Theses and Dissertations

Fall 2018

Characterization of the Spatial and Temporal Changes in River Geometry and Sand Load with Field Data Analysis and 1D Numerical Modeling

Zeyad Ayoob Sulaiman

Follow this and additional works at: https://scholarcommons.sc.edu/etd

Part of the Civil Engineering Commons

CHARACTERIZATION OF THE SPATIAL AND TEMPORAL CHANGES IN RIVER GEOMETRY AND SAND LOAD WITH FIELD DATA ANALYSIS AND 1D NUMERICAL MODELING

by

Zeyad Ayoob Sulaiman

Bachelor of Water Resources Engineering
University of Mosul, 2004

Master of Irrigation & Drainage Engineering
University of Mosul, 2007

Submitted in Partial Fulfillment of the Requirements

For the Degree of Doctor of Philosophy in

Civil Engineering

College of Engineering and Computing

University of South Carolina

2018

Accepted by:

Enrica Viparelli, Major Professor

Raymond Torres, Major Professor

Jasim Imran, Committee Member

Shamia Hoque, Committee Member

Cheryl L. Addy, Vice Provost and Dean of the Graduate School

ii

DEDICATION

To my parents

My beloved wife and sibling

And all my teachers and friends

Without whom it was almost impossible to finish this work

ACKNOWLEDGEMENTS

ABSTRACT

The quantification of the changes in channel geometry and sand load that have occurred on the Missouri River after engineering works and that characterize the Altamaha River in the fluvial-tidal transition zone is the main objective of this research. Dam construction and channelization on the Missouri River resulted in flow regulation, sediment shortage by dam reservoir trapping, channel straightening and narrowing. Quantifying the morphodynamic response of the Lower Missouri River to these engineering projects at short and long-time scales is a difficult problem that we approach with the analysis of the available field data and with the aid of a one-dimensional morphodynamic model. The results show that the peak discharge and suspended sand load have reduced remarkably downstream of Gavins Point Dam, i.e. the lowermost dam on the Missouri River mainstem, and have recovered gradually to pre-dam levels downstream of the junctions with major tributaries. The analysis of mean daily flows reveals no observable change in high flow magnitude and frequency downstream of the Missouri River – Grand River confluence. Model results show no significant change in mean annual sand load in the downstream-most part of the study reach for short and long-term simulations. Recent studies on river morphology in the fluvial tidal transition zone show significant changes in channel geometry and sediment size over relatively short distances with the cross-sectional area and the sediment size decreasing the oceanward direction. The collection and analysis of field data in the fluvial-tidal transition zone of the Altamaha River presented herein provides greater insight into

the characteristics and causes of these spatial changes. Stream power and Shields number were used to explain the observed changes, which occur over a distance ranging from 1 to 4 km. The analysis showed a sharp decline in stream power and Shields number at the boundary between the fluvial and tidal dominated reaches. This decline is thought to be responsible for the observed changes in channel geometry and sediment size.

TABLE OF CONTENTS

LIST OF TABLES

LIST OF FIGURES

LIST OF SYMBOLS

B coefficient of the entrainment relation (1);

B_c channel width (L);

C_f friction coefficient (1);

C_5 near-bed volumetric suspended sediment concentration averaged over turbulence at a distance z_b from the channel bed equal to $0.05H$ (1);

D geometric mean diameter (L);

D_{90} grain diameter such that 90% of the bed material is finer (L);

E total energy (L);

E_b non-dimensional entrainment rate of sediment in suspension (1);

Fr Froude Number (1);

g acceleration of gravity (LT^{-2});

H cross-sectionally averaged flow depth (L);

H_s cross-sectionally averaged flow depth associated with skin friction (L);

I Integral in the direction normal to the channel bed of the product between the velocity and the volumetric suspended sediment concentration (1);

xiii

k_c composite roughness height associated with flow resistances associated with skin friction and form drag (1);

k_s roughness height associated with skin friction (1);

N number of characteristics discharges bin in the flow duration curve (1);

p_i average fraction of the year in which the flow was equal to characteristic discharge(1);

q volumetric flow rate per unit channel width (L^2/T);

Q_{bm} total volumetric bed material transport capacity (L^3/T);

$Q_{bm,b}$ volumetric bedload transport capacity (L^3/T);

$Q_{bm,s}$ volumetric suspended bed material (L^3/T);

Q_s suspended sand transport capacity (L^3/T);

Q water discharge (L^3/T);

R submerged specific gravity of the bed material (1);

R_p particle Reynolds number (1);

S channel bed slope (1);

S_f friction slope (1);

t temporal coordinate (T);

U depth-averaged flow velocity (L/T);

u_* shear velocity (L/T);

u_{*s} shear velocity associated with skin friction (L/T);

v_s particle settling velocity (L/T);

x downchannel coordinate (L);

X non-dimensional entrainment parameter of sediment (1);

Zr Rouse number (1);

α parameter that accounts for stratification effects associated with suspended sediment transport (1);

η channel bed elevation (L);

η_i channel bed elevation at the downstream end of the modeled reach (L);

κ Von Karman constant (1);

λ_p bulk porosity of bed (1);

v kinematic viscosity of water ($L^2 T^{-1}$);

ξ water surface elevation (L);

ρ water density ($M L^{-3}$);

ρ_s sediment density ($M L^{-3}$);

τ bed shear stress ($M L^{-1} T^{-2}$);

τ_s bed shear stress associated with skin friction ($M L^{-1} T^{-2}$);

τ^* Shields number (1);

τ^*_s Shields number associated with skin friction (1);

ω Unit stream power (watt/ L^2).

CHAPTER 1

INTRODUCTION

Rivers transport water and sediment from continents to the ocean. Depending on the system slope, the flow regime, the sediment supply and the sediment characteristics, river morphology varies, adjusts, and adapts over multiple spatial and temporal scales (Leopold and Maddock, 1953; Julien and Wargadalam, 1995). Natural and anthropogenic events may induce changes in hydrology, sediment load and/or caliber that induce changes in river shape and form (Lane, 1937; Mackin, 1948; Gurnell, 1997; Schumm, 1968; Church, 1995).

Rivers respond to natural and human-induced changes with a series of channel adjustments, e.g. changes in channel geometry and morphology, in slope or in channel pattern (Lane, 1955; Simon, 1989; Ortega et al., 2014; Boix-Fayos, 2007; Gregory, 2006; Lane et al., 2007). Examples of anthropogenic activities that result in changes in river characteristics include changes in land use, flow regulation, river engineering works. The adjustments to these activities are generally confined within the watershed and its river network. Natural conditions that can control channel shapes and processes include changes in flow characteristics due to e.g. the interaction between unidirectional river flows and bidirectional tidal currents or the confluence with a major tributary (Gurnell, 1997), changes in climate and sea level. The response to these factors varies over temporal scales that are much longer than those characterizing the response of a river reach to human activities and over spatial scales that are larger than a single watershed.

1

River adjustments to natural and anthropogenic forcing occur at different spatial and temporal scales. Small scale adjustments can be associated with changes in channel characteristics such as the changes in grain size distribution, channel width, and channel depth. The large scale response of a river can be characterized by changes in channel pattern, reach morphology and slope, and usually reflects the cumulative effect small scale processes (Church, 1995; Buffington, 2012).

The research work presented in this dissertation focuses on the response of the Missouri River to flow regulation and channel narrowing-straightening, and on the impacts that the interaction between river flow and tidal oscillations have on river morphology in the fluvial-tidal transition zone of the Altamaha River.

1.1 IMPACT OF FLOW REGULATION AND RIVER MODIFICATION ON RIVER MORPHOLOGY AND HYDROLOGY

More than 40,000 dams higher than 15 m have been built around the world for e.g. flood control, hydropower generation, navigation control, irrigation, industrial development, municipal water supply and sediment control (ICOLD, 1988). Further, river engineering works such as channel stabilization and straightening associated with the construction of dikes and other structures are realized for e.g. flood control, navigation, and prevention of bank erosion (Horsak et al., 2009; Painter and Heine, 2005).

With the increasing number of dam projects and river engineering works, the awareness of the impacts that these projects have on natural systems has grown as well. Thereby, the characterization of the impacts of imposed changes in flow regime, sediment supply and downstream base level on river morphology and hydrology received significant

attention last few decades (Williams and Wolman, 1984; Brandt, 2000; Benn and Erskine, 1994; Petts and Gurnell, 2005; Galay, 1983; Andrews, 1986; Gregory, 2006; Pišút, 2002; Horsak et al., 2009; Painter and Heine, 2005).

Morphological and hydrological changes associated with dam construction are generally characterized by 1) changes in flow rates and sediment loads delivered to the downstream reaches, and 2) a sudden increase in base level for the upstream reaches. Flow regulation downstream of dams is generally characterized by a reduction in the peak flood discharges. Flow management to ensure safe navigation may be associated with increasing magnitude in medium and low flows. In other words, the regulated flow regime downstream of a dam is characterized by changes in shape, magnitude, and frequency of the flow hydrograph compared to the natural conditions (Magilligan and Nislow, 2005). The response of different river reaches to these changes depends on the reach characteristics and as such it is very a complex problem that has to be approached with the study of a significant amount of field data (Petts, 1979; Church, 1995).

The closure and the operation of a dam not only impacts the flow regime, it also results in a reduction of the sediment that is supplied to the regulated reaches. In other words, the majority of the sediment contributed from the basin upstream of the dam is trapped in the reservoir and does not reach the regulated portion of a river. Depending on the reservoir size and on the dam operational rules, the sediment trapping efficiency of a reservoir may be as high as 95% (Williams and Wolman, 1984). As a result, the sediment transport capacity of the flow released from the dam is in general higher than the sediment supplied to the regulated reach and this may result in channel bed erosion and/or in the formation of a static armor (Livesey, 1965). Due to the increasing drainage area, further

3

downstream of the dam, the post-dam sediment supply and channel hydrology may recover to pre-dam level (Li et al., 2009).

1.2 IMPACT OF TIDAL OSCILLATIONS ON CHANNEL MORPHOLOGY

The interaction between tidal oscillations at the downstream end of a river channel and the sediment transport processes plays an important control on channel forms and processes. In rivers, bankfull channel width and depth increase in the streamwise direction as the flow discharges increases from the mountains to the ocean (Leopold et al., 1964). Predicting the spatial changes in channel geometry becomes more complex in tide-dominated settings due to the complex interactions between river flows and tidal oscillations.

The fluvial-tidal transition zone identifies the portion of a river at the boundary between the river-dominated reach, where the flow hydrodynamics is significantly impacted by the tidal oscillations (Dalrymple and Choi, 2007; Dalrymple et al., 2012; Ensign et al., 2013; van den Berg et al., 2007; Wright et al., 1973). The location of the fluvial-tidal transition zone depends on the flow regime, the channel morphology, and the characteristics of the tides (Dalrymple et al., 2015, Freitas et al., 2012).

Yankovsky et al. (2012) described the tidal-fluvial transition as the portion of the river in which the interaction between the unidirectional river flow and the bidirectional tidal flow becomes significant. Progressing from the ocean towards land, tidal amplitude, and current speed increase due to channel convergence. As the tide travels landward, energy is gradually dissipated due to bed friction and the interaction with the river discharge. In the transition zone significant dissipation of tidal energy occurs (Ensign et al., 2013; Yankovsky et al., 2012; Dalrymple et al., 2015). Due to the interaction between

4

unidirectional river flow from the land to ocean and bidirectional tidal flows, channel morphology in the fluvial-tidal transition zone is characterized by noticeable changes over relatively short distances (Gurnell, 1997; Sassi et al., 2012; Yankovsky et al., 2012).

Recent observations in tidal settings documented changes in channel morphology through the fluvial-tidal transition zone (Torres, 2017; Kastner et al., 2017; Yankovsky et al., 2012; Gurnell, 1997; Sassi et al., 2012; Ganju et al., 2004; Dashtgard and La Croix, 2017; Dalrymple and Choi, 2007; Lawrence et al., 2015). In particular, Yankovsky et al. (2012) and Torres (2017) reported on a sharp change in cross-section geometry in this part of the river (see also Kastner et al., 2017; Sassi et al., 2012). Ganju et al. (2004) and Dashtgard and La Croix (2017) used suspended sediment concentration measurements to determine the location of the fluvial-tidal transition over a tidal cycle. During flood flow the transition migrates landward and corresponds to the location of a maximum suspended sediment concentration. These studies notwithstanding, changes in channel morphology and sedimentary processes in the fluvial-tidal transition are still poorly characterized and interpreted due to the complex flow hydrodynamics and its interaction with sediment transport processes.

1.3 RESEARCH OBJECTIVES

The overall objective of this dissertation is the study of how temporal changes in flow regime, sediment supply and base level impact channel morphology. In particular, two field cases are considered. The first field study focuses on the impacts of dam construction and channelization works on the Lower Missouri River, USA, where widespread channel bed erosion is thought to be a consequence of human-induced flow regulation and channel

narrowing/straightening. The second field study focuses on the impacts of tidal oscillations (i.e. periodic, natural changes in base level) on the morphology and flow hydrodynamics of the fluvial-tidal transition zone in the unregulated Altamaha River in Georgia, USA.

The Lower Missouri River is the ~1300 km long reach of the Missouri River starting at Gavins Point Dam, SD, and ending at the Mississippi River − Missouri River confluence, MO. Water resources management in the Lower Missouri River basin focuses on different purposes including flood control, hydropower generation, irrigation, water supply and maintenance of navigation flows. Dam construction in the 1950s coincided with extensive engineering works such as channel alignment and bank stabilization, on more than 90% of the total reach length (Pinter and Heine, 2005; Simon and Rinaldi 2000, 2006; Halberg, 1981).

The impacts of the engineering works on the Lower Missouri River morphology can be summarized as widespread channel bed erosion and changes in sediment load, as well documented in previous studies (Pinter and Heine, 2005; Jacobson and Galat, 2008; Holly and Karim, 1986; Simon and Rinaldi 2000, 2006; Halberg, 1981). Due to the problem complexity, however, there are still questions on 1) the impact of dam closure and channelization works on the sand load delivered to the Mississippi River (e.g., Nittrouer and Viparelli, 2014; Blum and Roberts, 2014; Meade and Moody, 2010; Horowitz et al, 2001; Kemp et al., 2016; Syvitski et al., 2009), 2) the role of tributaries and the streamwise increase in drainage area on the regulated flow regime and sand loads, and 3) the response of the Missouri River channel to the engineering works.

The objectives of the proposed research on the impacts of changes in flow regime on the Lower Missouri River are:

6

a- Quantify, analyze, and discuss the spatial and temporal changes in flow regime and suspended sand load in the study reach.

b- Quantify the morphodynamic response of the Lower Missouri River to the engineering works at short and long time scales.

c- Determine the role of tributaries on the short and long term morphodynamic evolution of the study reach.

The second part of the proposed research is an investigation on the morphological and hydrodynamic characteristics in the fluvial-tidal transition zone. The study area is located on a 47 km long reach of the Altamaha River, USA, located ~30 km upstream of the river mouth. The flow regime in the study reach is non-regulated and tidally influenced in the lowermost part of the reach, in other words the fluvial-tidal transition occurs within the study reach.

The upper limit of the transition zone is generally identified by the tidal limit, i.e. the point where the influence of tidal oscillations on the river flow becomes negligible. The tidal limit does not have a fix position in time, it migrates upstream or downstream during a tidal cycle and due to the variability of the river discharge (Freitas et al., 2012; Dalrymple and Choi 2007; Dalrymple et al., 2012; Kastner et al., 2017; Gurnell, 1997; Sassi et al., 2012; Ganju et al., 2004; Dashtgard and La Croix, 2017; Lawrence et al., 2015).

Spatial changes in channel geometry and sediment characteristics have been observed across the fluvial-tidal transition zones (Torres, 2017; Kastner et al., 2017; Gurnell, 1997; Sassi et al., 2012; Ganju et al., 2004; Dashtgard and La Croix, 2017; Dalrymple and Choi, 2007; Lawrence et al., 2015). However, the physic processes that are responsible for these changes are still poorly understood. Investigating the causes of the

7

observed changes in channel geometry and sediment grain size is the main objective of the proposed second study.

Specific objectives of the proposed research are to combine field observations and one-dimensional calculations to:

a- Investigate the spatial changes in channel morphology and grain size distribution across the fluvial-tidal transition zone; and

b- Interpret the change in channel geometry and grain size distribution with respect to the spatial distribution of stream power and Shields number respectively.

The remainder of this document is organized as follows. The study on the short and long term morphodynamic evolution of the Lower Missouri River is presented in Chapter 2. The study on the changes in channel morphology and grain size distribution of a fluvial-tidal transition presented in Chapter 3. The summary and conclusion of the two case studies in Chapter 2 and Chapter 3 are presented in Chapter 4.

CHAPTER 2

NUMERICAL SIMULATION OF MISSOURI RIVER BED EVOLUTION AND SAND LOAD DOWNSTREAM OF GAVINS POINT DAM[1]

2.1 INTRODUCTION

The Missouri River originates in the Rocky Mountains in southwestern Montana and flows southeastward for ~3800 km before it joins the Mississippi River near St. Louis, Missouri. The US Army Corp of Engineers manages water resources in the Missouri River basin with particular attention to flood control, navigation, hydropower generation, irrigation and water supply. Dams and other engineering structures were built to regulate the Missouri River and its tributaries (Ferrell, 1993, Pinter and Heine, 2005). Dam construction started in the 1930s and about 100 dams have been built since the 1950s as part of the Pick-Sloan water development project (Ferrell, 1993, Pinter and Heine, 2005; Skalak et al., 2013). Gavins Point Dam, SD, is the most recent and downstream most dam on the Missouri River mainstem and was closed in 1954.

This study focuses on the ~1300 km of the Missouri River from Gavins Point Dam to the confluence with the Mississippi River, MO. This reach is generally called the Lower Missouri River and it is represented in Figure 2.1 with the main tributaries, USGS gaging stations, and locations that are relevant for this study. Downchannel distances in Figure 2.1

---

and throughout this chapter are measured in river kilometers, RK, upstream of the Mississippi River – Missouri River confluence, with RK= 0 indicating the Mississippi River – Missouri River confluence and RK = 1305 indicating the location of Gavins Point Dam.

Channelization works on the Lower Missouri River were performed in the 1960s from Sioux City, Iowa, to St. Louis, Missouri, to create a *stable channel* for navigation and to reduce flood magnitude and frequency. In particular, the channel width was narrowed to 220 m – 360 m, equal to one half to one third of the original width, the main channel was re-aligned, meanders were removed and the banks were armored to prevent lateral migration (Pinter and Heine, 2005; Heine and Lant, 2009; Jacobson and Galat, 2008; Simon and Rinaldi 2000, 2006; Halberg, 1981; Branyan, 1974). As a result, the Missouri River mainstem was shortened of ~110 km and the sinuosity was reduced (U.S Army Corps of Engineers, 2017).

Field observations show that the Missouri River response to these engineering works has been complex. The Missouri River from Gavins Point Dam (RK 1305) to Sioux City (RK 1178), IA and from St. Joseph (RK 719), MO to Kansas City (RK 589), MO experienced 2.0 m - 4.0 m of bed degradation (see locations in Figure 2.1), while the reach from Omaha (RK 991), NE, to Nebraska City (RK 937), NE, changed little since dam closure (U.S Army Corps of Engineers, 2012; Pinter and Heine, 2005).

Quantifying the morphodynamic response of the Lower Missouri River to the engineering works at short (decadal) and long (centennial) time scales is a difficult problem that we approach with the analysis of the available field data and with the aid of a one-dimensional morphodynamic model. In particular, we quantitatively analyze and discuss

10

1) the streamwise changes in the Lower Missouri River daily flows, 2) the spatial and temporal changes in suspended sand load in the study reach, 3) the morphodynamic evolution of the Lower Missouri River channel, and 4) the role of tributaries on the short and long term morphodynamics of the study reach.

The changes of the Lower Missouri River hydrology associated with the construction of dams have been thoroughly studied (Pegg et al. 2003; Pegg and Pierce, 2002; Galat and Lipkin, 2002; Jacobson and Galat, 2008). The vast majority of these studies, however, primarily focused on the changes in flow regime at few gaging stations and did not consider the impacts of water resources management on the flow regime of the entire Lower Missouri River. Here we present an analysis of the daily flow data collected at nine USGS stations to determine 1) the length of the Lower Missouri River where the flow regime has been significantly impacted by the closure of Gavins Point Dam, and 2) how the flow regime has changed in the Lower Missouri River due to flow regulation in the river basin.

It is well accepted that historically the Missouri River contributed roughly 12% of the total water and 50% of the total (sand and mud) sediment load to the Mississippi River (Meade and Moody, 2010). However, the impacts of flow regulation in the Missouri River basin on the sand and mud loads delivered to the Mississippi River are still a matter of debate (e.g., Nittrouer and Viparelli, 2014; Blum and Roberts, 2014). The uncertainties associated with the predictions of the sand load in the Lower Missouri River further complicate the interpretation of the field observations. Here we use the available field data and a model of river morphodynamics to predict the changes of the suspended sand load

upstream of the Mississippi River – Missouri River confluence from the closure of Gavins Point Dam at short (decadal) and long (centennial) time scales.

Finally, to the best of our knowledge the role of the main tributaries on the morphodynamic evolution of a large, regulated river is a largely overlooked problem in the engineering literature (Blom et al., 2016). Here a model of river morphodynamics is used to investigate the role of the Missouri River tributaries on the evolution of the regulated and engineered Lower Missouri River mainstem.

2.2 THE LOWER MISSOURI RIVER

The Missouri River basin occupies ~137,000 km^2 of the United States from South West Montana to Missouri (Galat and Lipkin, 2002). For water resources management the Missouri River is divided into three reaches, the Upper Missouri River from the headwater to Fort Peck Dam, MT, the Middle Missouri River from Fort Peck Dam, MT, to Gavins Point Dam (RK 1305) near Yankton, SD, and the Lower Missouri River from Gavins Point Dam to the confluence with the Mississippi River near St. Louis, MO (Jacobson and Galat, 2008; Holly and Karim, 1986; Alexander et al., 2013). It is worth mentioning here that in some studies the upstream end of the Lower Missouri River is located at Sioux City (RK 1178), IA (Pegg et al. 2003; Pegg and Pierce, 2002; Galat and Lipkin, 2002).

The major tributaries of the Lower Missouri River are listed in Table 2.1 with indication of the confluence location, tributary drainage area and confluence side, i.e. on the hydraulically left or right of the Missouri River. In general, the tributaries on the hydraulic left have low slopes and fine sediment load. The tributaries on the hydraulic right have relatively high slopes and transport relatively coarse sediment (Carlston, 1969).

12

The US Army Corps of Engineers conducted extensive bed sampling in the 1970s from Yankton (RK 1305), SD, to St. Joseph (RK 719), MO, and showed that the median bed material size ranges between 0.2 and 0.4 mm (Holly and Karim, 1986). Further, Keown et al. (1986) reported that there was no significant change in the bed material (sand) size at Hermann (RK 157) for the last 50 years, where the characteristics sand size varies between 0.2 mm and 0.45 mm.

2.2.1 Lower Missouri River hydrology

The hydrology of the Lower Missouri River is analyzed using daily flows recorded at nine USGS gaging stations on the Missouri River main channel. These stations are listed in Table 2.2 with their USGS ID number, location in RKM, period of record and watershed area. These stations were chosen based on the length of the period of record, the type of available measurements and on the location.

The USGS stations with daily flow measurements and with a record of suspended sediment measurements starting prior to 1954 were used to characterize the flow regime and sediment loads. The USGS stations located on the mainstem immediately downstream of the junctions with major tributaries were used to determine the streamwise changes in flow regime. The downstream most USGS stations on the major tributaries were considered to determine the input of sediment from major tributaries.

The majority of the Missouri River mainstem dams were completed in the 1950s and 1960s, and the flow record at the USGS stations on the Lower Missouri River considered herein starts in the late 1920s/early 1930s. We thus divided the flow record

13

into two periods: pre-1954 or pre-Garrison Dam (pre-dam), and post-1954 or post-Garrison Dam (post-dam).

Garrison Dam was completed in 1953 and it was the first large dam built on the Missouri River mainstem after the closure of Fort Peck Dam, MT, in 1937. The area of the Missouri River basin upstream of Fort Peck Dam is equal to 20% of the drainage area of the Missouri River basin at Gavins Point Dam. We thus assume that the construction of the Fort Peck Dam did not have a significant impact on the Lower Missouri River.

The same assumption cannot be made for Garrison Dam, ND, located ~610 km downstream of Fort Peck Dam and ~930 km upstream of Gavins Point Dam. The area of the Missouri River basin at Garrison Dam is equal to the 65% of the Missouri River basin area at Gavins Point Dam, and the assumption that the construction of Garrison Dam did not impact the flow regime at Gavins Point Dam cannot be reasonably made (Meade and Moody, 2010; Shalak et al., 2013). Thus, the pre-1954, i.e. pre-Garrison Dam closure, daily flow data are used to characterize the pre-dam flow regime of the Lower Missouri River.

The flow regime of the Lower Missouri River is here described with flow duration curves based on the mean daily flows measured at the nine USGS stations listed in Table 2.2. Pre- and post-dam flow duration curves are presented in Figure 2.2, where the continuous and the dashed lines respectively represent pre- and post-dam conditions. For analysis and comparison purposes, high flows are characterized by probabilities of exceedance are greater than 0.05 and low flows have probabilities of exceedance smaller than 0.6.

After the completion of the engineering works on the Lower Missouri River, dams were built on its major tributaries and management practices were introduced regulate

14

agriculture (Simon et al., 2004; Ferrell, 1993; Meade and Moody, 2010). To determine if the engineering works and the changes in land use and management practices in the Lower Missouri River basin had an influence on the daily flows of the Lower Missouri River, we compared the post-dam flow duration curves at the USGS stations of Table 2.1 for 20-year intervals (1955-1974, 1975-1994, 1995-2015) with the pre-dam flow duration curve.

The flow duration curves for the 20-year time intervals are presented in Figure 2.3, where the gray and black lines represent the pre-dam and the 1995-974 periods respectively. The continuous dashed and dotted black lines represent the post-dam periods between 1975 and 1994 and between 1995 and 2015 respectively.

The post-dam flow regime at Yankton (RK 1287), SD, immediately downstream of Gavins Point Dam, did not significantly change from a 20-year period to the other (Figure 2.3a). The only noticeable difference between the flow duration curves is an increase of the low flows (probability of exceedance greater than 0.6) for the period between 1975 to 2015.

From Sioux City (RK 1178), IA to Waverly (RK 467), MO, the 1955-1974 period has the lowest flow rates (Figure 2.3b to 2.3g). This decline in the post-dam flow regime is associated with impoundment of the large reservoirs that extended until the end of the 1960s (Galat et al., 1996; Pegg et al., 2003; Blevins et al., 2014). The 1975-2015 flow rates with a probability of exceedance larger than ~0.3 are of the same order of magnitude of the pre-dam flows with the same probability of exceedance (Figures 2.3c to 2.3h). Downstream of the Grand River – Missouri River confluence at Hermann (RK 158), MO, the 1975-2015 intermediate and high flow rates reach the pre-dam flow level with no significant differences (Figures 2.3i).

15

In summary, Figure 2.2 and 2.3 show that 1) the effects of the dams on the Lower Missouri River flows gradually decrease as major tributaries enter the mainstem, 2) post-dam low flows are generally larger than the pre-dam flows with the same probability of exceedance, 3) upstream of the Missouri River -Grand River confluence post-dam flows with a probability of exceedance greater than ~0.1 are smaller than the pre-dam flows with the same probability of exceedance, and 4) downstream of the Missouri River -Grand River confluence, the 1975-2015 post-dam flows with probability of exceedance smaller than ~0.1 are higher than pre-dam flows.

2.2.2 Mean annual suspended sand loads

The mean annual suspended sand loads are calculated using two approaches. The first approach uses the power relation between the daily flow and suspended sand load, as illustrated and discussed in the continuing of this section. The second approach uses the suspended sediment concentration rating curve. The calculation procedure and the estimated mean annual sand loads are reported in the Appendix A. The comparison between the mean annual sand loads at the USGS stations on the Missouri River mainstem (Table 2.3) using these two methods shows that the maximum reported difference between the calculated loads was less than 20% of the mean annual sand load based on the suspended sand rating curve, which is used for the calculations presented in the continuing of this chapter.

Mean annual suspended sand loads are calculated from the available data collected at five USGS stations on the Missouri River mainstem (Table 2.3) and at the downstream most USGS station on the nine major tributaries of Table 2.1 (Table 2.4). The station

16

information (name and USGS ID) is reported in Tables 2.3 and 2.4 with the estimated pre- and post-dam suspended sand loads based on the power relation between daily flow and suspended sand load, the period of record of suspended sediment concentration and the number of measurements used in the analysis. The procedures used to estimate the mean annual suspended sand loads is illustrated below.

2.2.2.1   Pre-dam mean annual sand load

A limited number of suspended sediment concentration measurements are available at four stations on the Missouri River (Omaha, NE, St. Joseph, MO, Kansas City, MO, and Hermann, MO) for the pre-dam period, but the volume fraction content of sand in suspension is not reported. To determine a pre-dam suspended sand rating curve the suspended sediment discharges were estimated as the product of the measured suspended sediment concentration, the discharge and the volume fraction content of sand in suspension (Grey and Simoes, 2008). Heimann et al. (2011) reported that the average fractions of sand in suspension was 0.43 at Omaha, NE, (39 samples); 0.26 at St. Joseph, MO, (13 samples); 0.15 at Kansas City, MO, (9 samples); and 0.2 at Hermann, MO, (12 samples). These fractions were used to estimate the pre-dam suspended sand rating curves. At Yankton, SD, where pre-dam suspended sand data are not available, the suspended sand rating curve based on data collected between 2000 and 2008 was assumed to be representative of pre- and post-dam suspended sand transport. At Omaha, NE, the pre-dam mean annual sand load is estimated based on the 14 available values. The mean annual suspended sand load was estimated by averaging the suspended sand rating curve over the flow duration curve.

17

2.2.2.2 Post-dam mean annual sand load

The post-dam suspended sand rating curves at the five stations on the Missouri River of Table 2.3 were built with all the available data collected after 1954 for which the volume fraction content of sand in suspension was reported. Due to the lack of measurements of instantaneous discharge for a significant number of post-dam data and for all the pre-dam data, the suspended sand load was estimated by multiplying the daily discharge by the suspended sand concentration. Although this method does not provide an accurate estimate of the instantaneous suspended sand load, it will give a reasonable estimate of the daily loads (Joshi and Xu, 2015).

The pre- and post-dam mean annual suspended sand loads of Table 2.3 were computed as the average sand transport rate over the pre- and post-dam flow duration curves. In particular, the flow duration curves of Figure 2.2 were modeled in terms of 36 characteristics discharges, Q_i, with p_i being the average fraction of the year in which the flow was equal to Q_i. The suspended sand transport capacity, Q_{si}, for each characteristic discharge was then computed with the suspended sand rating curves (USACE, 2006). The mean annual suspended sand load, $Q_{bm,s}$ was finally estimated as:

$$Q_{bm,s} = \sum_{i=1}^{n} p_i Q_{si} \tag{2.1}$$

After 1954 the mean annual suspended sand load decreased from 8.8 Mt/yr to 0.5 Mt/yr at Yankton, SD. The post-dam reduction in mean annual suspended sand load gradually diminishes in the downstream direction with the post-dam suspended sand load being equal to 57%, 29% and 20% of the pre-dam estimate respectively at Omaha, NE, St. Joseph, MO and Kansas City, MO.

18

The same procedure was used to estimate the suspended sand loads at the lower most stations on the major tributaries of Table 2.4. Due to the lack of pre-dam data on suspended sand transport and daily flows, only post-dam sand loads could be estimated. Thus, in the model simulations presented in the continuing of this chapter we assumed that the pre-dam loads were equal to the post-dam suspended sand loads.

Field measurements of bedload transport on the Lower Missouri River are scarce. Based on measurements and observations performed by the USACE in 2012 the bedload transport was assumed to be equal to ~10% of the suspended sand load (Joshi and Xu, 2015; USACE, 2012).

2.3 MODEL FORMULATION

Model governing equations are the shallow water equations of conservation of flow mass and momentum (Chaudhry, 2008) and the equation of conservation of bed material (sand), the Exner equation. Flow resistances and suspended sand loads are computed with the Wright and Parker (2004) formulation for large, low slope sand bed rivers and the bedload transport rate is estimated with the Ashida and Michiue relation, which was derived based on experiments performed with sand and pea gravel (Parker, 2008).

For the model application to the ~1300 km long Lower Missouri River the problem is simplified as follows:

1. The bed material load is assumed to be orders of magnitude smaller than the flow rate so that the quasi-steady approximation holds (De Vries, 1965).

2. The channel cross section is assumed to be rectangular with effective width for sediment transport calculations B_c.

19

3. The grain size distribution of the channel bed material is assumed to be uniform with characteristic grain size D equal to 0.3 mm.

4. The sediment fluxes between the Missouri River channel and its floodplain are not accounted for in the calculations. In other words, a perfect balance between erosion and deposition associated with channel migration and overbank deposition of suspended sediment is assumed (Lauer and Parker, 2008a, b).

2.3.1 Flow equations

The one-dimensional form of the shallow water equations for open channel flow is (Chaudhry, 2008)

$$\frac{\partial H}{\partial t} + \frac{\partial UH}{\partial x} = 0 \tag{2.2}$$

$$\frac{\partial UH}{\partial t} + \frac{\partial U^2 H}{\partial x} = -gH\frac{\partial H}{\partial x} + gHS - C_f U^2 \tag{2.3}$$

where H and U respectively denote the cross-sectionally averaged flow depth and depth-averaged flow velocity, C_f is a non-dimensional friction coefficient, S is channel bed slope and equal to $-\partial\eta/\partial x$ with η being the channel bed elevation, g is the acceleration of gravity and x and t respectively are the downchannel and temporal coordinates.

Equations (2.2) and (2.3) are simplified with the aid of the quasi-steady approximation (DeVries, 1965). The time dependence is dropped, and the one-dimensional shallow water equation reduces to

$$q = UH \tag{2.4}$$

$$\frac{U}{g}\frac{\partial U}{\partial x} + \frac{\partial H}{\partial x} + \frac{\partial \eta}{\partial x} = -\frac{C_f U^2}{gH} \tag{2.5}$$

20

where q denotes the volumetric flow rate per channel width and is equal to Q/B_c with Q being the flow discharge.

Recalling the friction slope S_f is equal to $C_f F_r^2$ with F_r denoting the Froude Number defined as $\sqrt{U/gH}$, equation (2.5) can be rewritten as

$$\frac{\partial E}{\partial x} = -S_f \tag{2.6}$$

where E denotes to the total energy defined as

$$E = \eta + H + U^2/2g \tag{2.7}$$

$\eta + H$ in equation (2.7) is equal to water surface elevation ξ.

2.3.2 Equation of conservation of bed material

The one-dimensional equation of conservation of bed material is used to compute the changes in channel bed elevation as

$$(1 - \lambda_p)B_c \frac{\partial \eta}{\partial t} = -\frac{\partial Q_{bm}}{\partial x} \tag{2.8}$$

where Q_{bm} denotes the mean annual bed material (sand) load and is equal to the sum of the suspended sand load and of the sand load transported as bedload, and λ_p denotes the bulk porosity of bed.

2.3.3 Flow resistance calculation

To numerically integrate equation (2.6), the friction slope, S_f, has to be computed as a function of the flow characteristics. The Wright and Parker (2004) formulation is here implemented and the non-dimensional friction coefficient, C_f, is computed as

21

$$\frac{1}{\sqrt{C_f}} = \frac{U}{u_*} = \frac{8.32}{\alpha}\left(\frac{H}{k_c}\right)^{1/6} \tag{2.9}$$

where k_c represents the composite roughness height, i.e. the roughness height-associated with skin friction and form drag, u_* denotes the shear velocity defined as $u_* = \sqrt{\tau/\rho}$ with τ denoting the bed shear stress, and α is a parameter that accounts for stratification effects associated with suspended sediment transport.

Based on field data collected in the Mississippi River basin Wright and Parker (2004b) proposed the following relation to compute α as a function of the near-bed volumetric suspended sediment concentration averaged over turbulence C_5 at a distance z_b from the channel bed equal to $0.05H$ and the channel bed slope S, which is substituted here with the friction slope S_f to account for gradually varying flow (Viparelli et al., 2015)

$$\alpha = \begin{cases} 1 - 0.06\left(\dfrac{C_5}{S_f}\right)^{0.77}, & \dfrac{C_5}{S_f} \le 10 \\[4mm] 0.67 - 0.0025\left(\dfrac{C_5}{S_f}\right), & \dfrac{C_5}{S_f} > 10 \end{cases} \tag{2.10}$$

Under the assumption of equilibrium suspension C_5 is equal to the entrainment rate of sediment in suspension, E_b. In the Wright and Parker formulation E_b is function of the shear velocity associated with skin friction u_{*s}, defined as the square root of the ratio between the bed shear stress associated with skin friction, τ_s, and the water density, the characteristics of the bed material, and the friction slope S_f, as reported in Equation (2.11)

$$E_b = \frac{BX^5}{1 + \dfrac{B}{0.3}X^5} \tag{2.11}$$

where B is a model parameter equal to $7.8 \cdot 10^{-7}$, and X the entrainment parameter, that in the case of uniform sediment is defined as

$$X = \left(\frac{u_{*s}}{v_s} R_p{}^{0.6}\right) S_f{}^{0.08} \tag{2.12}$$

with v_s being the particle settling velocity and R_p denoting the particle Reynolds number defined as $(RgD)^{0.5}D/v$ where v is the kinematic viscosity of water, and R is the submerged specific gravity of the bed material (1.65 for quartz).

The Wright and Parker criterion to partition the flow resistances between skin friction and form drag is expressed as follows

$$\tau_s^* = 0.05 + 0.7\left(\tau^* F_r{}^{0.7}\right)^{0.8} \tag{2.13}$$

where τ^* and τ_s^* are the Shields numbers respectively defined as $\tau/\rho RgD$ and $\tau_s/\rho RgD$.

The flow resistance calculation is characterized by four equations, i.e. (2.9)-(2.11) and (2.13), in the six unknowns S_f, k_c, $u^*{}_s$, α, E_b, C_f. Two more equations are thus needed to close the problem.

The first equation is analogous to equation (2.9) but it links the mean flow velocity with the values of water depth, shear velocity and roughens height associated with skin friction as

$$\frac{U}{u_{*s}} = \frac{8.32}{\alpha}\left(\frac{H_s}{k_s}\right)^{1/6} \tag{2.14}$$

where k_s is the roughness height associated with skin friction as it is equal to $3D_{90}$ with D_{90} denoting the diameter such that 90% of the bed material is finer.

The second equation to close the problem links the roughness heights with the flow depths H and H_s as follows

$$\frac{K_c}{K_s} = \left(\frac{H}{H_s}\right)^4 \tag{2.15}$$

23

Equations (2.9)-(2.11) and (2.13)-(2.15) are iteratively solved to determine the flow resistance and the entrainment rate of sand in suspension.

2.3.4 Calculation of mean annual bed material load

The bedload transport capacity is computed with the Ashida and Michiue (1972) relation:

$$Q_{bm,b} = 17\sqrt{RgD}DB_c(\tau_s^* - 0.05)\left(\sqrt{\tau_s^*} - \sqrt{0.05}\right) \tag{2.16}$$

The suspended-sand load $Q_{bm,s}$ is computed as (Wright and Parker, 2004)

$$Q_{bm,s} = \frac{9.7}{\alpha} C_5 u_* H B_c \left(\frac{H}{k_c}\right)^{1/6} I \tag{2.17}$$

where I is the integral and can be defined as

$$I = \int_{y_5}^{1} y^{1/6} \left(\frac{1-y}{y} \frac{y_5}{y_5 - 1}\right)^{Zr} dy \tag{2.18}$$

where Zr denotes the Rouse number defined as $v_s / \alpha \kappa u_*$ with κ being the von Karman constant set equal to 0.41, y a non-dimensional upward oriented coordinate normal to the channel bed such that $y = 0$ on the channel bed and $y = 1$ at the water surface, y_5 the non-dimensional distance from the channel bed where the concentration of suspended sediment is equal to C_5 ($y_5 = 0.05$) and I was numerically computed by Wright and Parker (2004b) as:

$$I \approx \begin{cases} 0.679 \exp(-2.23Zr), & Zr \leq 1 \\ 0.073Zr^{-1.44}, & Zr > 1 \end{cases} \tag{2.19}$$

The volumetric mean annual sand load, Q_{bm}, is equal the average over the flow duration curve of the transport capacity of sand in suspension (equations 2.17 and 2.19) and as bedload transport (equation 2.16) as:

24

$$Q_{bm} = \sum_{i=1}^{M} \left(Q_{bm,b,i} + Q_{bm,s,i} \right) p_i \qquad (2.20)$$

where *M* denotes the number of discharge bins used to discretize the flow duration curve, equal to 24 in the simulations presented below.

2.4 NUMERICAL IMPLEMENTATION AND BOUNDARY CONDITIONS

Equations $2.6 - 2.8$ are solved with a first order Euler scheme. The computational time step Δt and the distance between two computational nodes Δx for pre-and post-dam simulations are equal to 1/100 year and 4 km respectively. The channel bed porosity λ_p is assumed to be constant and equal to 0.35.

The schematic representation of the study reach is presented in Figure 2.4. In Figure 2.4, input flow discharge and sand loads at the upstream boundary of the reach and at the confluence with the major tributaries of Table 2.1 are respectively represented with blue and orange arrows. The green dots represent the USGS stations that are used to validate the model sand load predictions. In summary, the entire reach is divided into seven subreaches and the flow discharge and sand load are specified at the upstream end of each subreach.

Nine major tributaries are reported in Table 2.1 thus the modeled reach should have been divided into 11 subreaches. Due to the lack of information on daily flows and suspended sand loads between the confluences of the Missouri River with the Nishnabotna River (RK 870) and the Nodaway River (RK 745), with the Grand River (RK 402) and the Chariton River (RK 385), and with the Osage River (RK 209) and the Gasconade River (RK 170), these confluences are modeled as three (and not six) confluences, as illustrated

25

in Figure 2.4, and the modeled reach is divided into 7 subreaches. Each model confluence is located where the Missouri River meets the largest tributary, i.e. at RK 870 (Missouri River − Nishnabotna River confluence), and RK 402 (Missouri River − Chariton River confluence) and at RK 209 (Missouri River − Osage River confluence).

The flow discharge and the input sand load are specified as boundary conditions at the upstream end of the computational domain and at the confluences with major tributaries. At each confluence a flow duration curve is specified based on the USGS records at the stations of Table 2.2. Due to the lack of confluences with major tributaries between the stations at Sioux City, IA, and Omaha, NE, the flow duration curves at Omaha, NE, are not used in the numerical simulations. For same reason, flow duration curves at Waverly, MO, downstream Kansas City, MO, station are also not used in the calculations presented below.

The sand load at the upstream end of the modeled reach is equal to the mean annual sand loads estimated at Yankton, SD. At each confluence, the sand load is equal to the sum of the sand load supplied to the subreach upstream of the confluence plus the input sand from the main tributary (Table 2.4). The mean annual sand load computed at the USGS stations on the Missouri River mainstem downstream of Yankton, SD listed in Table 2.3 are not used as model input, but are used for model verification.

The hydraulic calculations at each confluence impose the conservation of energy and flow mass in the absence of local head losses (for details see Chaudhry, 2008). Equation (2.6) is integrated in the upstream direction, so that the energy level and the water surface elevations downstream of each confluence are known during the calculations.

26

The downstream boundary condition for equation (2.6) is a specified water surface elevation at the Mississippi River – Missouri River confluence, which is a function of the discharges in the Mississippi River, in the Missouri River, of the hydrodynamic conditions in the Mississippi River, and of the confluence geometry. In other words, predicting the water surface elevation at the Mississippi River – Missouri River confluence is not an easy task.

The problem was simplified as follows: the average daily flow measured at the USGS station on the Missouri River at Hermann, MO, (158 km upstream of the Mississippi River – Missouri River confluence) and the gage height measured on the Mississippi River at St. Louis, MO, (~24 km downstream of the Mississippi River - Missouri River confluence) in the same day have been plotted to find a relationship to express the downstream boundary condition as a function of the flow rate in the Missouri River.

The data points presented in Figure 2.5 show that the water surface elevation at USGS station at St. Louis, MO, can be reasonably approximated as a function of the flow rate at Hermann, MO, as $\xi_{St.Louis} = 68Q_{Herman}^{0.07}$ with $\xi_{St.Louis}$ denoting the water surface elevation at St. Louis and $Q_{Hermann}$ denoting the daily flow at Hermann, MO. To express the model downstream boundary condition, it is further assumed that the water surface elevation at the Mississippi River – Missouri River confluence is not much different from the water surface elevation measured at the USGS station in St. Louis, and the power low of Figure 2.5 is used in the calculations.

27

2.5 PRE-DAM MODEL ZEROING

Model zeroing is the first and necessary step in field scale applications of morphodynamic models. Depending on the problem of interest, these runs are performed with different objectives, e.g. parameter calibration (e.g. Lauer and Parker, 2008; Viparelli et al., 2011), definition of pre-disturbance conditions (e.g. Viparelli et al., 2015), characterization of an initial equilibrium (steady-state) for the model runs (e.g. Cui et al., 2006; Viparelli et al., 2013; Lauer et al., 2016).). Here the pre-dam model zeroing was performed to determine a reasonable equilibrium condition by comparing model results with the available field data. This equilibrium condition was then used as initial condition for the post-dam runs.

The seven subreaches of the Missouri River presented in Figure 4 were modeled as sediment-feed flume analogues, i.e. the flow rates and the bed material loads were specified at the upstream end of each subreach and the water surface elevation was specified at the downstream end of each subreach. Under these conditions the equilibrium profile is independent from the initial condition of the simulations (Parker and Wilcock, 1993). The channel width of the pre-dam Missouri River is assumed to be 460 m (Pinter and Heine, 2005).

Two types of zeroing runs were performed, one in which the streamwise increase of the drainage area was neglected and the flow rate and sediment loads at equilibrium did not change from Yankton, SD, to the Mississippi River – Missouri River confluence, and the other in which the streamwise increase in drainage areas was accounted for as illustrated in the previous section. Starting from an initial longitudinal bed profile with constant slope equal to 0.00013 m/m, model simulations were performed until the system reached

www.manaraa.com

conditions of equilibrium, i.e. when the longitudinal profile did not change in time. Model input parameters for the zeroing runs are summarized in Table 2.5.

Pre-dam equilibrium channel bed profiles are presented in Figure 2.6, where the dotted black line represents the equilibrium profile with spatially constant flow rates and sand load, and the continuous black line is the equilibrium profile that accounts for the streamwise increase in flow rate and sand load. The vertical dashed lines denote the location of the major tributaries, where changes in the flow duration curves and sand loads were specified. The black square dots are measurements of thalweg elevation in 1954 reported by the USACE (U.S Army Corps of Engineers: Omaha District, 1993) and the black cross dots are thalweg elevation measurements in 1952 reported by the USACE (U.S Army Corps of Engineers, 2012).

The equilibrium profile in the case of spatially constant flow duration curve and sand load has a constant slope of 0.00009 m/m, and sand transport capacity equal to the upstream input rate. The equilibrium profile in the simulation with input of water and sand from the main tributaries shows an upward concavity, i.e. decreasing slope in the downstream direction, that is commonly observed in alluvial rivers (Blom et al., 2016) and a reach averaged channel slope of 0.00022 m/m.

The comparison between predicted and measured pre-dam bed elevations of Figure 2.6 shows a reasonable agreement between measured and predicted bed elevations when the streamwise changes in flow rate and sediment loads are accounted for in the calculations suggesting that the model is able to reasonably reproduce the 1D morphodynamics of the pre-dam Lower Missouri River.

29

The comparison between the numerical predictions and field measurements of pre-dam suspended sand loads at the USGS stations at Omaha (RK 991), NE, St. Joseph (RK 719), MO, Kansas City (RK 589), MO and Hermann (RK 158), MO, are presented in Figure 2.7 for the simulation in which the spatial changes in flow duration curve and sand load are accounted for. In this figure the numerical predictions at equilibrium are represented with the black square dots and the measured data are represented with blue square dots. The vertical bars on the numerical predictions indicate an error of ±15 of the numerical value showing that the model reasonably reproduces the suspended sand load at the four USGS stations along the Lower Missouri River.

2.6 POST-DAM SIMULATIONS

In 1950s major engineering works were performed on the Lower Missouri River for water resources management, flood control and navigation. Gavins Point Dam was closed in 1954, and channel straightening and narrowing was completed prior to 1960 on 90% of the Lower Missouri River. Due to the lack of details on the channel straightening works, here channel narrowing only is considered in the post-dam simulations as a reduction in channel width from 460 m to 320 m from Sioux City (RK 1178), IA, to Mississippi River – Missouri River confluence.

Two sets of post-dam simulations were performed to investigate 1) how the equilibrium of the Lower Missouri River changes due to the closure of Gains Point dam and/or channel narrowing, and 2) the combined effect of the engineering works and the changes in flow duration curves (Figure 2.2) on the evolution on the Lower Missouri River

30

between dam closure and 2015. The initial conditions for these runs are the equilibrium profiles of Figure 2.6.

2.6.1 Post-dam equilibrium runs

Post-dam equilibrium runs were performed to determine the response of the Lower Missouri River to 1) Gavins Point Dam closure without channel narrowing, 2) channel narrowing with no closure of Gavins Point Dam, and 3) a combination of the two.

The numerical runs were performed in the idealized case of absence of streamwise changes in flow rate and sand load, and in the more realistic case in which the streamwise changes in flow duration curve and sand supply are explicitly accounted for. The flow duration curves used in these simulations are representative of the entire post-dam period, i.e. from 1955 – 2015 (Figure 2.2) and the mean annual sand loads are reported in Table 2.3 and Table 4 for the mainstem at Yankton, SD, and for the major tributaries.

The post-dam equilibrium results are presented in Figure 2.8. In Figure 2.8a the net changes in equilibrium profiles are reported for the runs with no streamwise change in flow duration curve and sand supply. The post-dam equilibrium runs with streamwise changes in flow duration curves and sand supply are presented in Figure 2.8b. The vertical dot grey lines in Figure 2.8b represent the location of the main tributaries, i.e. where the changes in flow duration curve and sand supply are specified. In Figure 2.8 the horizontal dashed line represents no net change in bed elevation. The black dot line represents the net change in equilibrium bed elevation in the case of dam closure only, i.e. the channel width in this numerical run was set equal to the pre-dam value of 460 m. The continuous grey line represents the net change in bed elevation in the case of a reduction in channel width

31

from 460 m to 320 m from Sioux City, IA, to the Mississippi River – Missouri River confluence. The continuous black line is the net change in equilibrium bed elevation in the case of dam closure and channel narrowing.

The comparison between net changes in bed elevation at equilibrium of Figure 2.8a suggests that most of the channel bed erosion on the Lower Missouri River is associated with channel narrowing with limited, but significant, contribution from dam closure. It is also interesting to note that for the idealized conditions of Figure 2.8a, i.e. when the streamwise changes in flow and sand load are not accounted for, significant changes in channel bed elevation occurred in the upstream most ~450 km of the modeled reach. Limited channel bed aggradation (less than 1 m) was predicted at the downstream end of the modeled reach at equilibrium. The net result of the changes in equilibrium channel bed profiles was a reduction of equilibrium bed slope from 0.000095 m/m to 0.000083 m/m for the case of dam closure only, to 0.000068 m/m in the case of channel narrowing only, and to 0.00005 m/m in the case of dam closure associated with channel narrowing.

The evolution of the bed profile is characterized by channel bed erosion in the upstream part of the domain with this erosion progressing downstream. The celerity of the waves of channel bed degradation induced by dam closure (black dot line in Figure 2.8a) and dam closure associated with channel narrowing (continuous black line in Figure 2.8a) are presented in Figure 2.9 where the black line represents the celerity of the degradational wave in the case of dam closure and the grey line is the celerity of the degradational wave in case of dam closure associated with channel narrowing.

The degradational wave celerity was computed as the length of the eroding reach divided by the simulated time, e.g. if after 10 years channel bed erosion occurred in the

32

upstream most 50 km of the domain the celerity of the degradational wave was equal to 5 km/yr. With this calculation procedure, degradation wave celerity could be computed until a sudden increase in channel bed slope is observable on the longitudinal profiles, i.e. up to ~170 – ~250 years.

Figure 2.9 shows that the of the degradational wave induced by dam closure (black line) is highest at the beginning of the simulation, i.e. when the disturbance is imposed on an equilibrium bed, and it rapidly decreases for ~10 years of simulated time. The degradational wave celerity continues to decrease at a relatively small rate for the following 250 years of simulated time.

In the case of dam closure associated with channel narrowing (grey line) the degradational wave celerity is equal to that obtained in the case of dam closure (black line) until the wave originated at the dam reached the narrowed portion of the modeled reach at Sioux City, IA, after 13 years of simulated time. At Sioux City, IA, the erosional wave induced by dam closure interacted with the erosion caused by channel narrowing with a consequent increase in wave celerity. After ~175 years of the simulated time the initial channel bed elevation mostly adjusted to the imposed channel geometry, flow regime and sediment supply and the downstream end of the erosional wave were not identifiable on the longitudinal profiles.

In summary, the degradational wave in the case of dam closure associated with channel narrowing was faster than in the case of dam closure only. Consequently, the time required for the adjustment of the long profile was shorter than in the case of dam closure only.

33

The net changes in equilibrium bed elevation in the runs in which the streamwise changes in flow discharge and sand supply are accounted for are presented in Figure 2.8b. The equilibrium profile in the case of dam closure only (continuous black dot line) was characterized by widespread erosion with localized deposition at the Missouri River – Platte River confluence and in the lowermost ~50 km of the modeled reach with the largest erosion occurring downstream of Gavins Point Dam. The localized deposition at the Missouri River - Platte River confluence (between Omaha, NE, and St. Joseph, MO) was caused by the relatively large input of sand from the Platte River. Downstream of the confluences with the Nishnabotna River and the Nodaway River channel bed erosion was associated with a relatively small increase in the sand load compared to the increase in the flow rates. The inputs of sand downstream of the Missouri River - Grand River confluence reduced the amount of channel bed erosion.

In the case of channel narrowing with pre-dam flows and sediment loads (grey line) widespread erosion was predicted in the entire domain with the largest erosion occurring in the upstream part in proximity of Sioux City, IA. Finally, in the case of channel narrowing associated with the closure of Gavins Point Dam (continuous black line) the erosion between Sioux City, IA, and ~ RK 750 was smaller than in the case of channel narrowing (grey line). On the contrary, downstream of ~RK 750 channel erosion was higher than in the case of channel narrowing only.

The different erosion patterns between the cases of channel narrowing (grey line) and channel narrowing associated with dam closure (continuous black line) can be explained as follows. Downstream of Sioux City, IA, channel bed erosion was limited by the reduction in flow discharge (and thus sand transport capacity) caused by the closure of

34

Gavins Point Dam (black line above the grey line). In the downstream part of the domain, due to high post-dam flows compared to the pre-dam conditions (Figure 2.2), the post-dam mean annual sand transport capacity was larger than in the pre-dam period, with a consequent largest erosion of the initial channel bed (grey line above the black line).

The channel bed erosion presented in Figure 2.8b resulted in a decline of the reach-averaged equilibrium slope from 0.00022 m/m to 0.00019 m/m in the case of dam closure, to 0.00015 m/m in the case of channel narrowing and to 0.00012 m/m in the case of dam closure associated with channel narrowing.

In summary, when the streamwise increase in flow rate and sediment supply was accounted for in the calculations (Figure 2.8b) the long-term channel response to changes in flow regime, sand supply and channel width was characterized by widespread erosion of the channel bed. When the streamwise changes in flow duration curve and sand supply were not accounted for in the calculations (Figure 2.8a), channel bed erosion was predicted in the upstream ~450 km of the modeled reach and channel bed deposition occurred in the downstream part of the modeled domain.

The evolutions of the initial equilibrium bed towards a new condition of equilibrium presented in Figure 2.8 significantly changed if tributaries were accounted for in the calculations. When the streamwise changes in flow regime and sediment supply were not accounted for (Figure 2.8a), a rotation of the longitudinal profile around a point located in the center of the modeled domain occurred. When the spatial changes in flow discharge and sand load due to the streamwise increase in drainage area were accounted for, widespread erosion was predicted in the entire modeled domain with a rotation of the

35

equilibrium bed profile around a point located less than 100 km upstream of the Mississippi River – Missouri River confluence.

2.6.2 Prediction of the transient evolution of channel bed

To determine if the model was able to reasonably capture the spatial and temporal changes in bed profile associated with Gavins Point Dam closure and channel narrowing between Sioux City, IA, and the Mississippi River – Missouri River confluence, model predictions were compared against the measured changes in water surface elevation between 1955 and 2015. The comparison was done in terms of water levels measured at a specified flow discharge at the USGS stations of Table 2.2. The comparison between measured and numerical changes in water surface elevation was not performed at the Missouri River at Nebraska City, NE, which is close to the stations located at Omaha, NE, and St. Joseph, MO.

The comparison between numerical and measured changes in water surface elevation is presented in Figure 2.10, where the measured values are represented with blue square dots. Model results obtained using a single post-dam flow duration curve (Figure 2.2) are reported with the continuous grey line. The dash grey lines represent the ±20% interval around the model results. The black lines represent net changes in water surface elevation predicted when the flow duration curves of Figure 2.3 were used as input parameters, i.e. one flow duration curve for the 20 year long period between 1955 and 1974, one for 1975-1994 and one for 1995-2015.

The comparison between numerical and measured water surface elevation changes at a flow rate of 850 m^3/s at Yankton (RK 1287), SD, is presented in Figure 2.10a. The

36

field data show a progressive decrease in water surface elevation associated with channel bed erosion. Between 1955 and 1995 a net change in water surface elevation of 2.8 m was measured. This change in water surface elevation was primarily associated with the closure of Gavins Point Dam. The comparison between field data and numerical results showed that the model could reasonably capture the measured changes in water surface elevation. Further, due to the lack in significant change in the post-dam flow duration curves, significant changes between model results obtained with one and with three flow duration curves were not observed.

The comparison between changes in water surface elevation at the USGS station at Sioux City (RK 1178), IA, was done for a flow rate of 850 m^3/s (Figure 2.10b). The water surface elevation did not significantly change prior to 1960, when the channelization works were completed. The channelization works caused a rapid decrease in water surface elevation between 1960 and 1975 with ~2 m drop over ~15 years. No significant changes in bed elevation occurred between 1975 and 1992. Significant water surface elevation changes were then observed after the 1993 and the 2011 floods. The comparison between numerical results and field measurements showed that the model captured the overall changes in channel bed elevation but, due to the model simplification and the use of a cycled flow duration curve, the model was not able to capture the erosion associated with large flood events.

The changes in water surface elevation at Omaha (RK 991), NE, at a flow rate of 850 m^3/s are presented in Figure 2.10c. The field data showed no net change before 1965, an increase in the stage of less than 0.8 m between 1965 and the early 1980s followed by a decrease in the stage to pre-dam valued prior to 1995. The model results with a single post-

37

dam flow duration curve (Figure, 2.2c) reasonably captured the increase in water surface elevation between 1965 and 1985 but did not reproduce the decrease in water surface elevation between 1985 and 1995, which was likely a consequence of the changes in flow duration curve showed in Figure 2.3c. When 20 year-long flow duration curves were used to describe the flow regime, the model predicted a rapid increase in water surface elevation prior to 1965, which did not match the field data, but it then reasonably reproduced the post-1985 decreasing stage (continuous black line in Figure 2.10c). However, given the model simplifications, the magnitude of the pre-1985 change in water surface elevation was reasonably predicted.

The changes in water surface elevation at St. Joseph (RK 719), MO, were recorded for a flow rate of 1100 m^3/s (Figure 2.10d). Field data show a relatively stable period (not much change) prior to 1965 followed by a rapid 2.5 m drop between 1965 and 1975 that was partially the result of man-made meander cutoffs and wing dams upstream of this station (Pinter and Heine, 2005). The water surface elevation then remained relatively constant between 1975 and 1985, increased between 1985 and 1990 and then stabilized ~1.5 m below the 1955 stage. These changes in water surface elevation cannot be captured with the one-dimensional model presented herein. This notwithstanding, the model predicted the observed ~1.5 m water surface elevation changes between 1955 and 2009. In addition, when the changes in the flow duration curve were accounted for (black line) the model reasonably reproduced the changes in water surface elevation between 1955 and 1968, i.e. prior to the meander cutoff.

The water surface elevation at Kansas City (RK 589), MO, at a flow rate of 1100 m^3/s decreased of ~1.2 m between 1955 and 1992 and then it dropped of ~ 1 m during the

38

1993 flood (Figure 2.10e). Significant changes in water surface elevation between 1994 and 2000 were not recorded. A drop of ~ 1 m in the water surface elevation was then recorded between 2000 and 2005. In the simulation with a constant flow duration curve, the model did not capture the slow decrease in water surface elevation that occurred prior to 1993 and the sudden drop in the early 2000s (continuous gray line in Figure 2.10e). However, the magnitude of the predicted changes in water surface elevation over the 60 year-long period were in reasonable agreement with the field measurements. The results of the numerical simulations with 20 year-long flow duration curves (black line) reasonably captured the measured changes in water surface elevation prior to 1993 and the magnitude of the 1993-2015 water surface elevation changes.

The water surface elevation at a flow rate of 1300 m^3/s at Waverly (RK 467), MO, and Bonneville (RK 313), MO, and at 1900 m^3/s at Hermann (RK 158), MO, decreased of ~ 0.5 m at Waverly, MO, and ~ 1 m at Hermann, MO. Relatively large changes in water surface elevation were observed at Boonville, MO, with a drop of 1.7 m between 1975 and 2007 (Figure 2.10f, 2.10g, and 2.10h). The comparison between model results and field observations showed that the model reasonably captured the declining water surface elevations at these three stations, and that the results of the simulations with the 20 year long flow duration curves better approximated the field data than the simulations with a single post-dam flow duration curve.

In summary, the model reasonably predicted the magnitude and temporal change of water surface elevation associated with Gavins Point Dam closure and with the reduction in channel width downstream of Sioux City, IA. Model results obtained with 20 year-long post-dam flow duration curves showed overall better agreement with the observed changes

39

in water surface elevation than the results obtained using a single flow duration curve for the 1955-2015 period. We can thus conclude that the changes in flow rate associated with water resources management in the Missouri River basin, i.e. the changes in the flow duration curve, play a significant control on the evolution of the Missouri River channel at decadal time scales.

2.6.3 Simulation of post-dam suspended sand load

The comparison between numerical predictions of suspended sand load averaged over 20 year periods and field-based estimates for the same time intervals is presented in Figure 2.11 for the simulation with the 20 year-long flow duration curves of Figure TTT. The comparison is done at the USGS gage stations Missouri River at Omaha, NE, Missouri River at St. Joseph, MO, Missouri River at Kansas City, MO and Missouri River at Hermann, MO (Figure 2.1).

In Figure 2.11 field measurements and numerical results are respectively represented with blue triangle dots and black circle dots. The error bars on the predicted values represents ±15% error. The model results were in reasonable agreement with field measurements at all the stations and for all the considered time intervals. At Omaha, NE, for the period between 1975 and 1995 (Figure 2.11 a1), the predicted suspended sand loads were smaller than the majority of the measured data and this was likely a consequence of the channel bed degradation (Figure 2.10c) that was not captured during the model simulations.

The summary of the suspended load calculations is presented in Figure 2.12 in terms of field-based estimates and numerical predictions of the mean annual suspended

40

sand load averaged over 20 years at the same stations of Figure 2.11. Field estimates are represented with colored bars (purple for pre-dam, pink for 1955-1974, green for 1975-1994 and grey for 1995-2015) and model predictions are represented with black dots and the vertical bars indicate a ±15% error.

The field-based estimates of the mean annual suspended sand load in Figure 2.12 show that the pre-dam load increased from Omaha, NE to Hermann, MO, from ~12 Mt/yr to ~25 Mt/yr. In the post-dam period the suspended sand load at Omaha, NE, and St. Joseph, MO, respectively was ~1/3 and 2/3 of the pre-dam loads. Downstream of the Missouri River – Kansas River confluence (station Missouri River at Kansas City, MO) the post-dam load was the ~75%-85% of the pre-dam value and virtually no change between pre- and post-dam loads were observed at Hermann, MO, for the post-1975 period.

The comparison between the three estimates of post-dam mean annual sand loads of Figure 2.12 showed a noticeable decrease in the suspended sand load between 1955 and 1974 everywhere in the modeled domain. This was a consequence of the flow regulation associated with the impoundment of the two Missouri River reservoirs upstream of Garrison Dam and Gavins Point Dam that extended until the late 1960s (Galat et al., 1996; Pegg et al., 2003; Blevins et al., 2014).

The 1955- 1974 was characterized by higher than pre-dam low flow (probability of exceedance larger 0.6) and lower than pre-dam high flows (probability of exceedance less than 0.05) (Figure 2.3). Due to the strongly non-linear dependence of the suspended sand transport capacity on the flow rate (equation 2.17), the lower than pre-dam high flows resulted in a significant reduction of the mean annual sand load.

41

In the 1974-2015 period, the frequency and magnitude of high flows at the Lower Missouri are larger than in the 1955-1974 interval and this resulted in higher mean annual suspended sand loads. It is interesting to note that at Hermann, MO, the 1974-2015 mean annual suspended sand loads were comparable with the pre-dam values.

The comparison between the model results and the field-based estimates showed that the model can reasonably reproduce the suspended sand loads in the Lower Missouri River. Significant differences (larger than 15%) between model results and field-based estimates occurred at the station Missouri River at St. Joseph due to the changes in bed elevation associated with an artificial cutoff and other engineering works (see Figure 2.10d).

2.7 DISCUSSION

The field data and the numerical results presented in the previous sections were performed to study 1) the streamwise changes in daily flow frequency and magnitude in the post-dam Lower Missouri River, 2) the spatial and temporal changes in sand load associated with the engineering works, 3) the morphodynamic evolution of the Missouri River channel, and 4) the impact of the major tributaries on the evolution of the Lower Missouri River at short and long time scales.

The pre- and post-dam changes in daily flow frequency and magnitude were studied using flow duration curves at the USGS stations of Table 2.2 for the time intervals: pre-dam (or pre-1954), 1955-2015, 1955-1974, 1975-1994 and 1995-2015. The comparison between pre- and post-dam flow duration curves showed that the impact of the flow regulation on the Lower Missouri River resulted in 1) higher than pre-dam low (probability

of exceedance larger than 0.6), 2) lower than pre-dam high flow (probability of exceedance greater than 0.05) magnitude upstream of the Missouri River – Grand River confluence, and 3) no observable change in high flow magnitude downstream of the Missouri River – Grand River confluence in the 1975-2015 period (Figure 2.2 and 2.3).

The spatial and temporal changes in flow duration curves revealed that as the Lower Missouri River drainage area increased from Yankton, SD, to the Mississippi River – Missouri River confluence, the change in daily flows associated with the closure of Gavins Point Dam became less significant. The Missouri River – Grand River confluence (903 km downstream of Gavins Point Dam) can be seen as the location that disconnects the reach of the Missouri River where the flow regulation at Gavins Point Dam has a significant impact on the magnitude of flood flows from the reach of the Missouri River in which flood flows are not much different from the pre-dam values (Figure 2.2 and 2.3).

The observed spatial and temporal changes in mean annual suspended sand load were not only associated with the changes in the flow regime, they were also a consequence of the engineering works designed to increase the sand transport capacity of the flow to create a *stable channel* for navigation (Pinter and Heine, 2005; Jacobson and Galat, 2008; Simon and Rinaldi 2000, 2006; Halberg, 1981; Branyan, 1974).

Estimates of the mean annual suspended sand loads based on data collected at the USGS stations of Table 2.3 and Figure 2.12 revealed that the post-dam suspended sand load decreased to ~95% , ~58%, ~30% and ~20% of the pre-dam values at the USGS stations Missouri River at Yankton, SD, Omaha, NE, St. Joseph, MO, and Kansas City, MO respectively, i.e. upstream of the Missouri River – Grand River confluence.

Downstream of this confluence, and virtually no change between pre- and post-dam loads (less than 10%) occurred at Hermann, MO, between 1975 and 2015 (Table 2.3).

Numerical predictions and field observations revealed that the suspended sand load in the Lower Missouri River between 1955 and 1974 was significantly smaller than in the pre-dam period due to the imposed reduction in high flow frequency and magnitude associated with impoundment of the large dam reservoirs (Galat et al., 1996; Pegg et al., 2003; Blevins et al., 2014).

The spatial changes in suspended sand load between Gavins Point Dam and the Mississippi River – Missouri River confluence showed that as the drainage basin increased, the reduction in suspended sand load associated with flow regulation became less important. At the lowermost USGS station on the Lower Missouri River, i.e. Missouri River at Hermann, MO, noticeable differences between pre- and post-dam suspended sand loads were not observed (Figure 2.12).

Long term (equilibrium) model simulation suggested that there was no significant change in mean annual suspended sand load at Hermann (RK 158), MO (Figure 2.13). In particular, the numerical results suggested that, if the flow duration curve does not change, a ~10% decrease in suspended sand load compared to pre-dam values can be expected at Hermann, MO, in the future 3000 years,. Thus, field data suggested that the amount of sand delivered to the Mississippi River at Saint Louis, MO has not been noticeably affected by the closure of the Missouri River dams and river engineering works. Numerical predictions showed that significant changes in the suspended sand load delivered to the Mississippi River should not be expected.

44

It is important to mention here, however, that the same conclusion, i.e. no change from pre-1954 conditions, does not necessarily hold for the wash load (silt and clay) due to the channel alignment works that significantly impacted the interaction between the Missouri River channel and its floodplain. Further, due to the lack of information on the wash load morphodynamics, quantifying the impact of dam sedimentation on the wash load budget remains an open problem.

The implementation and validation of a model of river morphodynamics on the Lower Missouri River showed that the channel response to engineering works and flow regulation was characterized by channel bed erosion downstream of Gavins Point Dam from Yankton, SD, to Sioux City, IA with up to 3 m of channel bed degradation between 1955 and 2015 upstream of the Missouri River - Platte River confluence (Figure 2.3a and 2.3b), i.e. where the post 1954 changes in flow duration curve are highest.

Downstream of the Missouri River – Platte River confluence, the magnitude of channel bed erosion was smaller than in the upstream reach due to the relatively large sand load of the Platte River. Downstream of the Missouri River – Kansas River confluence, the observed 3 m – 3.7 m of channel bed degradation were primarily associated with a change in channel width and channel straightening works, because the wave of degradation induced by the closure of Gavins Point Dam had not yet reached this portion of the Missouri River. Model results and field observation demonstrated that the amount of channel bed lowering at Waverly, MO, and Hermann, MO, are less than 1 m that resulted primarily from channel narrowing.

2.8 CONCLUSION

A mathematical formulation of river morphodynamics and its implementation in a one-dimensional numerical model were used to study the impact of dam closure and channel narrowing on large sand bed rivers. Model governing equations are the shallow water equation of open channel flow simplified with the aid of the quasi-steady approximation and the Exner equation of conservation of bed material. Flow resistances and suspended sand load were computed with the Wright and Parker (2004) formulation for large, low slope sand bed rivers.

The analysis of field measurements at the USGS stations and model simulations were used to investigate the impacts of dam construction and channel narrowing on a ~1300 km long reach of the Missouri River from Gavins Point Dam (RK 1305), SD, to the Mississippi River – Missouri River confluence, MO. The main objectives of this work were 1) the identification of the spatial and temporal changes in flow regime downstream of Gavins Point Dam, which had a direct impact on the sand transport capacity of the flow, 2) the quantification of the changes in suspended sand load to characterize the decline in suspended sediment concentration between 1955 and 1965 observed at the USGS stations on the modeled reach, 3) the prediction of the short and long term changes in channel bed elevation.

The comparison between pre- and post-dam flow duration curves showed that the closure of Garrison Dam and Gavins Point Dam significantly reduced high flow magnitude upstream of the Missouri River – Grand River confluence. Further, the controlled flow regime resulted in an increase in medium and low flows in the entire Lower Missouri River.

46

A ~60% decrease compared to pre-dam values in suspended sand load occurred upstream of the Missouri River – Platte River confluence. A decline in suspended sand load of about ~30% from pre-dam values occurred upstream of the Missouri River – Kansas River confluence. A ~20% decrease in suspended sand load from pre-dam values were observed at the USGS station downstream of the Missouri River – Kansas River confluence and virtually no change in suspended sand load was predicted and observed in the downstream of the Missouri River – Grand River confluence, i.e. Hermann, MO. It is important to mention here that, due to the low flow rates in the 1955-1974 period, the suspended sand loads were significantly lower than in the pre-dam and in the post-1974 periods.

The changes in channel bed elevation associated with flow regulation and channel narrowing resulted in widespread channel bed erosion. Larger erosion rates were observed and predicted in the upstream part of the domain, i.e. upstream of the Missouri River – Grand River confluence, where the most significant changes in sand load, high flow frequency and magnitude were recorded. Channel bed erosion on the order of ~1 m was measured and predicted downstream of the Missouri River – Grand River confluence and these changes were primarily associated with channel alignment and narrowing. Long term simulations (up to 3000 years in the future) revealed that, if the flow regime downstream of the Missouri River – Grand River confluence will not change, the reduction of mean annual sand load at Hermann, MO, will be at the most equal to ~10% of the pre-dam value

These results suggest that 1) the observed decline in suspended sediment concentration near the Mississippi River – Missouri River confluence has to be associated with a decline is wash load more than suspended bed material (sand) load, and 2) the long

47

term impact of the engineering works on the Missouri River will not be a major reduction in suspended sand load downstream of the Missouri River – Grand River confluence and thus the sand supply to the Mississippi River will likely remain close to historical values if major changes in the Missouri River flow regime and geometry will not occur.

Table 2.1: Major Lower Missouri River Tributaries.

Tributary name	Confluence location	Watershed area km^2	Confluence side
Big Sioux	RK 1187	21,818	left
Platte	RK 957	221,107	right
Nishnabotna	RK 870	7,268	left
Nodaway	RK 745	1,974	left
Kansas	RK 589	154,767	right
Grand	RK 402	17,819	left
Chariton	RK 385	4,843	left
Osage	RK 209	37,772	right
Gasconade	RK 170	7,356	right

Table 2.2: U.S Geological Survey (USGS) Gaging Stations in the Lower Missouri River considered in this study.

Station name	USGS ID	River KM	Period of record	Watershed area km^2
Yankton, SD	06467500	1287	1930-1995, 2017-2018	723,905
Sioux City, IA	06486000	1178	1928-2018	814,814
Omaha, NE	06610000	991	1928-2018	836,048
Nebraska City, NE	06807000	937	1929-2018	1,061,900
St. Joseph, MO	06818000	719	1928-2018	1,104,635
Kansas City, MO	06893000	589	1928-2018	1,253,819
Waverly, MO	06895500	467	1928-2018	1,258,481
Boonville, MO	06909000	313	1928-2018	1,296,813
Hermann, MO	06934500	157	1928-2018	1,353,275

49

Table 2.3: Pre- and Post-dam Mean Annual Suspended Sand Load in the Lower Missouri River. The asterisks identify measurements for which the volume fraction content of sand was not recorded.

U. S Geological Survey ID	Pre-dam load	Post-dam load	Period of available record	Number of measurements used in the analysis
USGS ID: 06467500 Missouri River at Yankton, South Dakota	8.80	0.49	2000-2008	57
USGS ID: 06610000 Missouri River at Omaha, Nebraska	12.89	5.48	1940-1954*; 1971-1986, 1996-2015	14*; 432
USGS ID: 06818000 Missouri River at St. Joseph, Missouri	17.28	12.2	1948-1976*; 1977-1993, 2002-2015	600*; 400
USGS ID: 06893000 Missouri River at Kansas City, Missouri	22.25	17.89	1948-1968*;1969-1991, 2009-2015	255*; 241
USGS ID: 06934500 Missouri River at Hermann, Missouri	25.9	23.8	1948-1971*; 1972-2015	5049*; 811

Table 2.4: Pre- and Post-dam Mean Annual Suspended Sand Load in the Lower Missouri River main Tributaries. The asterisks identify measurements for which the volume fraction content of sand was not recorded . Also, the number with asterisks means the number of measurements belongs to the period of record that has also asterisked. All number of measurements regardless with asterisks or not are used in the calculations of the mean annual suspended sand load.

U. S Geological Survey ID	Pre-dam load	Post-dam load	Period of available record	Number of measurements used in the analysis
USGS ID: 06485500 Big Sioux River at Akron, Iowa	-	0.29	1966-1976*; 1977-2002	57*; 90
USGS ID: 06805500 Platte River at Louisville, Nebraska	-	2.9	1965-1978*; 1979-1995	89*; 68
USGS ID: 06810000 Nishnabotna River at Hamburg, Iowa	-	0.74	1977-1993	62
USGS ID: 06817000 Nodaway River at Clarinda, Iowa	-	0.38	1976-1992	82
USGS ID: 06892350 Kansas River at DeSoto, Kansas	-	2.31	1979-2015	719
USGS ID: 06902000 Grand River at Sumner, Missouri	-	1.75	1974-1995	159
USGS ID: 06905500 Chariton River at Prairie Hill, Missouri	-	0.55	1978-1986	63
USGS ID: 6926510 Osage River at St. Thomas, Missouri	-	0.85	1974-1994	133
USGS ID: 06933500 Gasconade River at Jerome, Missouri	-	0.23	1979-1986	12

Table 2.5: Model input parameters for the zeroing runs.

Parameter	Value	Description
B_c	460	Channel width (m)
D	0.3	The geometric mean diameter of the Missouri River sediment (mm)
D_{90}	0.5	Diameter such that 90% of the bed material is finer (mm)
S	0.0001	Initial channel bed slope (m/m)
dt	1/100	Computational time step (yr)
dx	4000	The distance between two computational nodes (m)
L	1300	The total length of modeled reach (km)
Nr	7	Number of subreaches in modeled reach
η_i	109.4	Channel bed elevation above NAVDD88 datum at the downstream end of the modeled reach (St. Louis KM 0) in 1954 (Jordan, 1965).
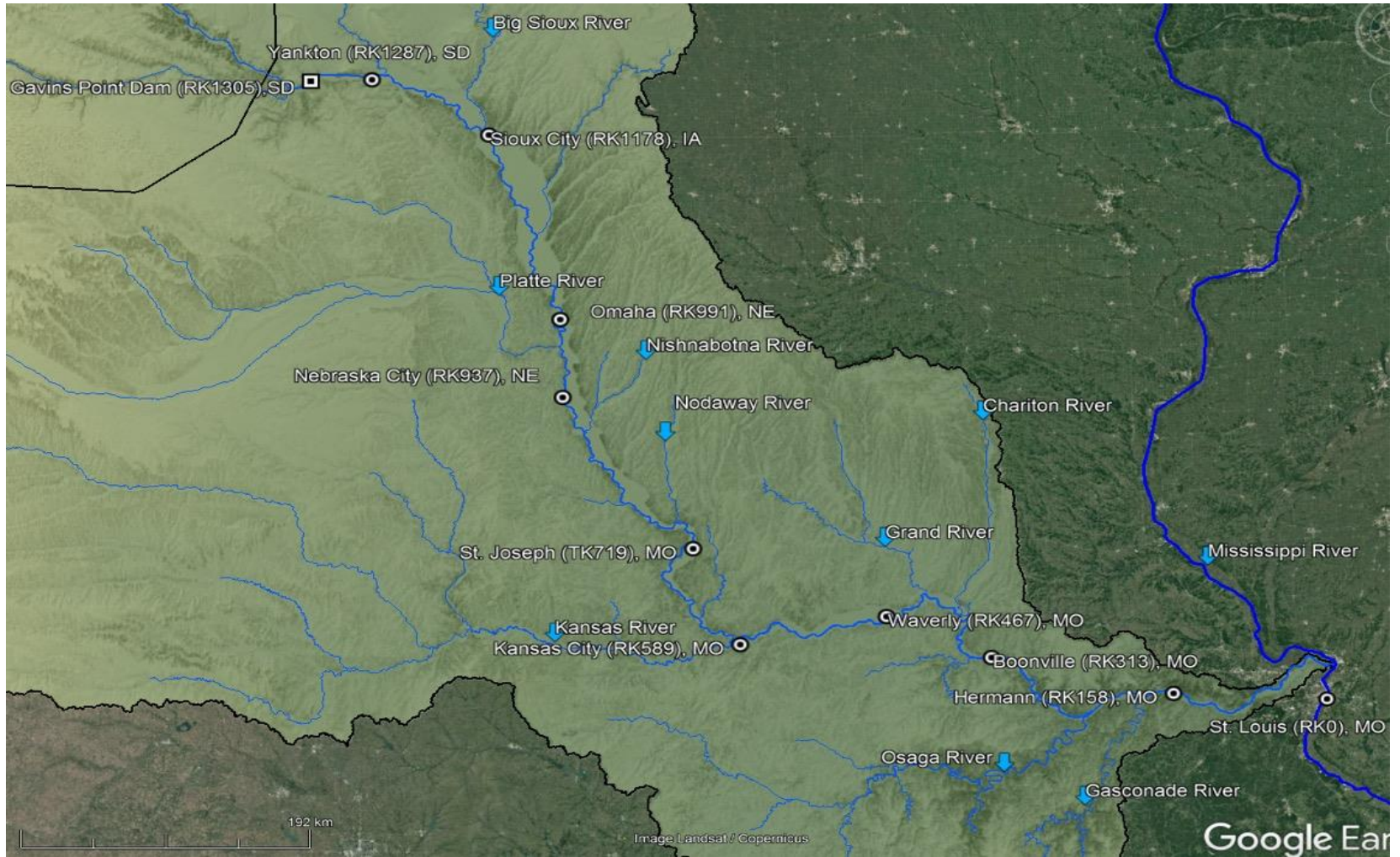
Figure 2.1: The Lower Missouri River, its main tributaries (blue arrows) and the USGS gaging stations used in this study (dots) (from USGS, google earth and GIS)

a: Yankton (RK 1287), SD
b: Sioux City (RK 1178), IA
c: Omaha (RK 991), NE
d: Nebraska City (RK 937), NE
e: St.Joseph (RK 719), MO
f: Kansas City (RK589), MO
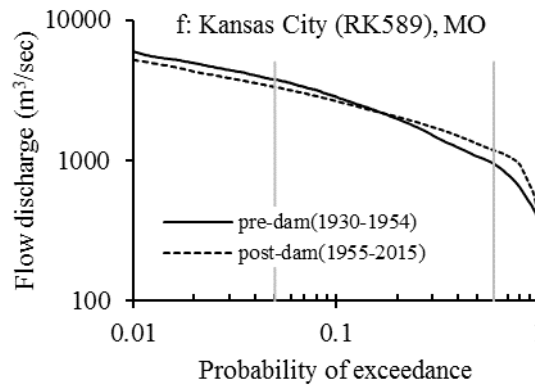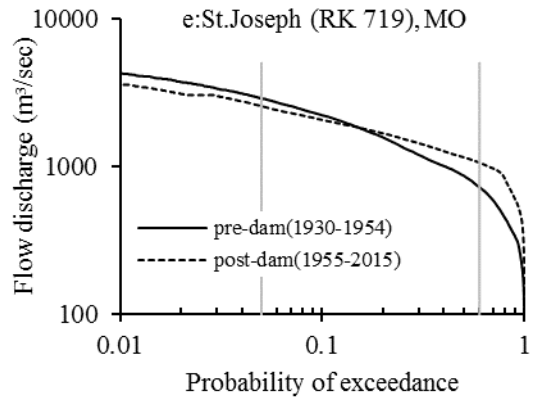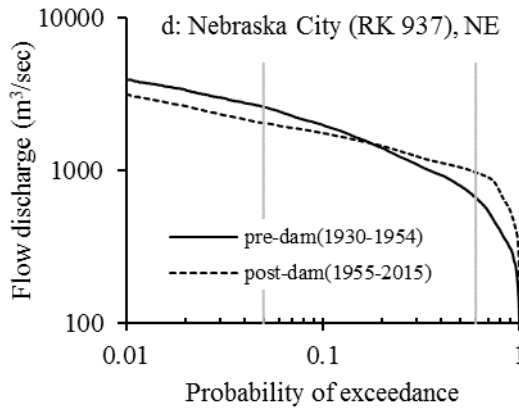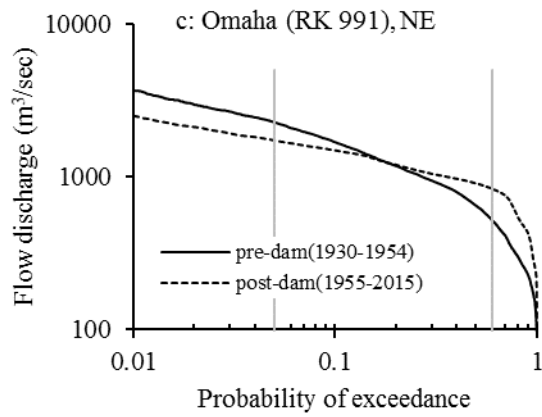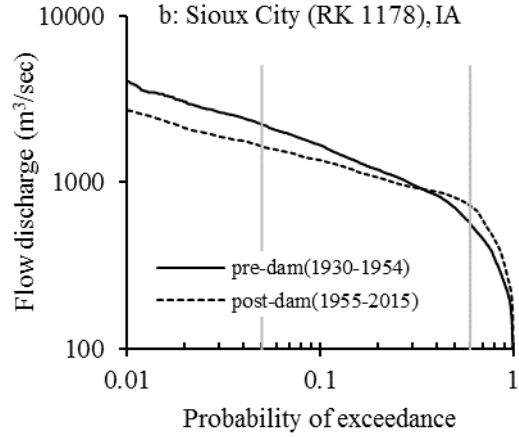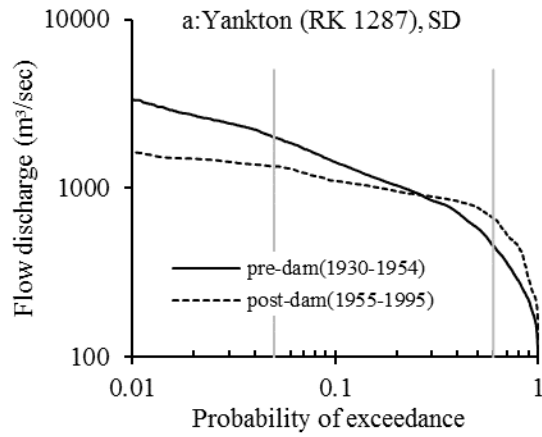
Continoue…………
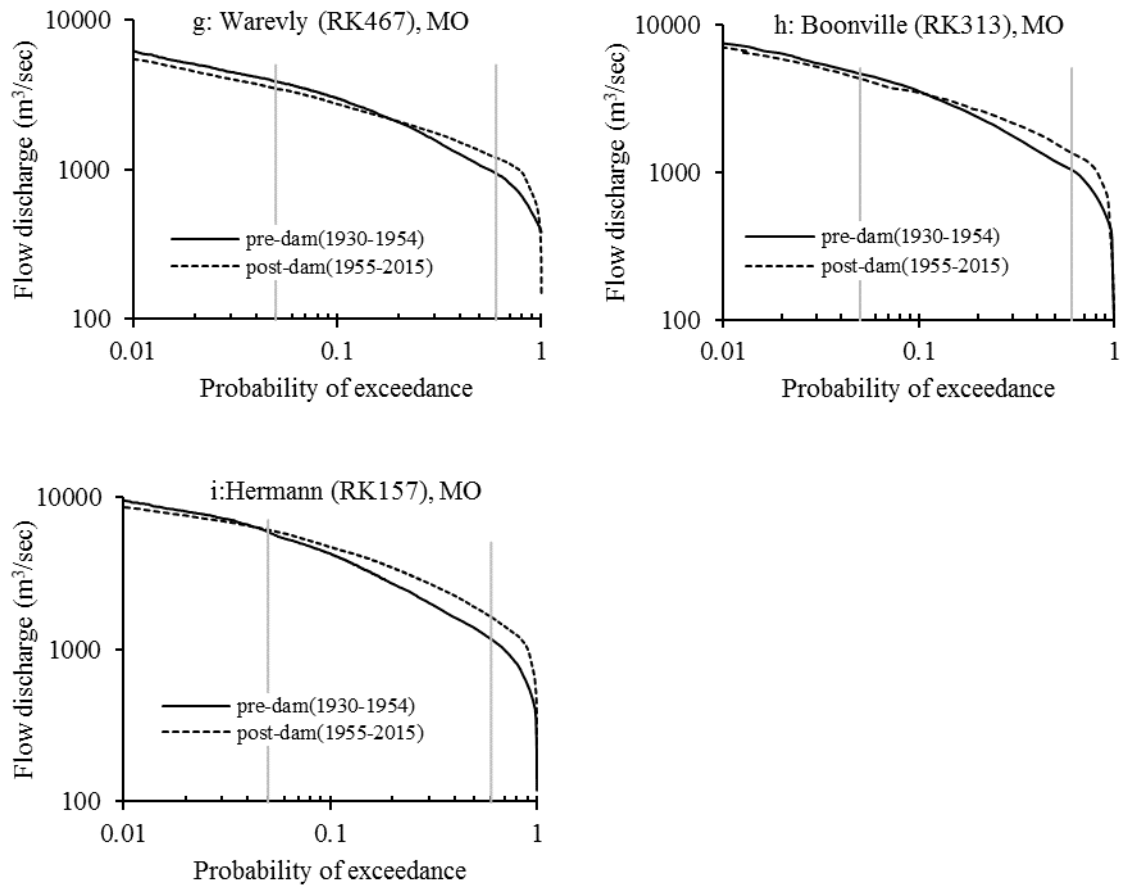
Figure 2.2: pre-dam and post-dam flow duration curves for selected USGS gage stations at Lower Missouri mainstem. Continuous horizontal gray lines represent probabilities of exceedance are equal to 0.05 and 0.6.

a:Yankton (RK 1287), SD

b: Sioux City (RK 1178), IA

c: Omaha (RK 991), NE

d: Nebraska City (RK 937), NE

e:St.Joseph (RK 719), MO

f: Kansas City (RK589), MO

Continue…………

www.manaraa.com
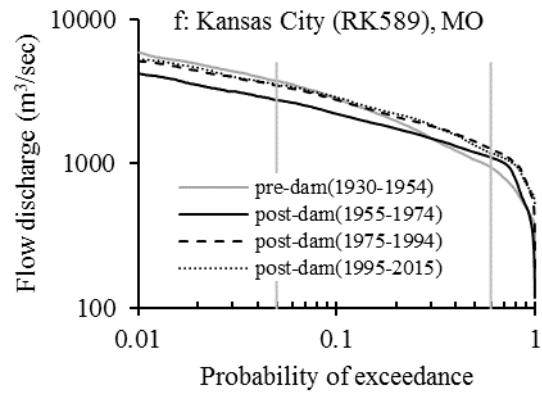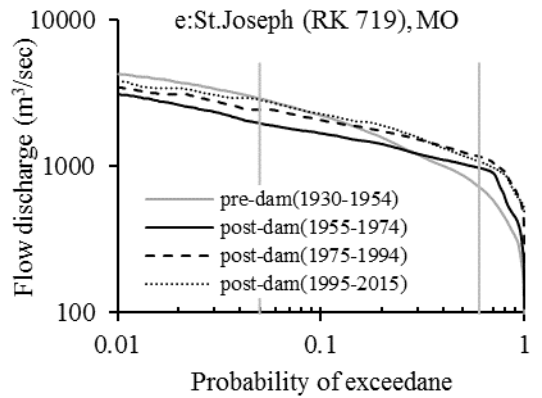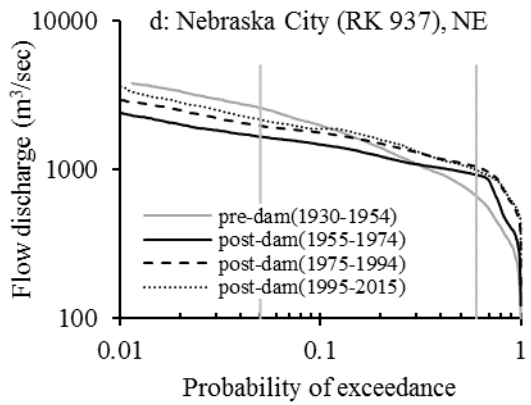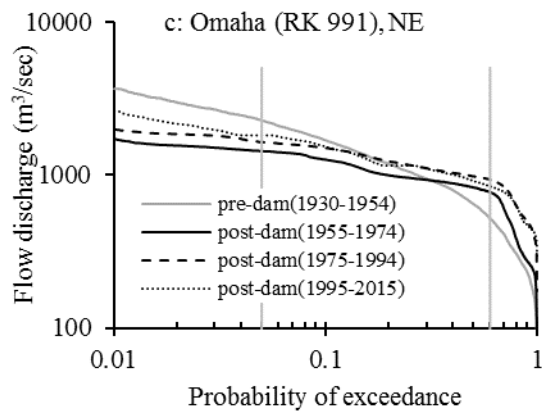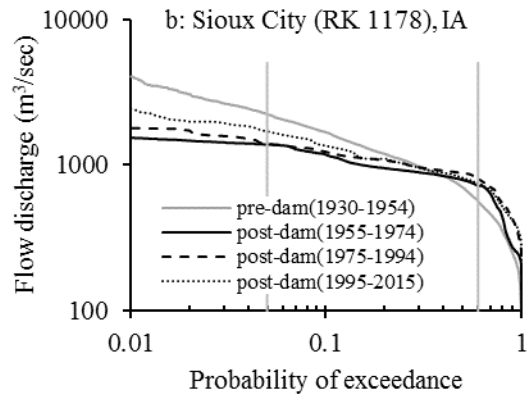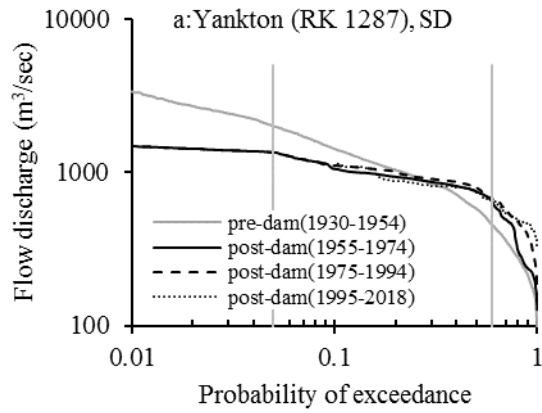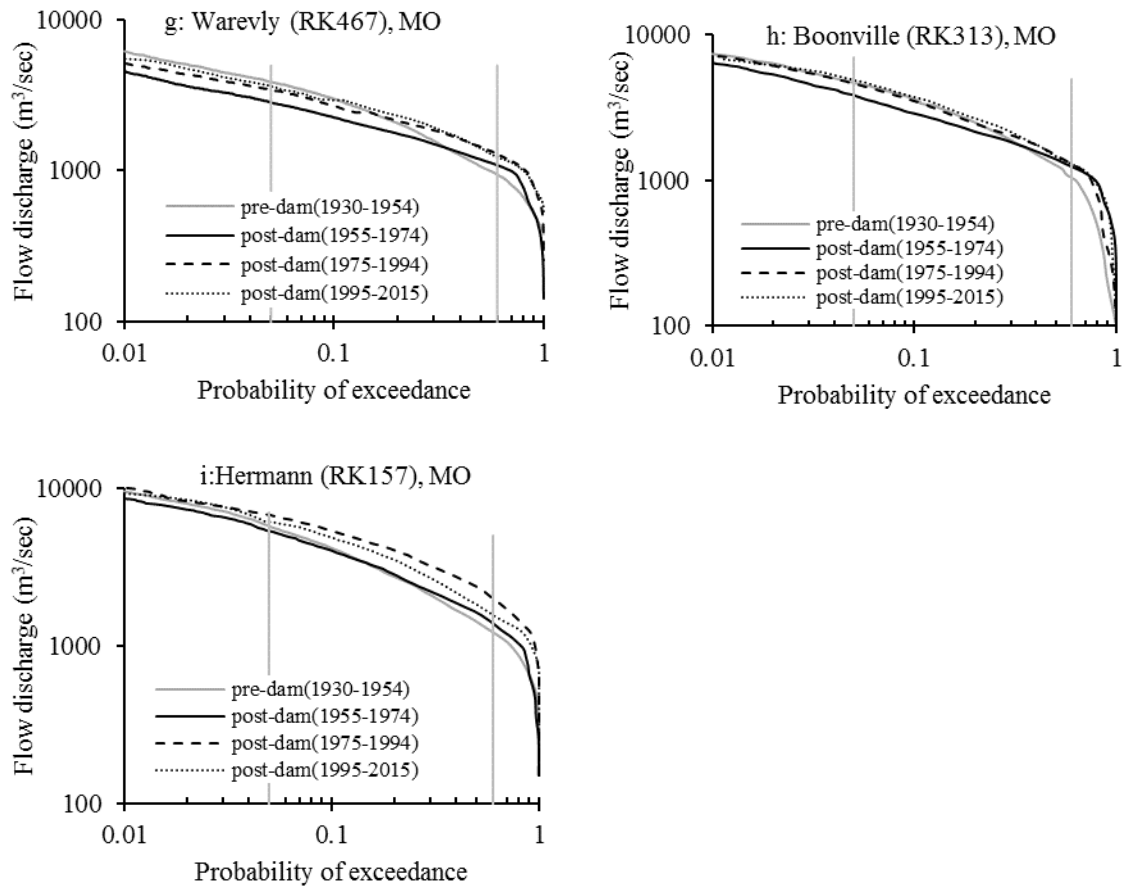
Figure 2.3: pre-dam (1930-1954) and 20 year-long period post-dam flow duration curves for Lower Missouri River at the USGS gage stations of Table 2.2. the continuous gray and black lines represent the pre-dam 1995-974 periods respectively. The continuous dashed and dotted black lines represent the post-dam periods between 1975 and 1994 and between 1995 and 2015 respectively. Continuous horizontal gray lines represent probabilities of exceedance are equal to 0.05 and 0.6. In

subfigure a, there is a gap in data from 1996 to 2016, therefore, data of 1995, 2017, and 2018 are used as a post-dam (1995-2015).
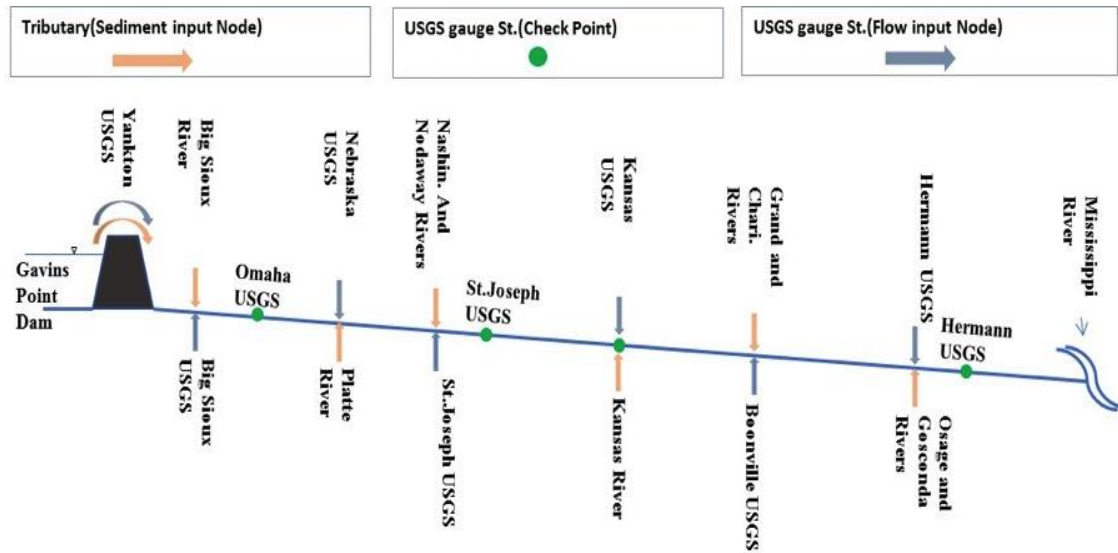
Figure 2.4: Schematic representation of the study reach. Gray and orange arrows represent the flow and sediment load inputs at computational nodes respectively, and green dots represent the U. S Geological Survey gage stations that used to validate the model sand load predictions.
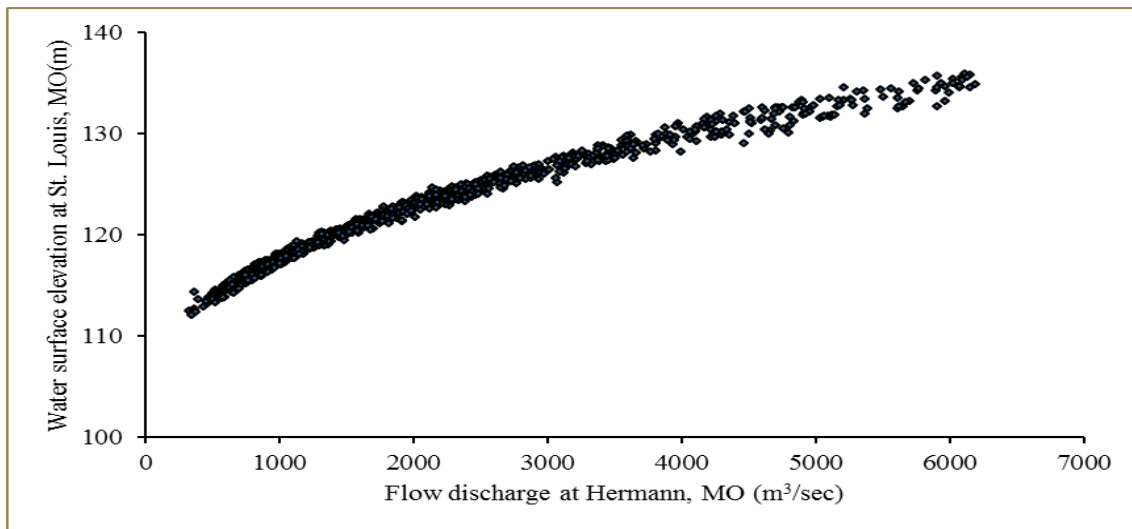
Figure 2.5: Relationship between water surface elevation above NAVDD88 at St. Louis, MO and flow discharge at Hermann, MO at the confluence of Missouri-Mississippi River system.

58
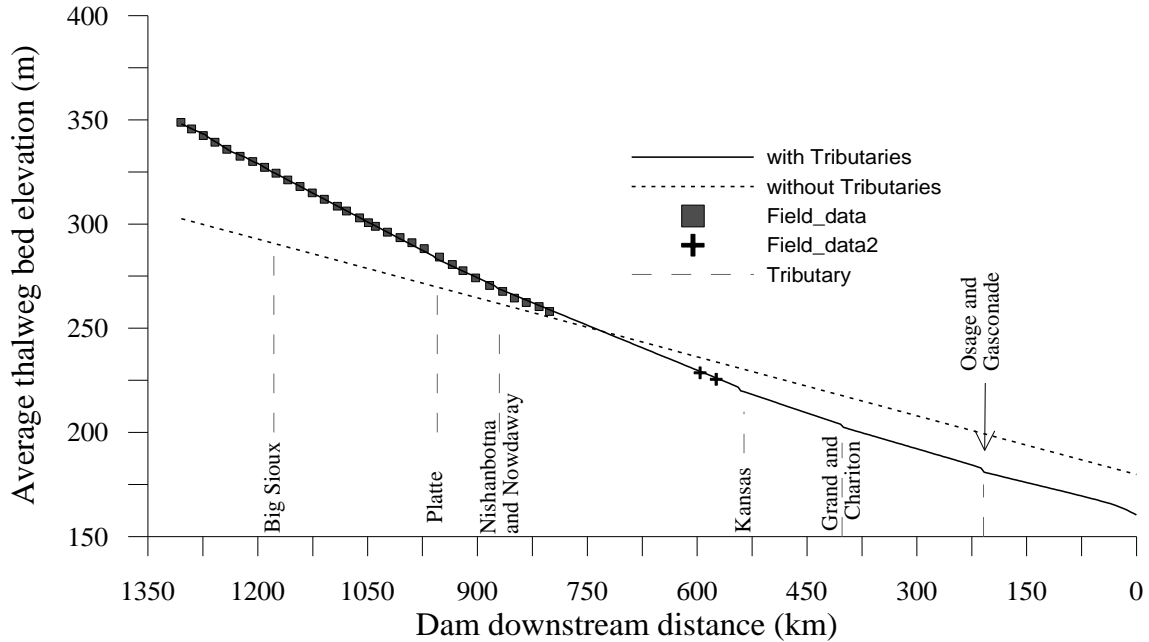
Figure 2.6: Comparison between numerical and measured (black square and cross dots) average channel bed elevation above NAVDD88 at mobile bed equilibrium. The numerical channel bed elevation with present of tributaries is represented by a continuous black line and dashed black line for numerical bed elevation with no including tributaries. A gray dash line represents the locations of tributaries. The black square dots are measurements of thalweg elevation in 1954 reported by the USACE (U.S Army Corps of Engineers: Omaha District, 1993) and the black cross dots are thalweg elevation measurements in 1952 reported by the USACE (U.S Army Corps of Engineers, 2012).

a) Omaha (RK 991), NE

b) St.Joseph (RK 719), MO
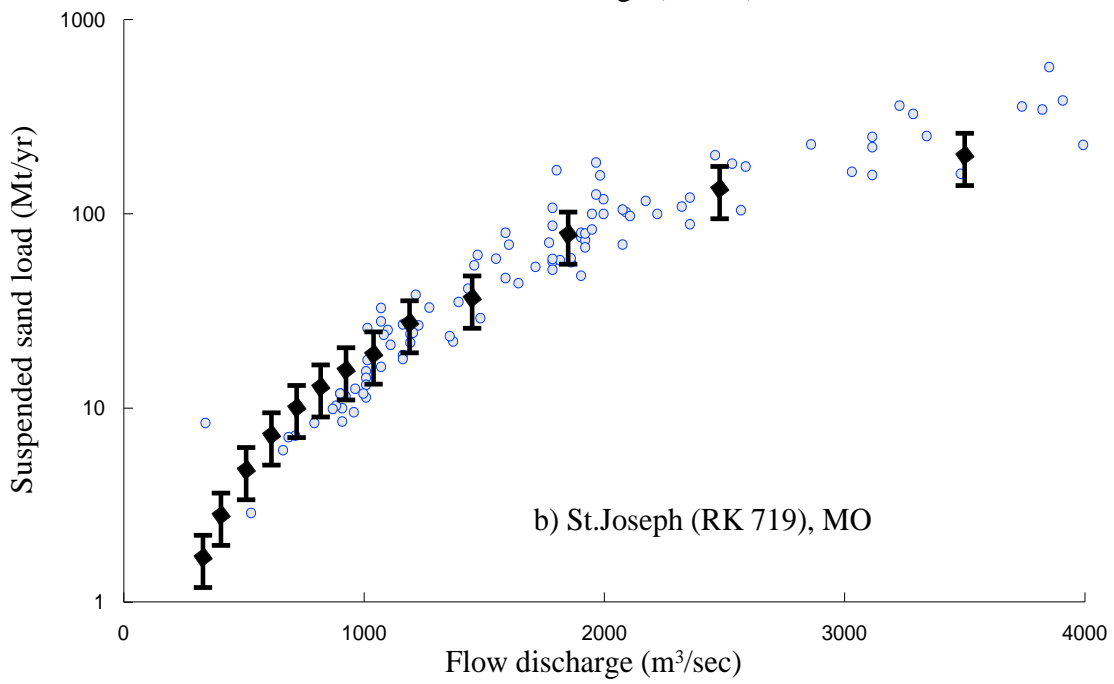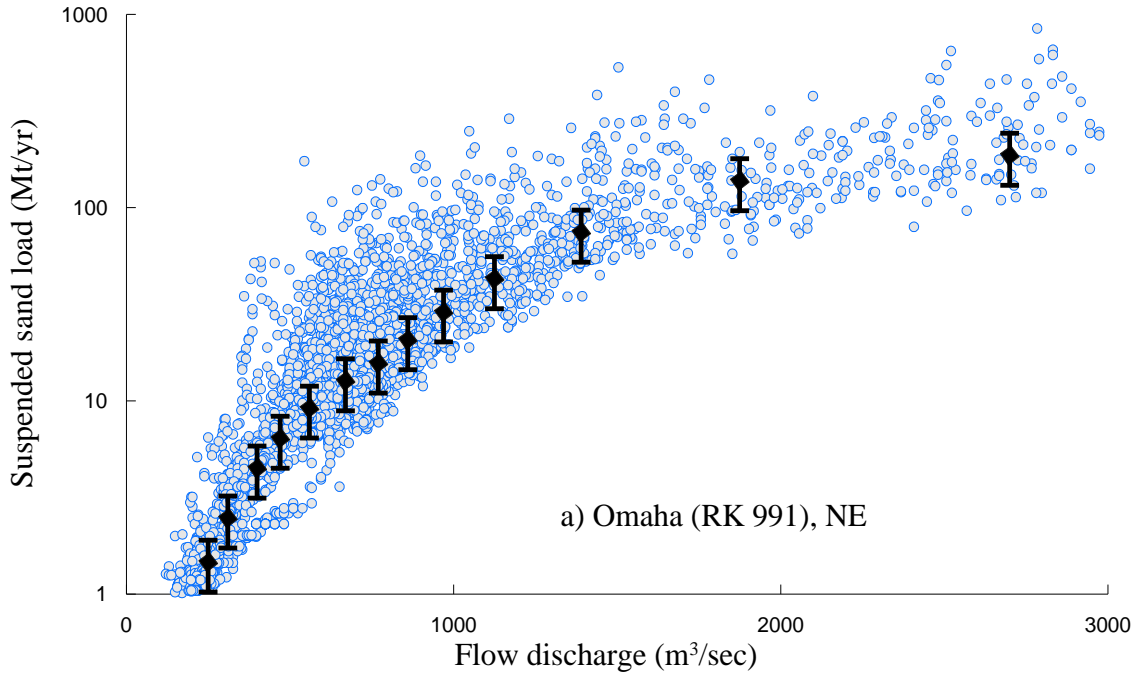
Continue………
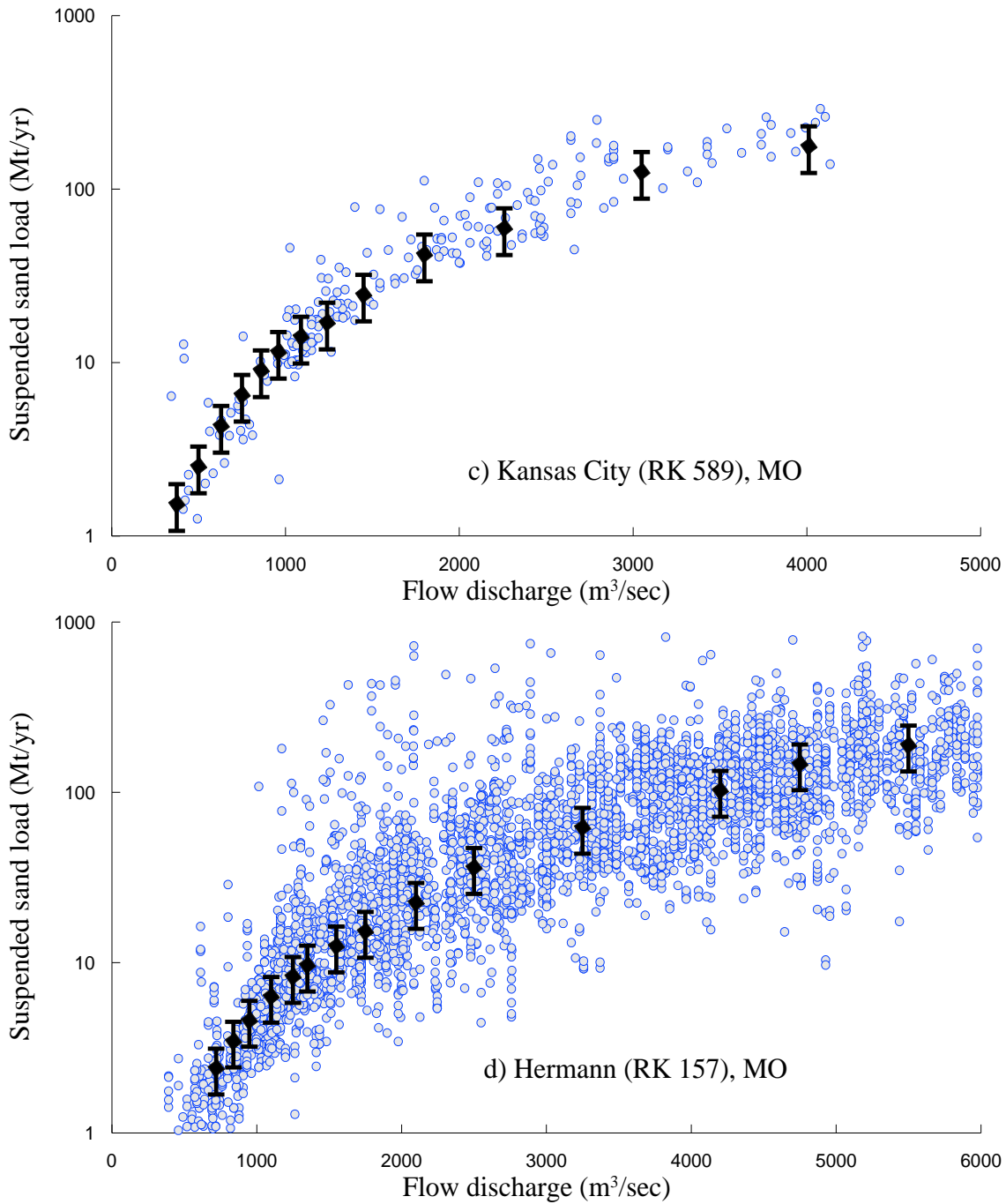
Figure 2.7: Comparison between numerical (black square dots) and measured (blue square dots) pre-dam suspended sand load. Numerical results pertain to equilibrium conditions. The vertical bars on the numerical results indicate error of ±15%.

a) no spatial changes in the flow duration curve and the suspended sand load

b) with spatial changes in the flow duration curve and the suspended sand load
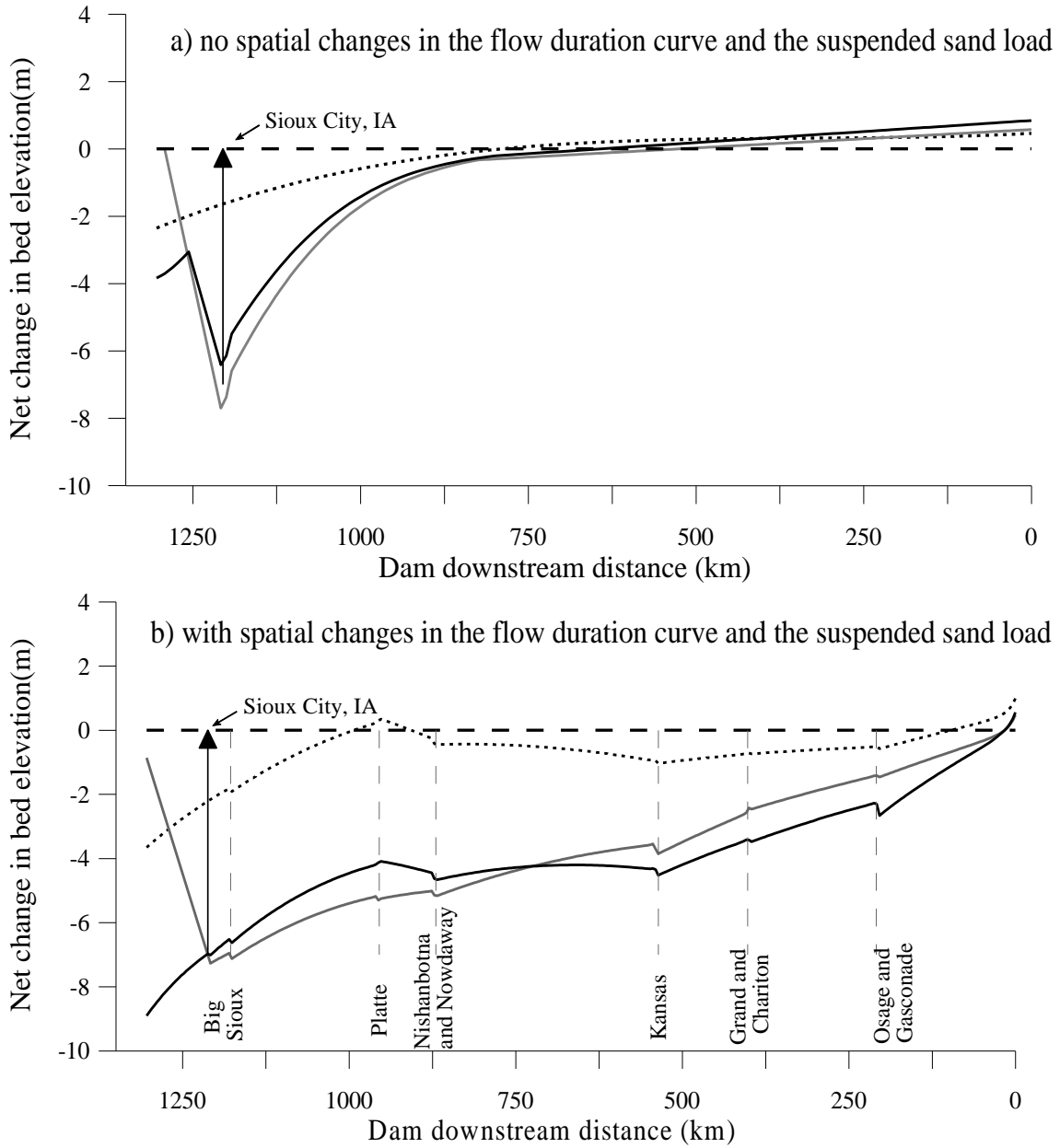
Figure 2.8: Long term changes in channel bed elevation associated with the closure of Gavins Point Dam (dash line), channel narrowing (grey line), and dam closure associated with channel narrowing (continuous black line). The vertical gray line represents the location of the main tributaries and horizontal continues dashed line represents the condition of no net change in channel bed elevation. The vertical arrow refers to the most upstream of the channelized portion of the Lower Missouri River at Sioux City, IA. The results in panel (a) pertain to simulations in which the flow duration curve and the sand load were specified at the upstream end of the

modeled reach. The results of the panel (b) accounted for changes in flow duration curve and sand load downstream of the confluences with major tributaries.
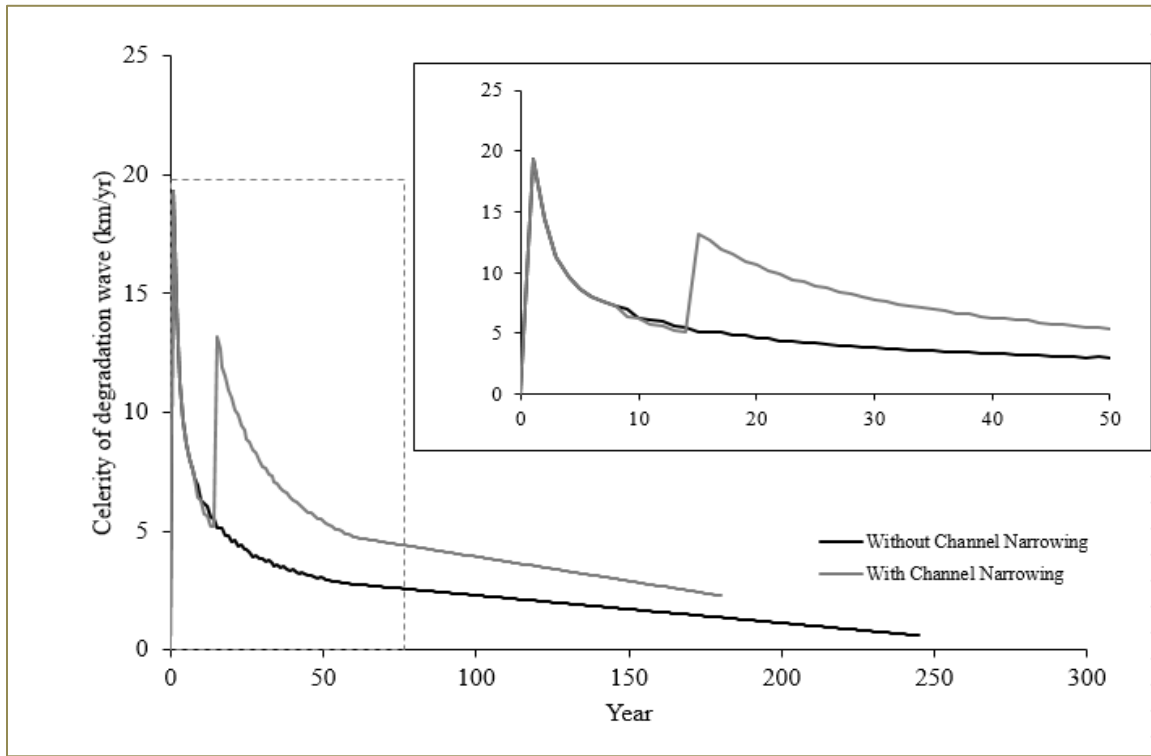
Figure 2.9: Celerity of the wave of degradation in the case of dam closure (black line) and dam closure associated with channel narrowing (grey line).

a) Yankton (RK 1287), SD (Qw=850m³/sec)

b) Sioux City (RK 1178), IA (Qw=850m³/sec)

c) Omaha (RK 991), NE (Qw=850m³/sec)

d) St.Joseph (RK 719), MO (Qw=1100 m³/sec)

e) Kansas City (RK 589), MO (Qw=1100 m³/sec)

f) Waverly (RK 467), MO (Qw=1300 m³/sec)
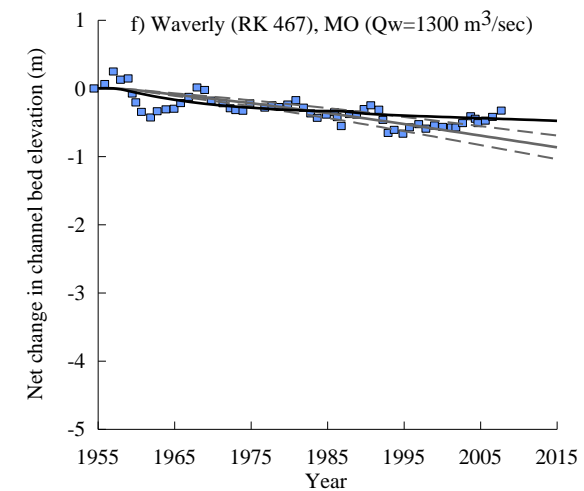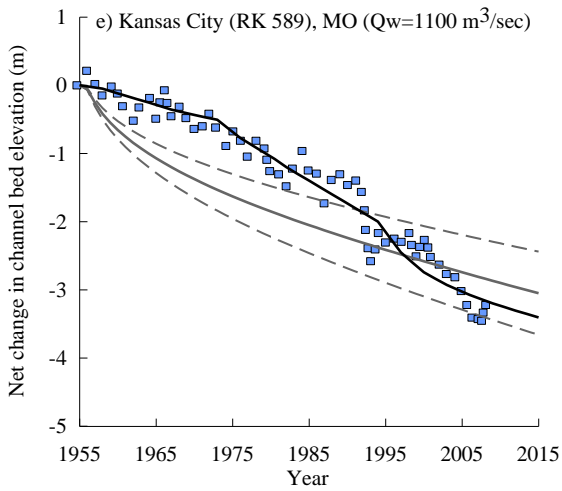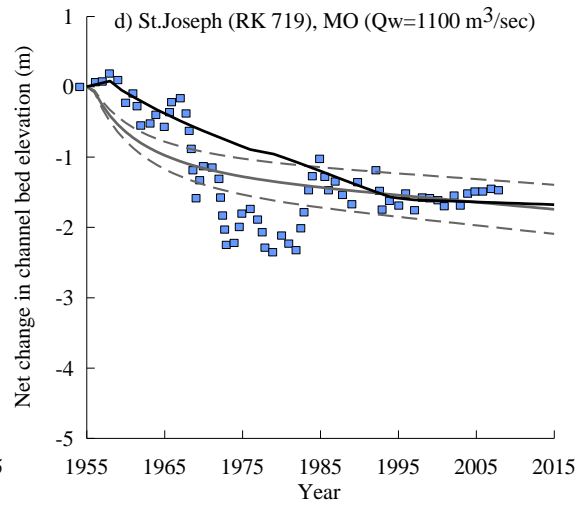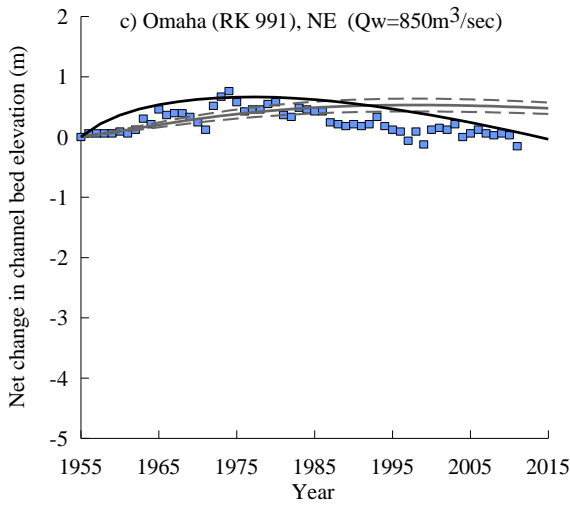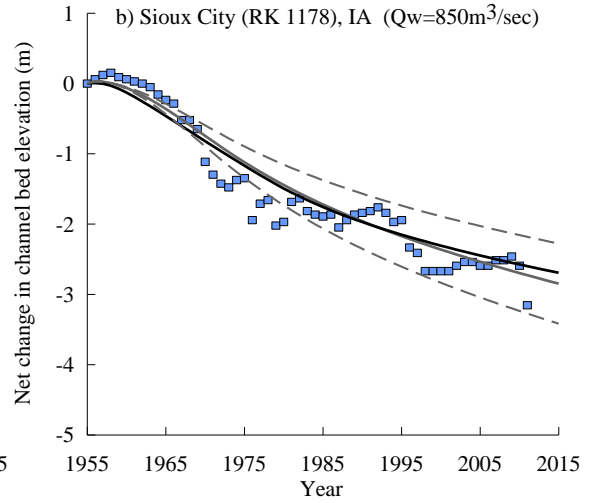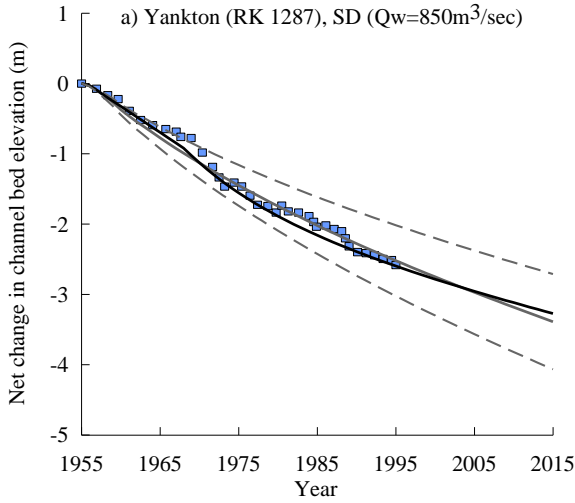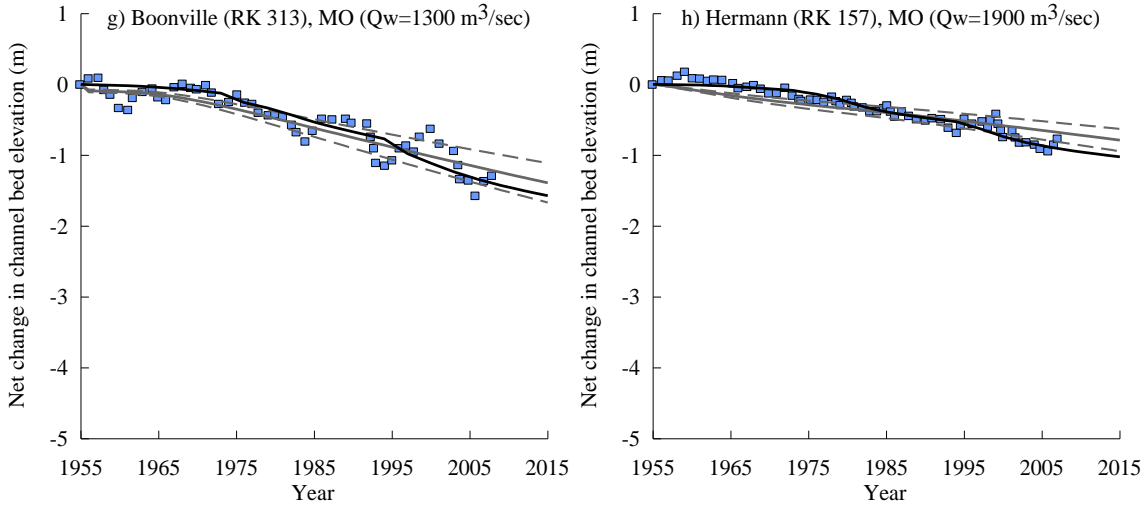
Continue……..

Figure 2.10: Comparison between numerical (lines) and measured (blue square) for net change in channel bed elevation along the modeled reach. The continuous gray and black lines respectively represent the model results obtained with a single post-dam flow duration curve, and three flow duration curves are describing 20 year-long post-dam time intervals. The continues dashed gray lines indicate the ±20% of the value predicted with a single post-dam flow duration curve (continuous grey line).

Continue……..

a2) Omaha (RK 991), NE

Field(1995-2015)

Model(1995-2015)

b1) St.Joseph (RK 719), MO

Field (1975-1994)

Model(1975-1994)

Continoue……….

b2) St.Joseph (RK 719), MO

c1) Kansas City (RK 589), MO

Continoue………

c2) Kansas City (RK 589), MO

d1) Hermann (RK 157), MO
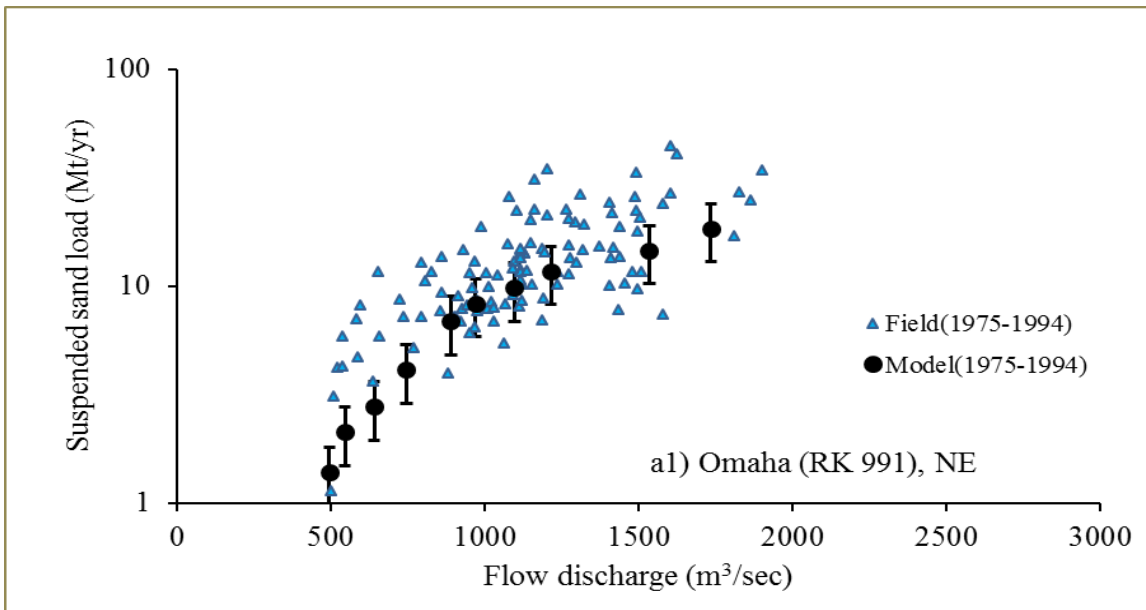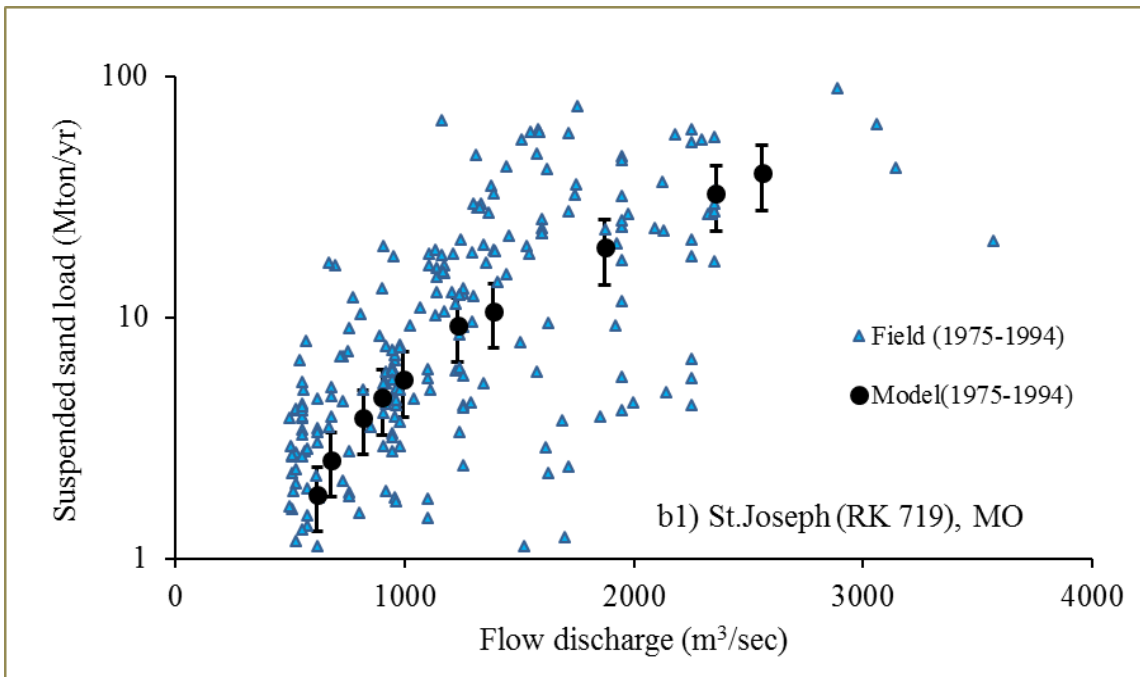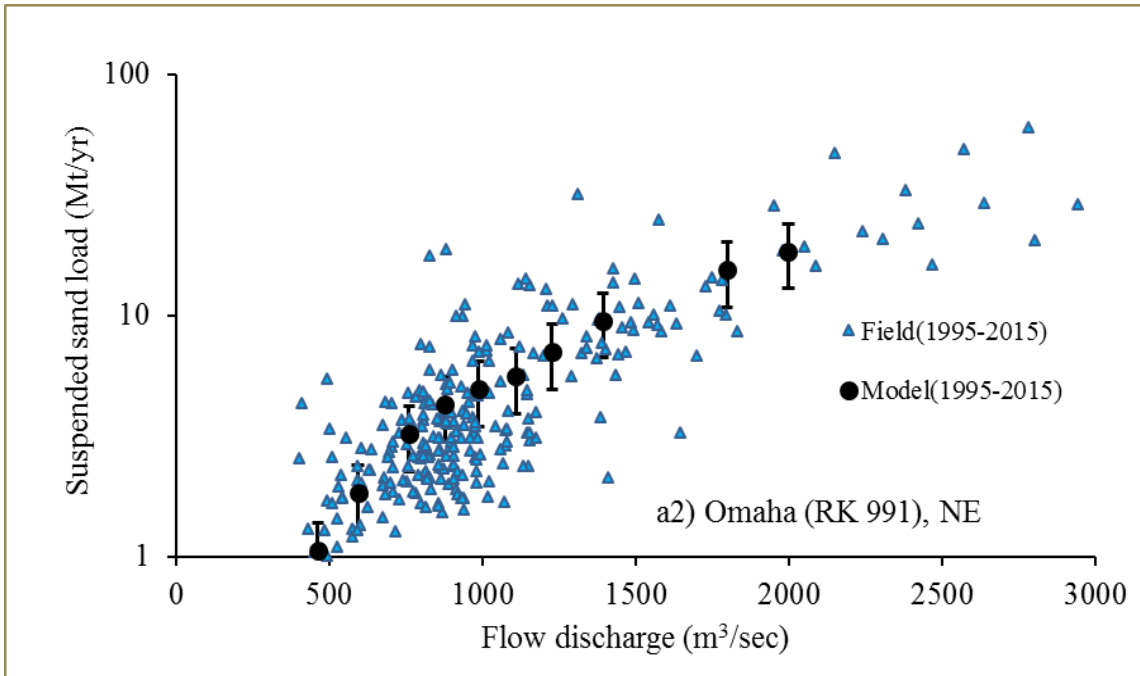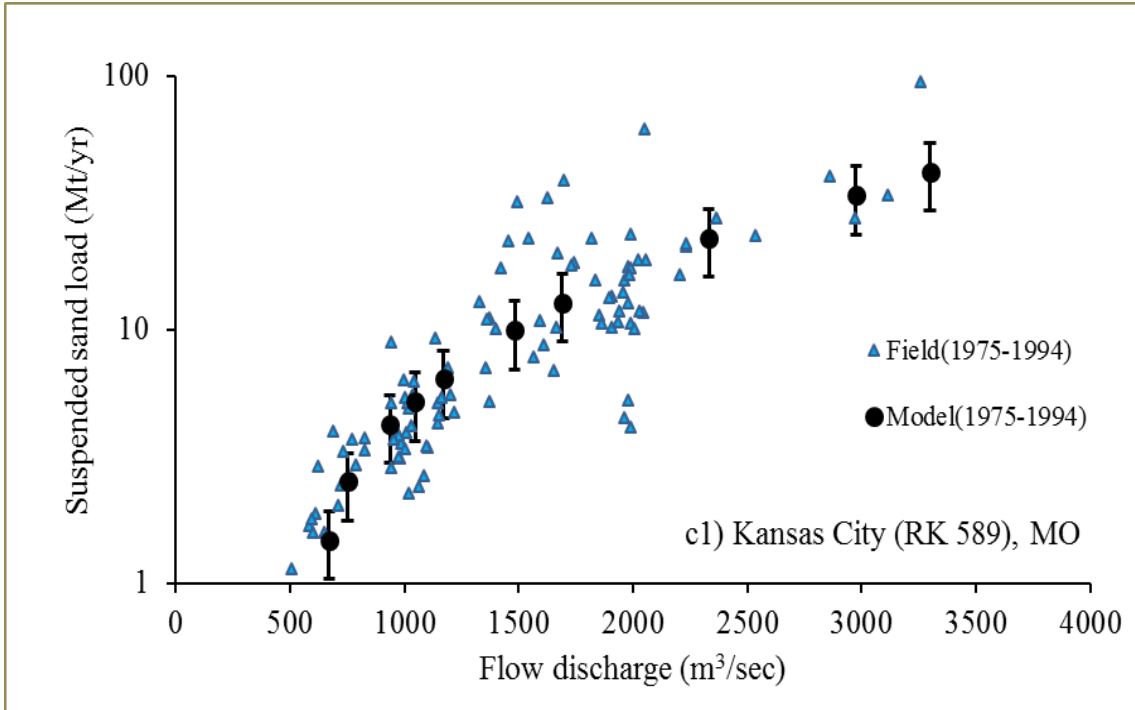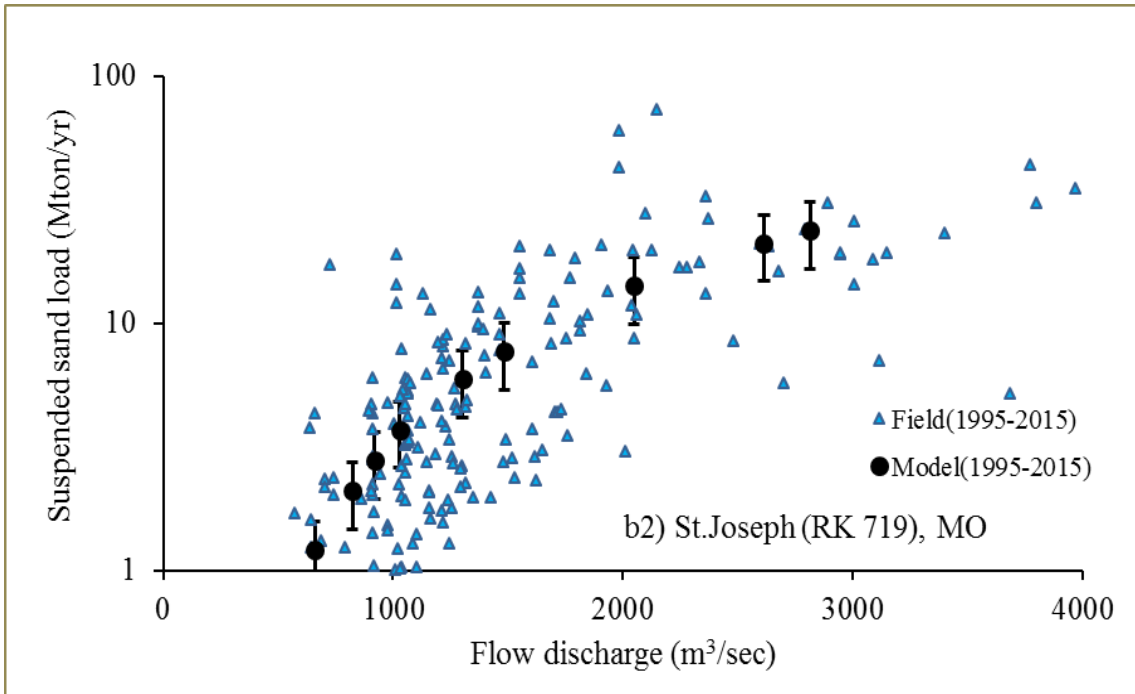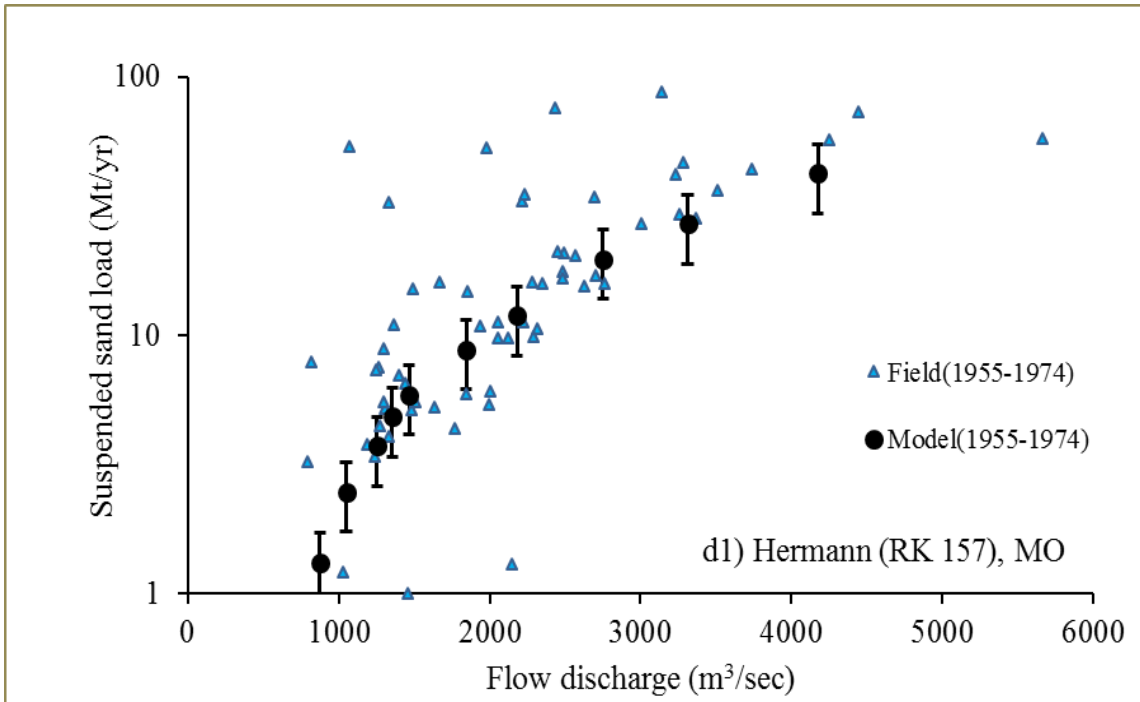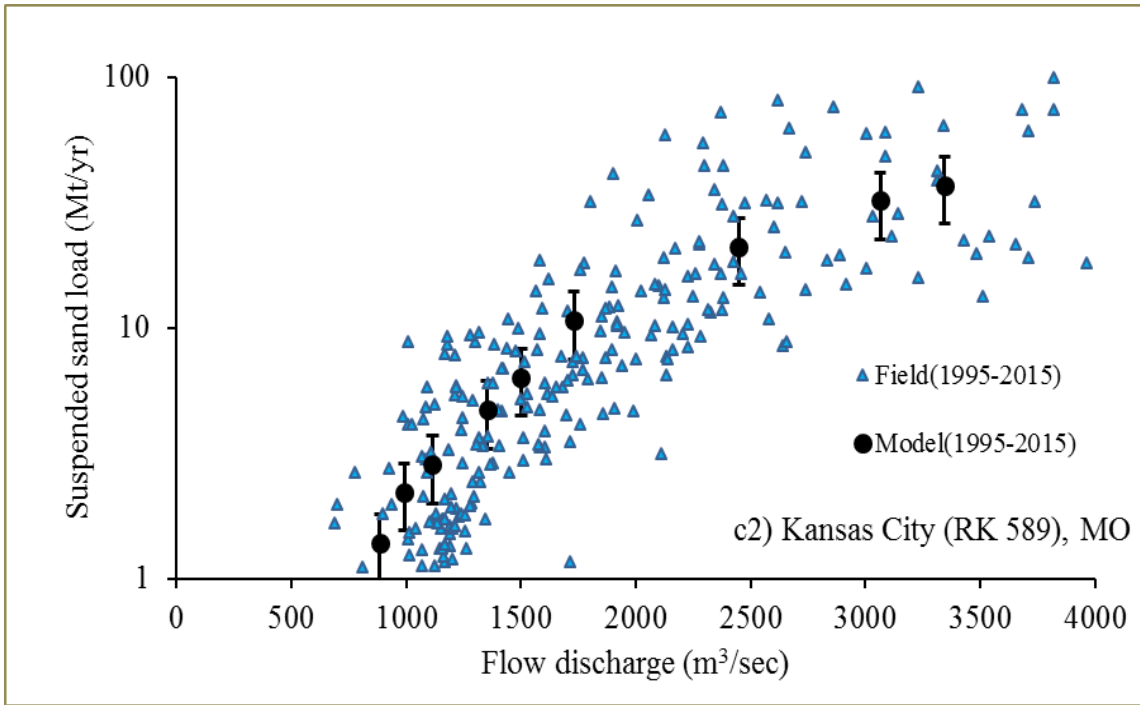
Continue……….
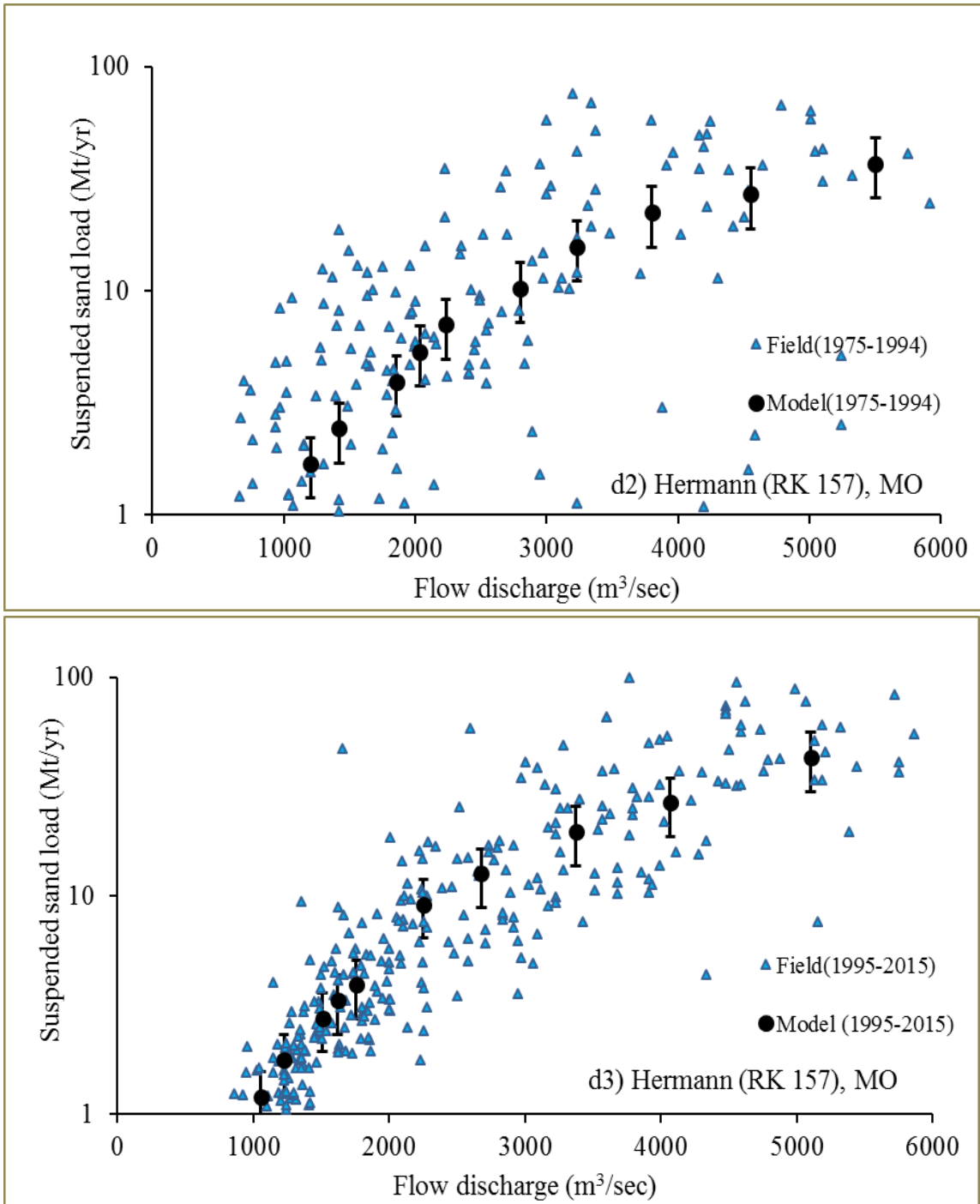
Figure 2.11: measured (blue triangles) and predicted (black dots) suspended sand loads. The error bars represent a ±15% difference from the numerical value.
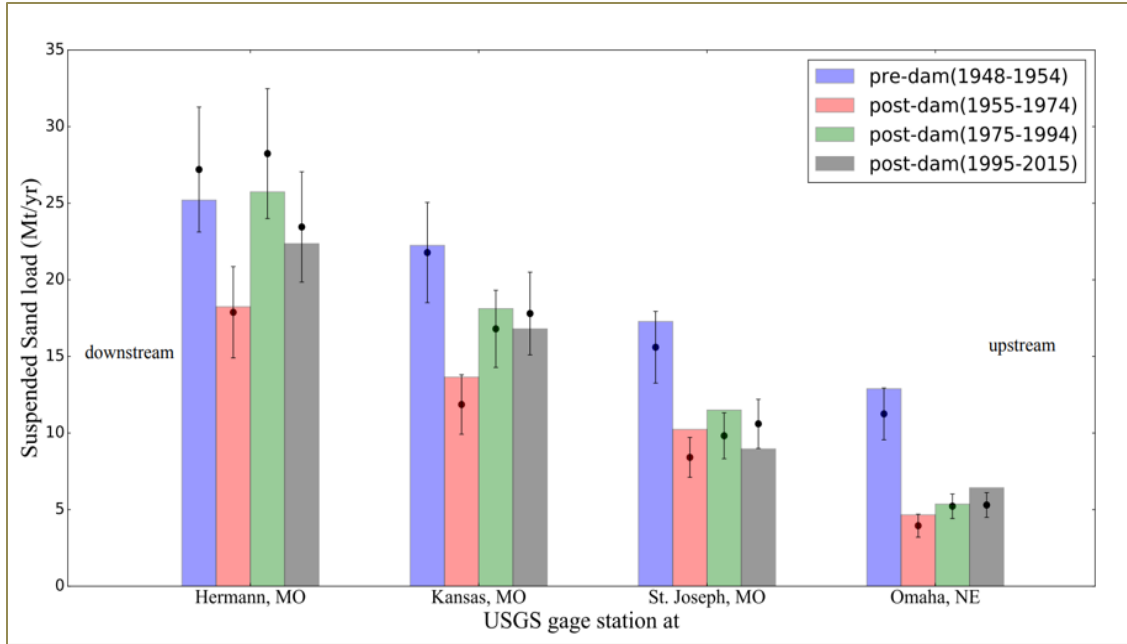
Figure 2.12: Pre- and post-dam mean annual sand load. Field estimates and model results are respectively represented with colored bar and black dots. The error bars indicate ±15% of the numerical value.
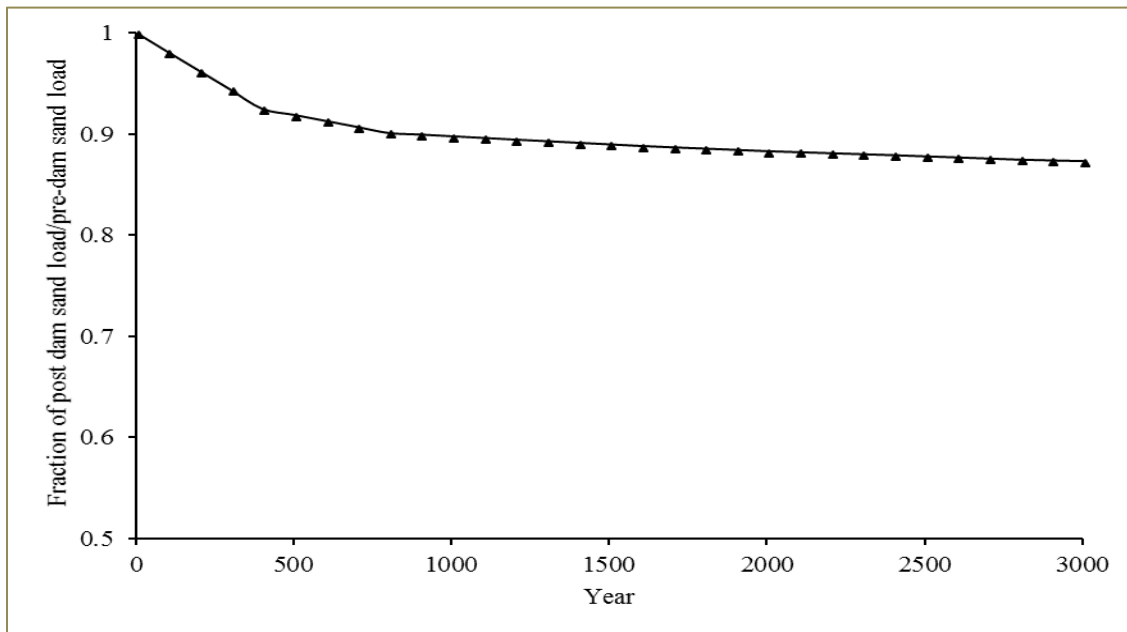
Figure 2.13: Long term prediction of the ratio between the post-dam and the pre-dam suspended sand load at Hermann, MO.

70

CHAPTER 3

THE FLUVIAL-TIDAL TRANSITION ZONE OF A COASTAL PLAIN RIVER

3.1 INTRODUCTION

Coastal plains are low elevation and low gradient landscapes that occur along many continental margins and they extend up to hundreds of kilometers inland, occupying $5.7x10^6$ km^2 worldwide (Colquhoun, 1968). They result from depositional processes associated with recurring sea transgressions and regressions (Colquhoun, 1969). In North America a large coastal plain extends from Long Island in the northeastern USA to the Yucatan Peninsula, southern Mexico, and up to 600 km inland. Rivers that traverse coastal plains facilitate floodplain development and their forested ecosystems have high productivity and a range of habitats that account for many of the floodplains intrinsic values (Sharitz and Mitch, 1993; Barko et al., 2006; Osterkamp and Hupp, 2010). In the lower coastal plain the distinction between the terrestrial river system and the tide-influenced estuary has been an active area of research (sensu Savenije, 2015).

Coastal rivers may be affected by tidal oscillations in stage and the system response has been presented in a conceptual model of along channel sediment-transport, particle size distribution, and the relative energy level (Dalrymple and Choi, 2007, Lawrence et al., 2015). In addition to these effects, fluvial-tidal interactions give rise to a transitional channel reach that links terrestrial and marine dominant components of the river system (Dalrymple and Choi, 2007), typically referred to as the fluvial-tidal transition zone

71

(FTTZ) (Dalrymple et al., 2012; Freitas et al., 2012). Researchers have identified the FTTZ as a zone of sediment storage (Dalrymple and Choi, 2007; Ensign et al.,2015; Ensign et al.,2017) of finer bed material (Dalrymple and Choi, 2007; Wang et al., 2009; Kastner et al., 2017; Gugliotta et al., 2017), with a reduced sediment transport capacity (Dalrymple and Choi, 2007; Nittrouer et al., 2011; Lamb et al., 2012) and high sediment accumulation rate (Dalrymple and Choi, 2007; Ensign et al.,2014; Lawrence et al., 2015). Others have shown how these effects translate to FTTZ channel morphology (Gurnell, 1997; Ensign et al., 2013; Kastner et al., 2017) and Torres (2017) referred to the transitional effects as a "fluvial-tidal discontinuity". However, a clear mechanistic understanding of FTTZ processes that can be used to explain these changes has not been well-developed.

In unsteady or tide-influenced river reaches the momentum equation can be used to determine the energy gradient in order to help shed light on FTTZ dynamics. With tidal freshwater rivers the energy gradient is mainly controlled by water surface slope (Knight, 1981), and therefore tidal effects can lead to disturbances in the energy gradient (Martinius and Gowland, 2011; Yankovsky et al., 2012). Moreover, energy perturbations can be expected to influence channel morphology and sedimentary processes. For example, Wright et al. (1973) have shown that the lateral and vertical convergence in channel morphology ceases at the upstream limit of tidal influence due to an inland declining tidal prism. Also, Yankovsky et al. (2012) observed that a transition from fluvial to tidal dominance can be distinguished by abrupt increase in energy dissipation and a distinct channel geometry, and a downstream decline in particle size has been shown to occur at the head of the tide (Chen et al., 2005; Dashtgard et al., 2012; Ensign et al., 2015; ; Gugliotta et al., 2017).

In this study we propose to provide greater insight on the development of channel morphology and bed material size distributions between fluvial and tidal dominant reaches. The spatial gradient in energy dissipation and sediment transport capacity are used to highlight the morphodynamic interaction between the channel morphology and tidal river hydrology. Hence, this study is guided by the hypothesis: Fluvial and tidal interactions cause discontinuities in the energy gradient and corresponding channel metrics. Here a "discontinuity" is taken as an abrupt or large change in along channel hydraulic or geometric properties that occur over approximately kilometer scale distances.

3.2 STUDY SITE

The Altamaha River is a tide-affected river in Georgia, USA and it runs for ~200 km from the confluence of the Ocmulgee and Oconee rivers to the Atlantic Ocean. The watershed area is ~36,200 km^2 and the vast majority of the system is within the US southeastern coastal plain (Di Iorio and Kang, 2003; Gotvald et al., 2004). The tidal range at the mouth is 1.5-3.0 m and the lower reach experiences bidirectional flows (Kang and Di Iorio, 2006). The zero salinity isoline is typically within 20 km of the ocean (Sheldon and Alber, 2002) making most of the lower reach a tide-influenced, freshwater system. These attributes and the absence of large dams were the main factors in site selection and thus one can infer that much of the Altamaha can be considered as a reference coastal plain, fresh water, tide-influenced river system. The study reach is a ~47 km long section between 29-76 km (0 km at the mouth, Figure 3.1). From 0-29 km there are several distributary channels, hence, the work presented here is designed to preclude the effect of distributary channel and therefore is focused on the single-threaded part of a meandering-straight, freshwater, tidal

73

river section. Six tributaries are located along the study reach and all have nominal watershed area limited to the local floodplain (Figure 3.1). Hereafter, we report along channel distance from the mouth with a "km" prefix followed by the distance, e.g., km41 means 41 kilometers from the estuary mouth.

From 2008-2017 the mean water surface elevation at the mouth is 1.1 m (all elevations reported here are referenced to NAVD88) based on a US Geological Survey (USGS) gaging station on the Brunswick River, 11km south (USGS 02226180; 31°08'00"N, 81°23'48"W). Data from a real time USGS gaging station (#02226160) at km41 (31°25'37″ N, 81°36'20″W) shows that the Altamaha flow regime exhibits strong seasonality but with large fluctuations within the seasonal highs and lows, and with a maximum tidal range of 1.2 m. The mean daily discharge ranged from -173 m^3/sec to 3,255 m^3/sec, with an average of 347 m^3/sec, and a median of 200 m^3/sec. All discharge values reported here are taken from this station. The corresponding relationship between magnitude and frequency, P_i, (P_i is percent exceedance) of daily discharge is concave up and resembles $y=a+x^{-1}$ where y = discharge, and x = fraction of exceedance (Figure 3.2). Thus, the magnitude of discharges with P_i lower than 0.1 are highly variable and generally represent large flood events. Further, the steep decline of the curve indicates the low frequency of flood events. From $P_{0.15}$ to $P_{0.5}$ the discharge gradually decreases from 480 m^3/sec to 200 m^3/sec, while from $P_{0.5}$ to $P_{0.75}$, the discharge magnitude decreases by only 100 m^3/sec. Also, 10% of time ($P_i \leq P_{0.9}$) discharge at this location experiences bidirectional flows with discharge values below zero. The minimum discharge and stage height that seems to damp the tidal oscillations are 495 m^3/sec and 3.05 m, respectively. Overall, 34%

74

of the daily discharge values exceed the mean daily flow for the lower four stations tidal signals can be observed during the median discharge (Figure 3.2).

3.3 DATA AND METHODS

The field surveys and instrument deployments were conducted in 2014 and 2016, the tasks and field conditions are shown in Table 3.1. River cross-section and longitudinal profile soundings relied on a Seafloor Sonar Mite (Hydrolite_TM) echo sounder connected to a Trimble R8 real-time kinematic global position system (RTK GPS) system using a wifi connection to a Georgia virtual reference station (eGPS Solutions). Soundings were conducted at 6 Hz with a source frequency of 235 kHz. The expected error associated with this set of equipment is ±0.03 m in the vertical and ±0.02 m in the horizontal coordinate.

A total of 69 cross-channel profiles at intervals of 0.2-1.2 km were surveyed perpendicular to flow direction. At times the boat drifted off of the perpendicular track and so the transect data within 5 m of the transect line were collapsed onto a single line, and those outside of this threshold were deleted. The long profile was surveyed along the middle of the river for straight reaches and closer to the outer bank at bends, both at 2.5 m spacing. Because of losing the GPS connection, channel bed long profile data have some gaps with no elevation data especially between km72 and km45. Standard deviation of a 3 km running mean of the long profile elevations were computed and river sinuosity was determined for 2 km long reaches centered about each transect. We also collected 43 bed samples between km33 and km73 at ~1 km spacing using a Ponar, Standard 1725-F10, Box of 23×23 cm. During bed sampling on May 14, 2016, the average discharge and water elevation at km41 were 212 m^3/sec and 2.13 m, respectively, with tidal range of 0.34 m.

75

The average wet weight of samples is about 720±190 gm. Samples were dried and homogenized, and 400 gm dry material was sieved with mesh sizes of 0.15-4.0 mm, and 10 size classes.

Four HOBO U20 Water Level Loggers were deployed at km36, km45, km51 and km56 to record pressure (water column length above sensor) and temperature every 5 minutes for a total of 75 days, March 5 – May 19, 2016. The logger operational range is 0-9 m with typical depth accuracy ± 0.5 cm. The absolute pressure readings were compensated for air pressure by using a fifth sensor as a barometer, the difference between absolute and barometric pressure gives water depth. During deployment water surface elevation was acquired at each station, giving sensor elevation, and this combined with depth gives free surface elevation. The corresponding discharge values were highly variable, ranging from 96 m^3/sec to 1290 m^3/sec, and the water surface elevation at each varied by 2-3 m. Four different discharge values corresponding to the probability of exceedance of 75, 50, 25 and 10% respectively, or Q_{75}, Q_{50}, Q_{25} and Q_{10} were used to explain the changes in water elevation data. A fifth water depth/elevation measurement was taken from the USGS gauge at km41.

Cross-channel properties including channel width, mean hydraulic depth, cross-section area, wetted parameter, and hydraulic radius at 0.1 m increments in the vertical were computed using WinXSPro (Hardy et al., 2005) while the river was at or near bankfull conditions. Also, since these transect data were collected during two different surveys, the variability of river stage had to be compensated. For example, on March 8, 2014 and March 6, 2016 the water levels at km41 were (3.31-3.34) m and (3.41-3.43) m respectively (Table

76

3.1). Despite these relatively small differences all transects were compensated by linearly extending the bank to the higher level.

Cross-sectional stream power per unit channel width (unit stream power) was calculated using Lane (1955) as :

$$\omega = \rho\, g\, Q\, S_\eta / w \ \dots\dots\dots(3.1)$$

where w is the channel width, ρ is the density of water, g is gravitational acceleration, Q is the discharge and S_η is the water surface slope. The water surface slope, S_η, was computed between each set of two consecutive water level stations where η is water level.

We use the USGS instantaneous discharge values to constrain discharges computed with the Manning formula:

$$Q = \frac{1}{n} \times A \times R_h^{2/3} \times S_\eta^{1/2} \dots\dots\dots\dots\dots\dots (3.2)$$

where n is Manning's roughness coefficient, A is cross-sectional area of flow and R_h is the hydraulic radius. All parameters are computed as a function of the observed water level η. Thus, we use the five channel transects to calculate discharge. We then determine A, h, R_h, η and channel width w and water level at each transect.

Here, the n values at km41 were estimated using discharge from the USGS station (average $n = 0.028$ sec/m$^{1/3}$), as were A, and R_h. S_η at this location is taken as water surface slope between km45 and km 41 as S_3, as well as S_1, S_2, S_3 and S_4 representing water surface slopes at km56 and km51, km45, km41 and km36, respectively; S_1 is applied to both km56 and km51 transects. With this simplification and with no major tributaries between km56 to km36, n is computed for all water level observations and it is assumed to be equal for all other transects. Hence, discharge at 4 pressure transducer locations can be computed using equation (3.2).

77

Shield criterion (Shields,1936) for initiation of sediment motion is expressed with dimensionless Shields number, τ^*, and calculated as:

$$\tau^* = \frac{R_h\,S_n}{R\,g\,D} \ldots \ldots \ldots \ldots \ldots \ldots (3.3)$$

where D is grain size diameter and R is the specific weight of the particle. The τ^* estimates for 0.5 mm particles are compared to the threshold value of the Shields number for the initiation of motion. The critical value of Shields number (τ_c^*) is empirically related to particle Reynolds number, based on the modified Bronwlie (1981) and assumed to be $\approx$ 0.01614 for non-cohesive particles (Parker, 2004). Further, the effect of hiding or exposure is neglected here.

The total study reach was split into the upstream fluvial reach, or "upstream reach" and the mixed tidal-fluvial, or "downstream reach". Here, we assume that the station with maximum tidal amplitude <0.05 m is not significantly affected by tides and the station is assumed to be at or near the head of tides. For brevity, hereafter we refer to the upstream and downstream reaches as "*Upstr*" (km75 to km51) and "*Downstr*" (km51 to km29). Details on this distinction are presented in the results section. Trends in the *Upstr* and *Downstr* data were assessed using linear regression. Further, we used box plots to explain the variability in the data and to distinguish grouped sets of data. The quantiles of each box are represented with D_{10}, D_{50}, and D_{90} which respectively denote the value at which 10, 50 and 90% of the bed particle are equal or less.

Channel properties, river bed profile, sinuosity, and bed grain size data are examined with Spearman's rho non-parametric (SR) test to reveal the trends of these parameters along the study reach. The test is conducted at 0.05 significance level and it is

78

applied to various properties taking channel distance as the independent variable. The Spearman's rho ,Rs, and standardized, Z_{SR} test statistics are computed as:

$$Rs = 1 - \frac{6 \sum_{i=1}^{m}(Ri - i)^2}{(m^3 - m)} \dots \dots \dots \dots \dots \dots (3.4)$$

$$Z_{SR} = R_s \sqrt{\frac{m-2}{1-R_s^2}} \dots \dots \dots \dots \dots \dots \dots \dots \dots (3.5)$$

Ri denotes the rank of ith observation along the reach measuring from the upstream end of the study reach and m is the number of measurements at each reach. The positive and negative values of Z_{SR} indicate increasing and decreasing trends, respectively (Yue et al, 2002; Agha and Şarlak, 2016).

3.4 RESULTS

3.4.1 River discharge and stage

Altamaha River annual discharge is characterized as having strong seasonality (Jiang et al., 2008; Roebuck et al., 2018) and during our observation interval the km41 (Figure 3.1) USGS hydrograph varied by one order of magnitude, from 96-1290 m^3/s (Figure 3.3). Initially, the hydrograph has a slight declining trend until March 18, and a much steeper decline to March 31 (inferred). The discharge increases to the peak value on April 16, followed by a sharp decline until April 24 and then a much more gradual decline until May 18. Tidal oscillations are evident for discharges <550 m^3/s, and are particularly well developed at all stations and for the lowest discharges (Figure 3.3).

Likewise, the five water level time series for the same time interval show similar variability with averages of 4.49 ± 0.71, 3.85 ± 0.69, 3.37 ± 0.55, 3.05 ± 0.49 and 2.75 ±

79

0.43 at km56, km51, km45, km41 and km36, respectively (Figure 3.3). Water levels attain clear peaks of 2.0 to 2.9m at all sites on April 16; the minimum values occur at the end of the monitoring period (Figure 3.3). The range of water level at each site varies depending on the magnitude of discharge and tidal range. The water level range (the difference between max and min observed) decreases in the downstream direction (Figure 3.3). At all stations tidal oscillations are greatest during the lower discharge conditions; for instance, water level time series during May, 2016 show the greater tidal amplitude. During low discharge conditions the tidal amplitudes are 0.83 m at km36, 0.46 m at km41, 0.31 m at km45, 0.14 m at km51 and 0.04 m at km56 (Figure 3.3, Table 3.2); similar to other studies (e.g., Horrevoets et al., 2004). The discharge that completely damps tidal oscillations at km36, km41, km45, km51 and km56 is 973, 541, 501, 237 and 116 m^3/sec respectively.

The average and standard deviation of water surface slope between successive sites and for all 7,105 measurements per site are of the order 10^{-4} m/m. In particular, from up-to downstream the values vary as 1.3 ± 0.1, 0.8 ± 0.3, 0.8 ± 0.2 and $0.6 \pm 0.2 \times 10^{-4}$ m/m, S_1, S_2, S_3 and S_4 respectively. The corresponding 50% and 75% quantile values also decline downstream, but the 25% quantiles have no clear pattern (Figure 3.4). Also, in general, the inner quartile range is least for the inland observations and S_1 is statistically significantly higher; the next three decrease in downstream direction although they are not statistically significantly different (Figure 3.4). Together, the data reveal a clear and frequently occurring break in slope at or near km51 (Figure 3.4).

In summary, during the observation interval river discharge varied 96-1,290 m^3/s, and the corresponding river stage varied by 2.0-3.0 m at all stations. Tidal amplitude is greatest during low discharge, reaching ~0.83 m at km36, but no tidal oscillations occurred

80

at either station when the discharge exceeded 973 m^3/sec. Also, tidal oscillations declined upstream, leading to a head of tides near the km56 station. The surface slopes between successive stations varied considerably, but between km56-km51 there is a statistically significantly higher slope relative to those further downstream. This change is slope represents a type of discontinuity at km51, separating the previously defined upstream and downstream reaches.

3.4.2 Long profile and channel planform shape

The centerline river-bed elevation is highly variable, ranging from to -7.9 m to 6.2 m, but overall it declines from upstream to downstream, and with a slight upward concavity (Figure 3.5A). The steepest part of the river is from km73 to km67, with fluctuations of about 2 m. At km66 there is channel deepening followed by a step-up, and these together mark the start of a more gradual slope extending to km56, followed by a 5 km long, 2 m deep trough. Km51 is the starting point for frequent 3-8 m fluctuations that persist to the shoreward end of the survey. The standard deviation (*sd*) of river bed elevation ranges from 0.53 m to 1.91 m and it tends to increase in a stepwise fashion toward the ocean, at km72 and km42. From km42 to km32 *sd* varies from 0.7 m to 1.9 m. (Figure 3.5A). The minimum values coincide with small fluctuations in bed elevation at km73 to km64. In contrast, *sd* values increase sharply from 1.0 m to 1.8 m at km42 and another sharp change occurs at km38 to km34.

Patterns in along channel variability reveal a statistically significant decreasing trend with *Upstr* (*Rs*=-0.78), while the *Downstr* had a significant but moderate trend (*Rs*=-0.40). We applied a linear fit to the *Upstr* and *Downstr* data and found bed slopes of 2.0×10$^-$

81

^{4} and 0.7×10^{-4}, respectively. These values are comparable to the average water surface slopes of 1.3×10^{-4} for the *Upstr* S_1 and 0.7×10^{-4} for *Downstr* at S_2, S_3 and S_4. The *Upstr* slope (S_1) is about three times the *Downstr* values (S_2, S_3 , S_4) and the transition from S_1 to S_2 coincides with a noteworthy break in the river bed profile at km54 (Figure 3.5A).

Channel sinuosity (*S*) varies from 1.1 to 2.7, and it has a declining trend with distance downstream before reaching a quasi-steady range (Figure 3.5B). In particular, *S* values decline between km75 to km51 with average sinuosity >1.8, but from km51 to km30 average sinuosity is <1.3 (Figure1 and Figure 3.5B). The *SR* test for the *Upstr* reveals a statistically significant decreasing trend with strong correlation (*Rs*=-0.69) while the *Downstr* showed no significant change. Linear trends along the *Upstr* give a slope of 0.4×10^{-4} while the *Downstr* trend does not depict significant change with distance (Figure 3.5B).

In summary, the slope of the river bed profile declines with distance downstream and it is concave up. There is a large break in river bed slope at km54 and a decline in the magnitude and along channel variability in sinuosity at km51 (Figure 3.5A and 3.5B). These distinct changes channel properties coincide with the boundary between the previously define *Upstr* and *Downstr*. The *Upstr* (km75 to km51) is characterized as having higher channel bed slope and sinuosity relative to the *Downstr* (km51 to km29).

3.4.3 Channel geometry

Channel width, *w,* varies by a factor of ~4 from 64 to 259 m with average 134 ± 45 m. (Figure 3.6A). There is also substantial scatter along the channel, but with an overall increase downstream. Locally, however, width can decline over 5+ kilometer long reaches

82

(e.g., km75-km67). The rate of increasing width is higher for the *Downstr* by a factor of 3, and with more scatter relative to *Upstr*. The *SR* test detected a moderate but statistically significant increase ($Rs = 0.45$) for *Downstr* with non-significant increase ($Rs=0.22$) for *Upstr*.

Likewise, the cross-section area of flow, *A,* varies substantially and also by a factor of ~4, ranging from 205 to 844 m^2, averaging 520 ± 161 m^2. The along channel response however, differs from that of *w*. *A* increases downstream to a maximum and then gradually declines (Figure 3.6B), giving an asymmetrical, convex pattern. The *Upstr* trend was significant ($Rs=0.79$); while the test for *Downstr* was non-significant ($Rs=-0.24$). There are local departures from these overall patterns, however. From km76 to km67 *A* persists at 200-310 m^2, followed by a step increase from 250 m^2 to 425 m^2. From km66 to km57 *A* is between 380 m^2 to 610 m^2, but at km56 there is an abrupt decline from 610 m^2 to 420 m^2. This is followed by a slightly increasing trend with nominal variability to km51. Downstream of km50 *A* varies considerably and in the absence of comparable trends. This distinct behavior was also reported by Sheldon and Alber, (2002) and with other rivers (Torres, 2017). Thus, a peaked along channel trend of *A* in the single strand channel appears to be an endemic feature of the FTTZ along southeastern coastal plain rivers..

The hydraulic radius R_h ranges from 2.38 to 5.10 m with average 3.74 ± 0.65 m. The along channel values have a peak at km53 (Figure 3.6C) and gives a net quasi-symmetrical pattern. Amongst the two *Upstr* and *Downstr* reaches we find significant trends in each, although the latter is declining ($Rs = 0.91$, and $Rs = -0.71$, respectively). R_h trend for *Upstr* increases with values range from 2.40 to 4.85 m. Upon closer inspection however, the reach can be characterized as having one part of nominal variability with a

clearly increasing trend (km69 to km64) surrounded by sections with much higher variation. The *Downstr* has no discernible smaller scale patterns. Nevertheless, these observations indicate that the downstream trend is for greater efficiency up to km51, followed by decreasing efficiency or bed and bank drag.

Width to mean depth ratio *w/d* provided more insight to channel shape and showed seaward deepening and shallowing for *Upstr* and *Downstr* respectively (Figure 3.6D). *w/d* values range from 15-101with average = 37. The average value of *w/d* for *Upstr* and *Downstr* are 27 and 46 respectively. The along channel values of *w/d* show high scattering for *Downstr* compared to *Upstr*. The *w/d* trend for the *Upstr* shows a non-significant decrease (*Rs*=-0.14); while the *w/d* trend for *Downstr* shows a significant increase (*Rs*=0.6). The transition in the trend of *w/d* also occurred between km55 and km51 at which *w/d* values reach minimum and range only from 15-23.

Taken together, from km76 to km51 it appears that A, R_h and w increase, albeit at different rates. Below km51 however there is a departure in responses where w increases but A declines. This response is translated to R_h as a clear peak with an apparently symmetrical trend. Moreover, it appears the km51 is the focal point along the channel where large changes are detected, and the channel becomes less efficient downstream.

3.4.4 Grain size distribution

For all river bed grab samples, the D_{10}, D_{50} and D_{90} quantile values range from 0.16 to 0.51 mm, 0.35 to 0.84 mm, and 0.59 to 1.9 mm, respectively, and the corresponding averages are 0.34±0.09 mm, 0.57±0.15 mm, 1.06±0.30 mm. Hence, the bed material consists of fine to coarse sand, but the median grain size is ~0.6 mm. However, the *Upstr* can be

84

characterized as having poorly sorted coarse sand while the *Downstr* is more uniform (Figure 3.7). The transition in sorting occurs from km51 to km44.

The *Upstr* and *Downstr* patterns of particle size show increasing but non-significant (*Rs*=0.12), and decreasing significant, (*Rs*=-0.5) trends, respectively (Figure 3.7). From km72 to km51 D_{10} values are highly variable but decline slightly between km51 and km44, and at km44 the values are grouped around 0.28 mm. On the other hand, D_{90} trends show decreasing and increasing trends along the *Upstr* and *Downstr*, respectively, but both were not statistically significant. The weak trends are related to the large scatter from km72 to km51, with a sharp decline over km50 to km47 followed by an overall increase toward km44; downstream of km44, D_{90} values are mostly consistent and close to 0.9 mm. The average D_{50} for the *Upstr* bed samples is 0.72 ± 0.08 mm compared with 0.45 ± 0.05 mm for the *Downstr*. Also, both reaches show that particle size decreases downstream with a sharp decline from km51 to km47; and these lower D_{50} values persist to the limit of the survey. The high scatter at km72-km51 gives rise to a weak trend (Rs=-0.28) whereas *Downstr* the trend is less scattered and significant (*Rs*=-0.46).

Overall, the median particle sizes have substantial variability along the inland reach. Further downstream however, the median values are remarkably uniform. These two distinctive patterns of variation are bridged by a 4km long reach of gradually declining particle size; from km51 to km47 particle size declines from about 0.71 to 0.41 mm.

3.4.5 Unit stream power and sediment transport capacity

Stream power, ω , represents the rate of potential energy loss and it is a measure of the channel's ability to perform geomorphic work (Bagnold, 1966; Bull, 1979; Knighton,

85

1999). Therefore, it can be used to provide insight on expectations for bed material size under a given discharge. Hence, a reach with high ω is more likely to have a high stream capacity and competence relative to a reach with low ω. Thus, spatial variations in bed size can be expected in response to longitudinal changes in ω.

An assessment of ω at each station shows that it is more variable but overall higher for the inland stations by up to a factor of 5 (Table 3.3). The stations at km56 and km51 have comparable ω conditions and they are statistically significantly higher than the values from stations further downstream. Also, the range of ω at km56 and km51 shows wide scatter relative to those further downstream (Figure 3.8). At km36 it is remarkably consistent with low variability and an inter-quartile range of ~0.5 watt/m^2. Using the predefined reaches described above we find that ω estimates for *Upstr* are of the same magnitude for the Clearwater River, Idaho in Bagnold (1980). Also, ω estimates across the FTTZ of Columbia River reported by Gies and Jay (1989) show that the ω of the fully fluvial part of Columbia River decreases downstream (from 7.8 to 1.4 watt/m^2) but remains significantly higher than the tidal part (1.9 to 0.2 watt/m^2), and that ω reaches minimum at the FTTZ. Our estimates of ω for Altamaha River are comparable in patterns and magnitude relative to the Columbia River.

Dimensionless Shields number, τ^*, can provide deeper insight on trends in particle size by providing estimates of the conditions necessary for initial or threshold sediment motion. We thus compare the Shields number at the five stations with the critical Shields number, τ_c^*, for $D_{50} = 0.5$ mm, the median grain size between *Upstr* and *Downstr* (Figure 3.7). The quartiles of τ^* decrease from km56 to km41 and then slightly increases at km36. Both average and median values at km56 and km51 are comparable and significantly

higher than τ^* at km45, km41 and km36. For the *Downstr*, the average and median of km45 are 0.0148 and 0.0158, respectively, and slightly higher than at km41 and km36. τ^* at km56 and km45 has high scatter compared to km51, km41 and km36. The recurrence of conditions where τ^* values exceed the critical value at km56 and km51 exceeds 80%. This percentage then decreases to 47%, 19% and 7% at km45, km41 and km36, respectively. This result shows that 80% of τ^* estimates at *Upstr* are beyond the predicted threshold of incipient motion, while *Downstr* the initiation of motion ranges from 7%-47%.

In summary, the range and magnitude of ω are comparable between km56 to km51. From km51 to km45 there is a 75% energy loss while from km45 to km36 ω gradually declines. Hence, the reach from km56 to km36 can be divided into an upstream high energy reach but below km51 the river system is comparatively low energy. Likewise, τ^* decreases in the downstream direction and shows a clear step-like decline from km51 to km45. The median of τ^* for *Upstr* is higher than the *Downstr*, and overall the median values decline seaward. The transect at km41 shows the lowest boundary shear stress among all transects.

3.5 DISCUSSION

The FTTZ has been a theme of focused research on sedimentology, geomorphology and hydrodynamics, as detailed in the introduction. Here we assert that our study reach includes the Altamaha River FTTZ in that the km56 station with maximum 0.04m tidal oscillations is at or very near the head of tides. This combined with our non-quantitative observations that current reversals do not occur at the station leads us to infer that the FTTZ is downstream of km56. Further along, at station km41 we find that tidal oscillations persist for discharge values up to the 10% exceedance probability (Figures 3.2, 3.3), with

87

the tidal amplitude ranging from 0.0 during high discharges to 0.83 m when the terrestrial runoff is distinctly lower (Figure 3.2). Also, the current reversals or negative discharges serve to highlight the intermittent tidal dominance at this station, hence, we propose that the fluvial-tidal transition zone is between km56 and km41. However, additional data will allow us to refine and more definitively identify the FTTZ position.

The trends in channel geometry, stream power and particle size have distinct attributes between the previously defined upper reach, from km75 to km51, and the lower reach, km51 to km29 or the *Upstr* and *Downstr,* respectively. In particular, the data collectively show a break in slope or inflection in the vicinity of km51. This is true for bed elevation and sinuosity (Figure 3.5), for channel width, cross-section area of flow, hydraulic radius and depth (Figure 3.6). Moreover, there are several equally identifiable breaks or discontinuities that occur over a distance of several kilometers, but typically between km51 and km45. For instance, this is true for water surface slope (Figure 3.4), particle size (Figure 3.7), stream power (Figure 3.8) and to a lesser extend Shields number (Figure 3.9). Lastly, it is noteworthy that three independent studies show the fluvial tidal transition reach in coastal plain rivers is upstream of the distributary system, and within the largely single strand river where there is a characteristic peak in cross-section area of flow (this study; Sheldon and Alber; 2002 and Torres, 2017). We propose that the peak is a feature endemic to tide influenced coastal plain river's fluvial tidal transition reaches. Overall, these data indicate that the fluvial tidal transition reach is about 4 km long, extending from km51 to km47. Also, with the area, *A*, there is a distinct departure from the general *Upstr* trend apparent as a step-decline in the area the starts upstream at km57,

and ends at km51. A similar trough in the area trend was noted by Torres (2017), and this may likewise be a FTTZ attribute.

Several studies report high energy dissipation rates associated with the FTTZ that is coincident with the peak in cross-section area (Gies and Jay, 1989; Yankovsky et al., 2012). For the Altamaha the high rate of energy dissipation (order 75%) and corresponding decline in Shields number (about 40%) occur between km51 and km45 (Figures 3.8 and 3.9) where A, R_h and d are maximum and w/d is minimum (Figure 3.6). Also, at the inland stations ω values are significantly higher than the shoreward stations, and average ω decreases systematically downstream. Moreover, the Shields number decreases in the downstream direction between km56 to km41, and with a significant decline at km51 (Figure 3.9 and Table 3.4). The downstream variations of ω and τ^* are associated with changes in water surface slope, channel bed slope and channel geometry (eq. 3.2 and 3.3). Water surface slope between km56 and km36 is highly variable (Figure 3.4) but there is a statistically significant break from km51 to km45, where the median values transition from 1.3 to 0.9×10^{-4} m/m. In other words, there is a remarkable decline in water surface slope near the boundary between *Upstr* and *Downstr*. Further along the channel the median values show a more gradual decline. The declining water surface slope is likely associated with tidal waves advancing upstream (e.g., Gies and Jay, 1989; Yankovsky et al., 2012; Kastner et al., 2017; Gugliotta et al., 2017) giving rise to a highly irregular and declining channel bed slope (Figure 3.5A). During high discharge periods ($Q>Q_{10}$), the tidal range is less than 0.07 m at km36 (Figure 3.3, 3.4 and Table 3.2). Thus, changes in water surface slope are most likely associated with upstream variations in terrestrial runoff (Gies and Jay, 1989).

During low discharge conditions, water surface elevation from km56 to km36 is affected by tide oscillations although tides at km56 are <0.04m. Hence, we assume the head of tides is at or near km56. However, the head of tides varies with discharge (e.g., Horrevoets et al., 2004; Freitas et al, 2012), therefore the head of tides may advance downstream but the data show it is limited to remaining between km56 and km45 (Figure 3.2). On the other hand, average water surface slopes at *Upstr* and *Downstr* reaches were comparable to the river bed slope (2.0×10^{-4} m/m for *Upstr*, and 0.7×10^{-4} m/m for *Downstr*). Thus, the *Upstr* is has a relatively higher water surface slope and lower variability compared to the *Downstr*. Similarly, the estimates of ω and τ^* are high in the *Upstr* but below km51 they are lower (Figure 3.8 and 3.9 ; Table 3.3 and 3.4). This pattern of ω are in good agreement with the magnitude and trend of ω across the FTTZ of Columbia River (Gies and Jay, 1989). It is likely that the *Upstr* meandering planform is required to dissipate excess available power and the transition from the meandering *Upstr* to the mostly straight *Downstr* developed to utilize available stream power needed to maintain a progressive movement of sediment over the lower slope (Figure 3.5A and Figure 3.1).

Along the channel a decline in median grain size is predicted as relative energy decreases along the FTTZ (Dalrymple and Choi, 2007). Thus, spatial variation in bed size and range are expected due to longitudinal changes in ω. Comparing the downstream trend of D_{50} in Figure 7 with downstream variations of ω (Figure 3.8) it is apparent that both ω and D_{50} have an abrupt decline going from km51 to km45 where ω declines by more than 75% and D_{50} by 50%. Thus, large bed particles are excepted along the *Upstr* while for *Downstr* the particles are expected to be relatively smaller due to the large decline in ω downstream km51. Further, by comparing the τ^* with expected critical shear stress τ_c^* for

D_{50}= 0.5 mm we find that more than 80% of τ^* for the *Upstr* exceed τ_c^*. This indicates that median grain sizes are larger than 0.5 mm. The discordance of τ^* with τ_c^* declines to 47% at km45 and to less than 20% at km41 and km36 shows that the median grain size for *Downstr* is <0.5 mm. This set of conditions appears as a sharp decline in D_{50} between km51 and km47 and is coincident with the abrupt decline in τ^* downstream km51. Consequently, the downstream trend of median grain size in Figure 3.7 can be reasonably measurable and quantified through the analysis and trend of τ^*.

The spatial changes in sediment transport capacity may help explain some adjustment processes between channel geometry and channel hydraulics. *Upstr* has relatively high transport capacity and may tend toward downcutting while the *Downstr* tends toward lateral cutting (Bull, 1979). These can be detected in the downstream trend of *w/d* where *Upstr w/d* is slightly decreasing shoreward while for *Downstr* it is highly variable, but overall increasing downstream (seaward shallowing). As a result, the *A* for *Upstr* increases as *w* and *d* increase but for *Downstr*, *w* increases more rapidly and *d* decreases (Figure 3.6). Thus, the trend in *A* for *Downstr* has a non-significant downstream decrease. If the typical increase of *w* to seaward along *Downstr* is associated with tidal flux (e.g., Dalrymple et al., *2012*), the downstream decrease of *d* may be associated with low transport capacity and an aggrading reach with relatively low bed slope (Figure 3.5A). The trend of channel morphology and bed particle size abruptly changes over a short distance across the fluvial tidal transition zone, km51 to km47. This geomorphic transition is associated with a sharp decline in stream power and sediment transport capacity that caused by change in water surface slope near the head of the tide. These results with other recent related studies (e.g., Dalrymple and Choi, 2007; Yankovsky et al., 2012; Torres, 2017;

Kastner et al., 2017) help define the fluvial tidal transition zone with common geomorphic and hydrodynamic features.

3.6 CONCLUSIONS

The fluvial-tidal transient reach is approximately 1-4 km long. We found that the abrupt changes in trends of channel geometry and median grain size that can be associated with a remarkable decline in estimates of unit stream power and dimensionless Shields number which declined by 82% and 42%, respectively. These analyses further illustrate that the fluvial reach has higher stream power and transport capacity than the downstream tide-dominated reach. The distribution of stream power and Shields number can be used to explain some of the fluvial-tidal transition channel adjustments in channel hydraulics, geometry and planform, and it provides some insight on the channel conditions that transition from seaward-deepening along fluvial reach to seaward shallowing along the tidal reach, leading to adjustments in, for example, cross-section area of flow. This may explain why the channel planform displays meandering and associated dissipation of the excess energy and the maintenance of straight channel for tidal dominated reach to ensure enough power for sediment transport over the relatively low slope.

Table 3.1: Coverage of fieldwork data used in this paper.

Period	Kind of Survey	Discharge range during survey at km41 (m³/sec)	Stage range during survey at km41(m)
March 8/2014	43 transects along the study reach.	649-665	3.31-3.34
March 6/2016	26 transects along the study reach.	713-724	3.41-3.43
	longitudinal profile along the study reach.	713-719	3.41-3.42
March 5-May 18/2016	water level data	96-1290	1.83-3.98
May 14/2016	river bed sample	161-258	1.99-2.23

Table 3.2: Maximum and minimum tidal ranges with their corresponding discharges.

Site	Max tidal range (m)	Corresponding Q (m³/sec) of max. tide	Min tidal range (m)	Corresponding Q (m³/sec) of min. tide	Tidal range at discharge with frequency is equal to			
					Q_{75} 100m³/sec	Q_{50} 200m³/sec	Q_{25} 480m³/sec	Q_{10} 815m³/sec
km36	0.83	119	0.06	897	0.78	0.67	0.21	0.07
km41	0.46	139	0.06	544	0.41	0.29	0.08	-
km45	0.31	182	0.06	413	0.34	0.17	-	-
km51	0.14	171	0.06	326	0.18	0.08	-	-
km56	0.04	116	0.04	116	-	-	-	-

Table 3.3: Statistical summary of the unit stream power estimates.

Site	Average of ω (watt/m^2)	Median of ω (watt/m^2)	Range of ω (watt/m^2)	Inter-quartile range of ω (watt/m^2)
Km56	6.7	7.1	1.8-12.2	3.6
Km51	6.4	6.9	2.4-12.1	3.8
km45	2.2	3.1	0.1-6.2	2.2
Km41	1.8	1.9	0.1-5.8	1.1
Km36	1.3	2.8	0-2.8	0.5

Table 3.4: Statistical summary of the Shields number.

Site	Average of τ^*	Median of τ^*	Range of τ^*	Inter-quartile range of τ^*	Percent of values at which $\tau^* > \tau_c^*$ %
Km56	0.0237	0.0248	0.0107-0.0353	0.0082	83
Km51	0.0215	0.0225	0.0120-0.0288	0.0054	85
km45	0.0148	0.0158	0.0010-0.0198	0.0110	47
Km41	0.0127	0.0124	0.0021-0.0145	0.0059	19
Km36	0.0120	0.0134	0-0.0183	0.0036	7

94
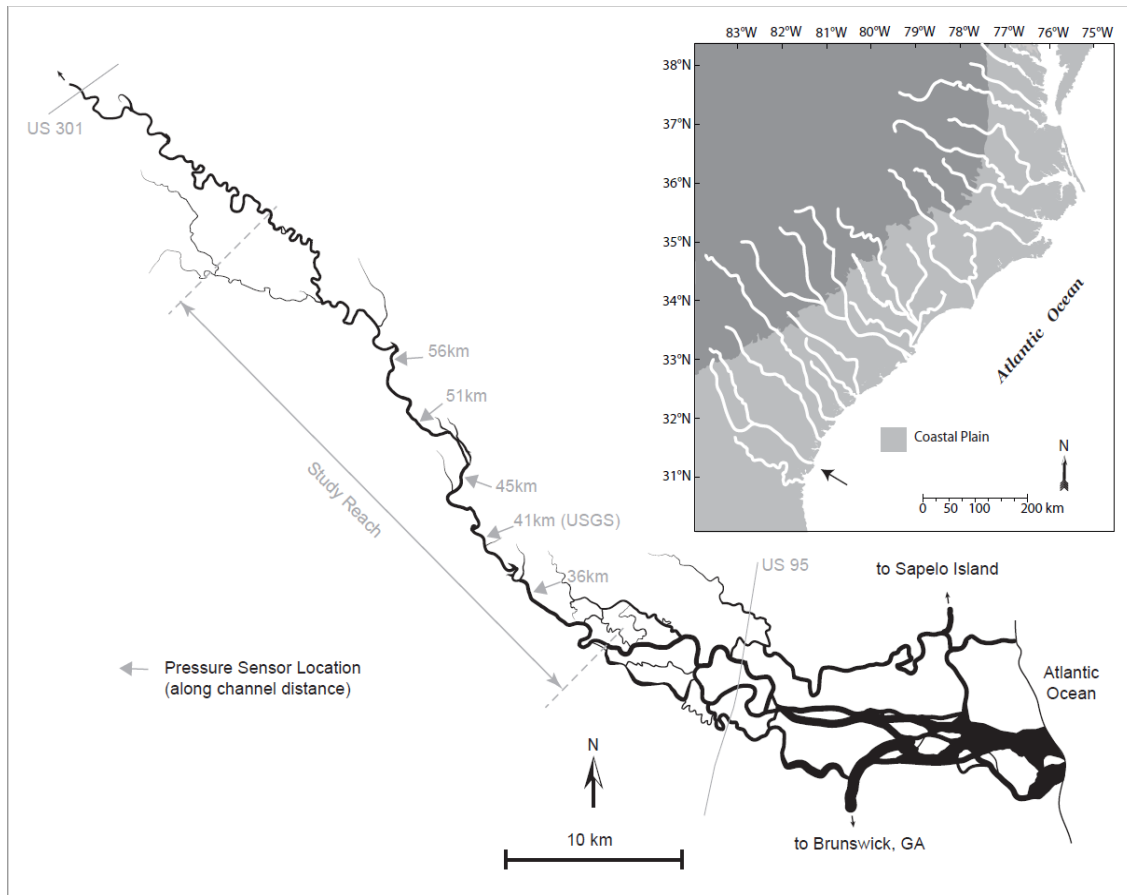
Figure 3.1: The main stem of the lower Altamaha River. The U.S. Geological Survey (USGS) gauging station (USGS ID:02226160, Altamaha River near Everett City, 31º25′37″ N, 81º36′20″W) is on a bridge pier at km41 from the river mouth.
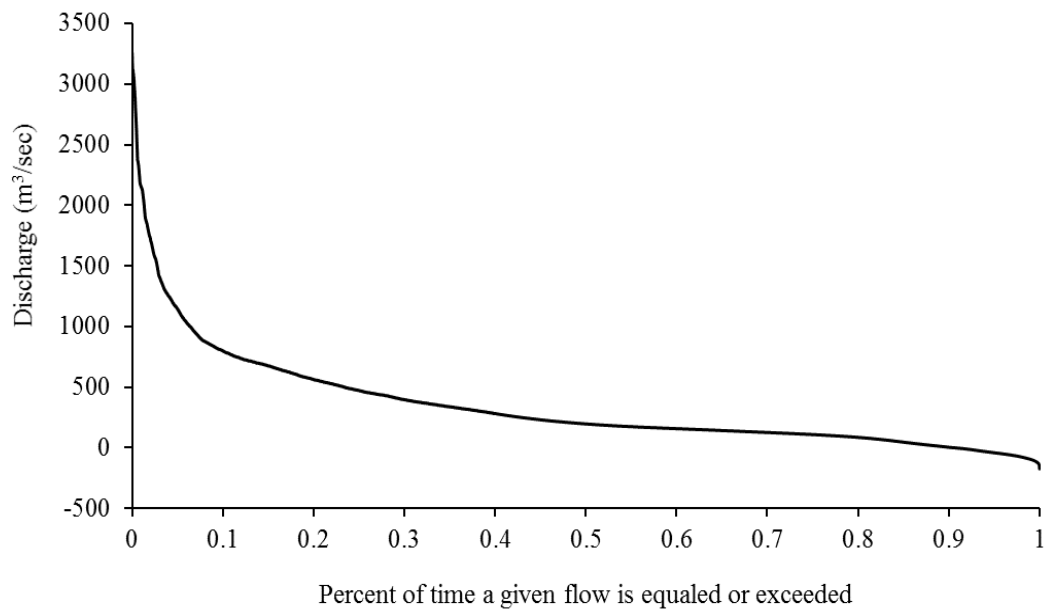
Figure 3.2: Flow discharge duration curve of the Altamaha River for available mean daily recorded data (2008-2017).
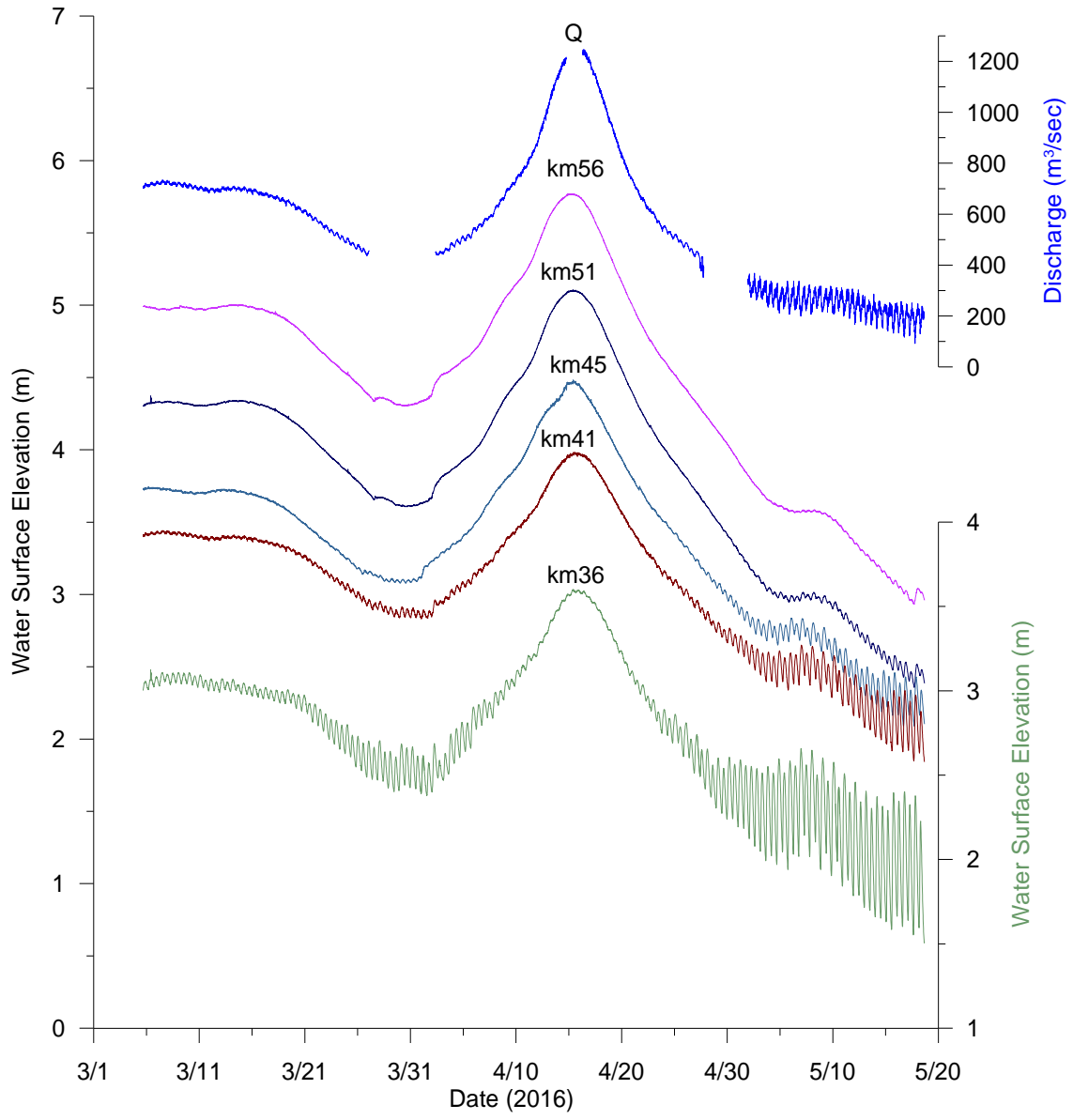
Figure 3.3: Simultaneous water level for monitoring stations. Where the main axis represents the water surface elevation at km41, km45, km51, and km56; while discharge at km41 at and water surface elevation at km36 are represented with a secondary axis.

97
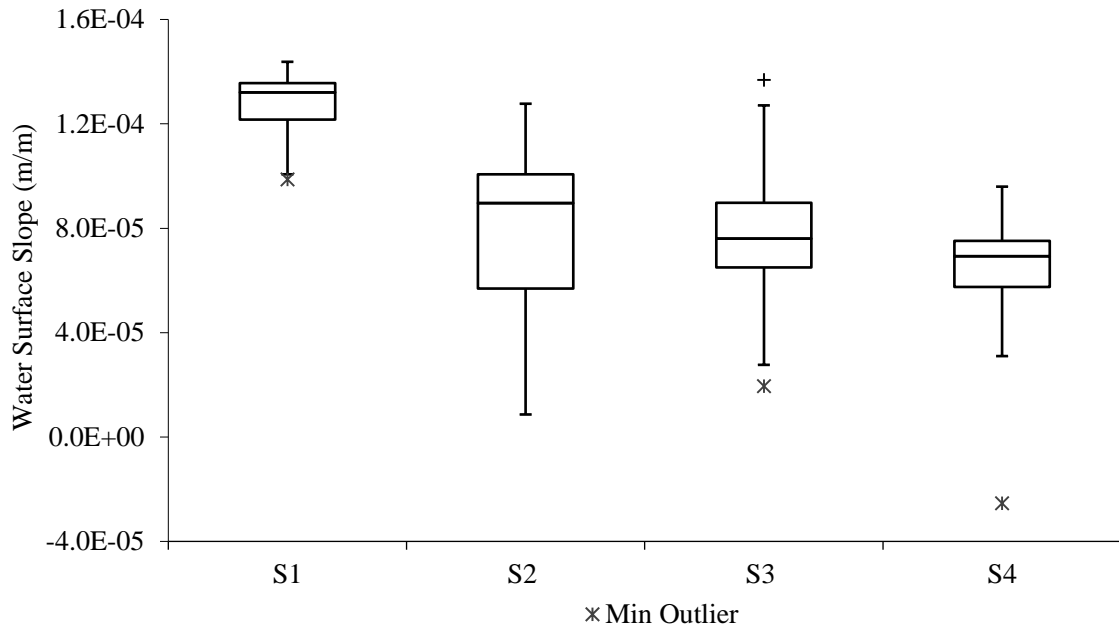
Figure 3.4: Water surface slope at four subreaches between km56 and km36 S_1, S_2, S_3 and S_4 respectively represent water surface slopes between km56-km51, km51-km45, km45-km41 and km41-km36.
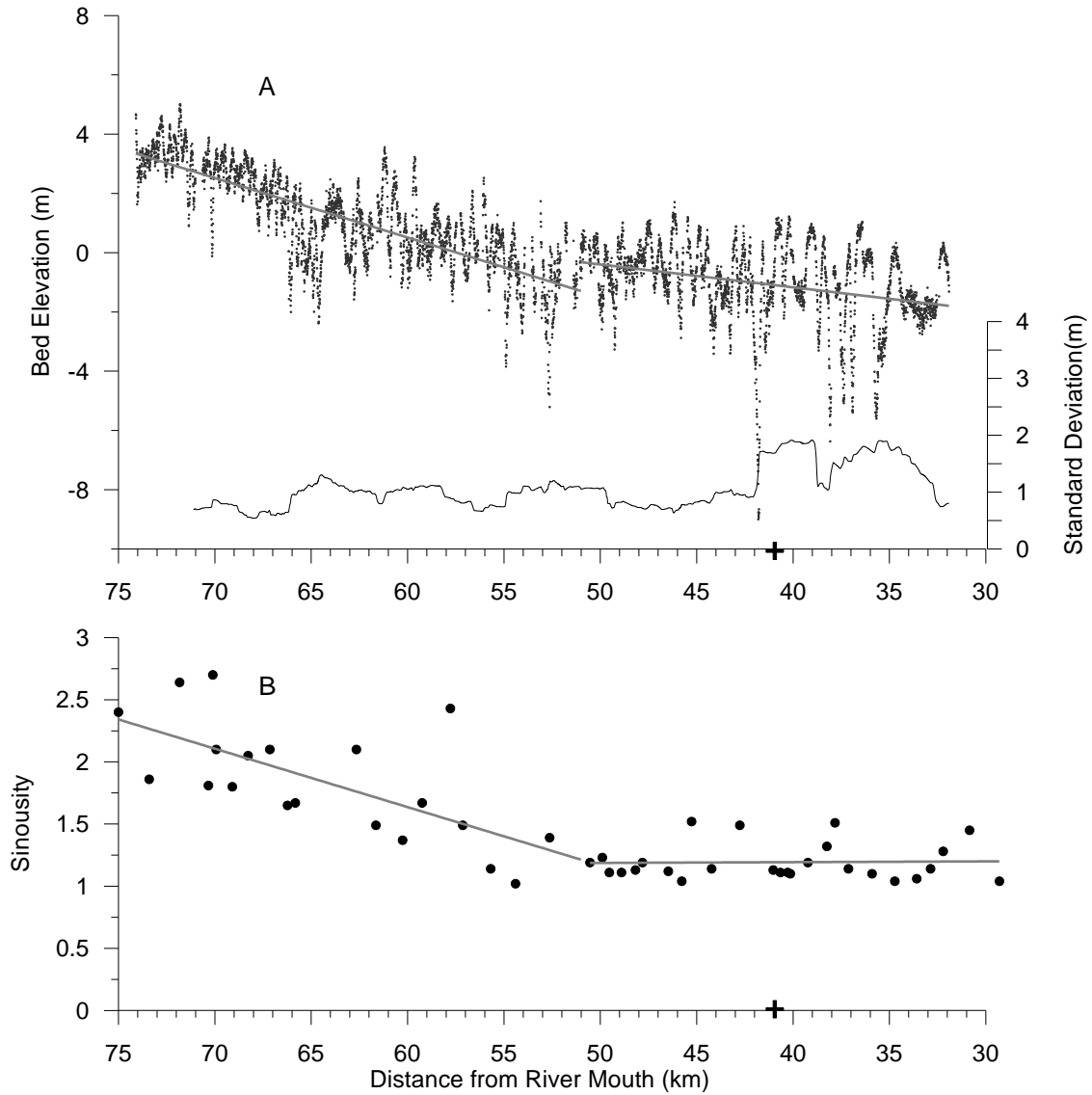
Figure 3.5: Along-channel variations in channel bed elevation and sinuosity. A- Main axis is the riverbed long profile elevation (black points) as a function of the along-channel distance. Secondary axis (inset) is the 3km running average long profile standard deviation. The cross sign is used to identify the location of the bridge. B-2km average sinuosity (black points) along the study reach. Sinuosity here is used to describe the meandering of the study reach and defined as a ratio of channel

length measured between two points along the river to straight-line length between the two selected points.

Continue………………

100
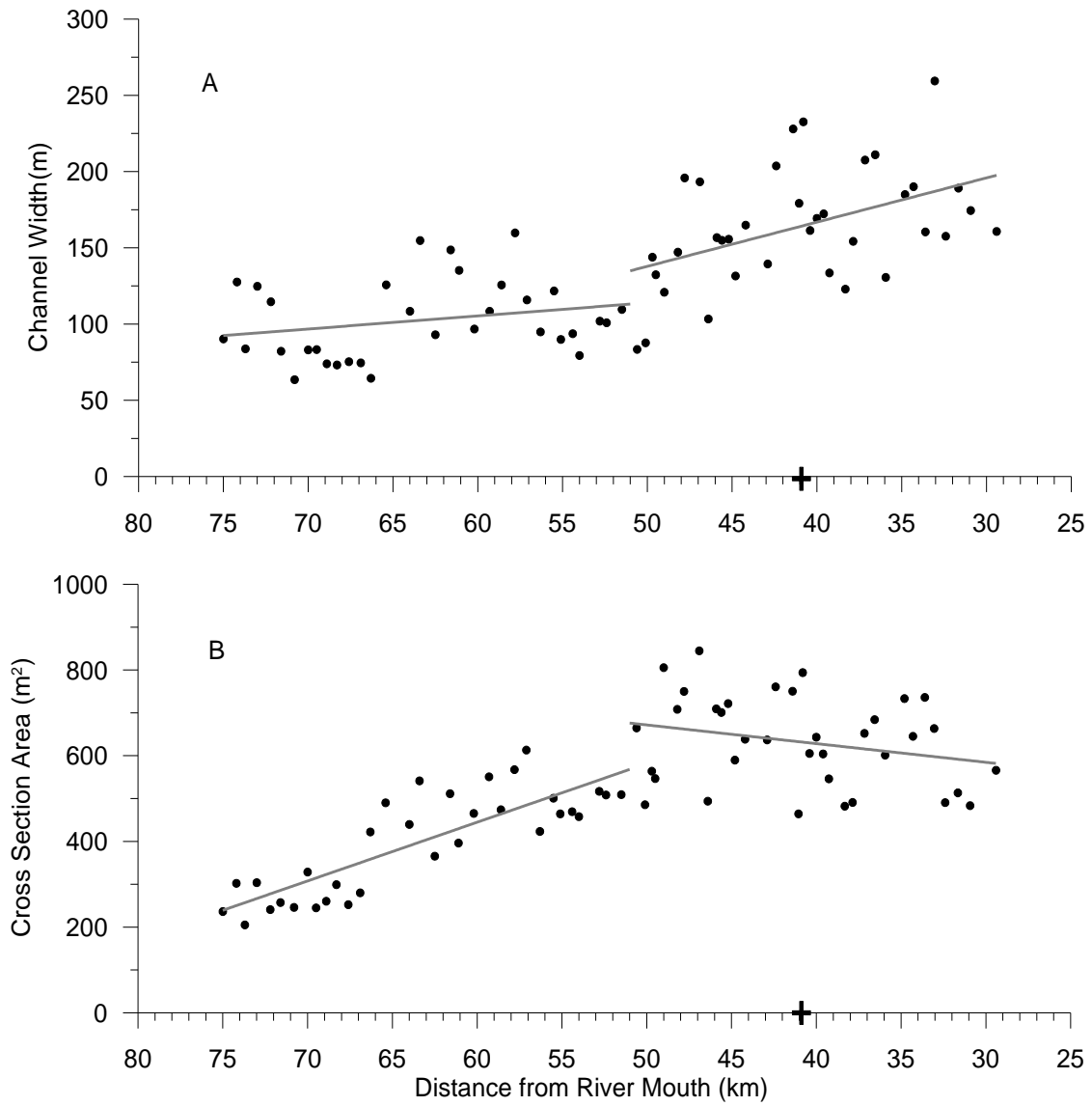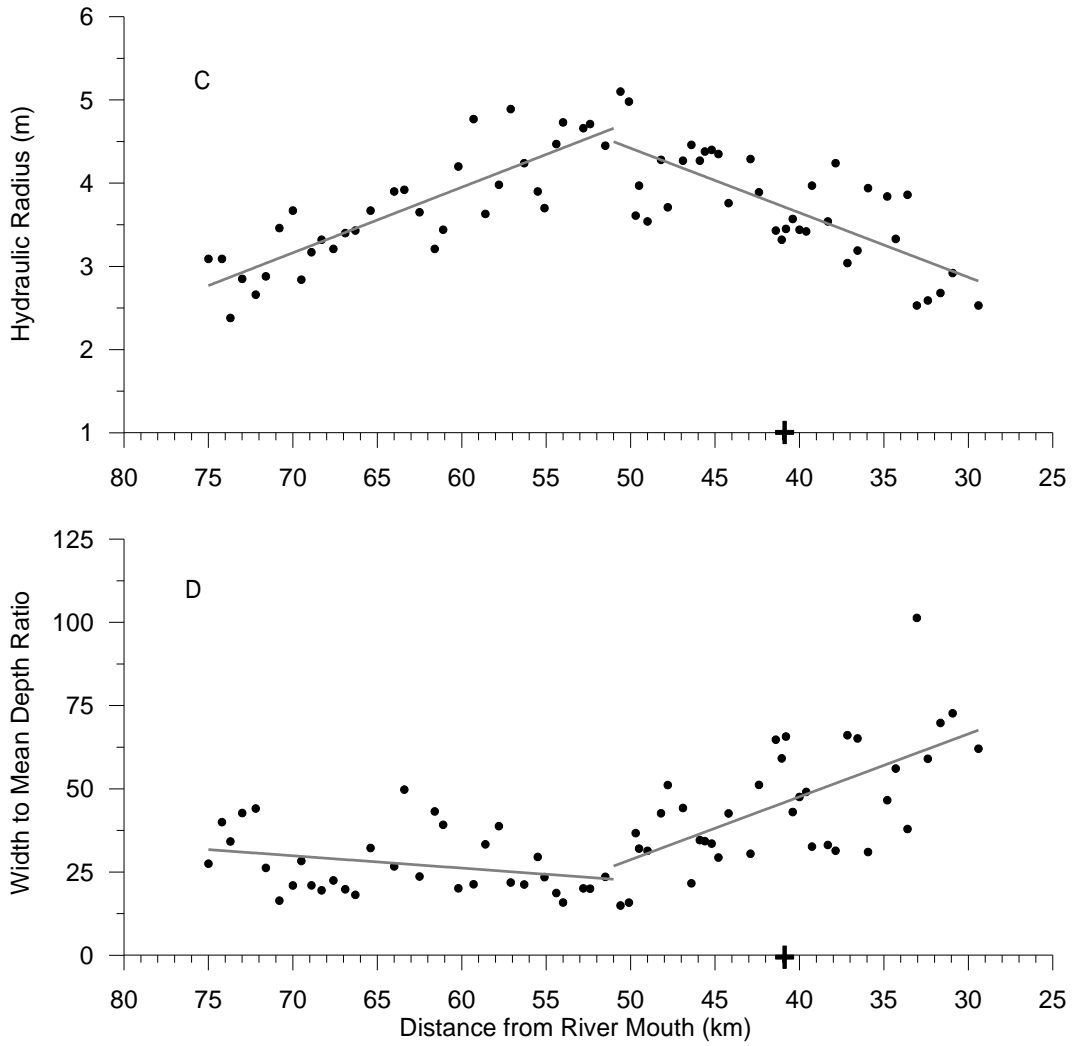
Figure 3.6: A long-channel variation in: A- Channel width *w*, B- The cross-section area *A*, C- Hydraulic radius R_h and D- Width to depth ratio *w/d*.
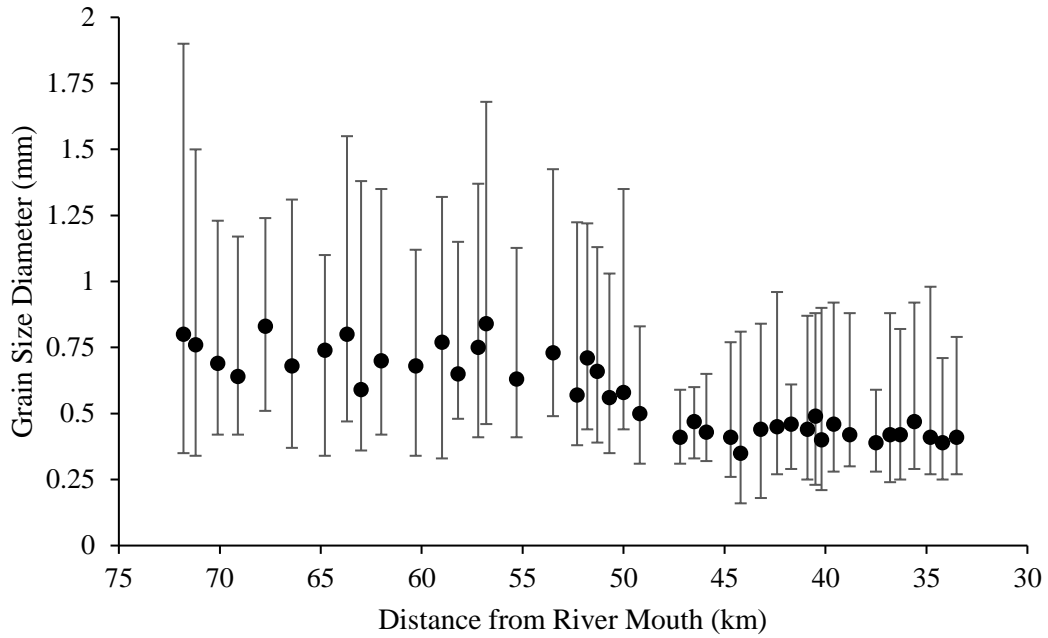
Figure 3.7: Downstream change in median grain size distribution along the study reach. Positive and negative errors bars represent D_{90} and D_{10} respectively.
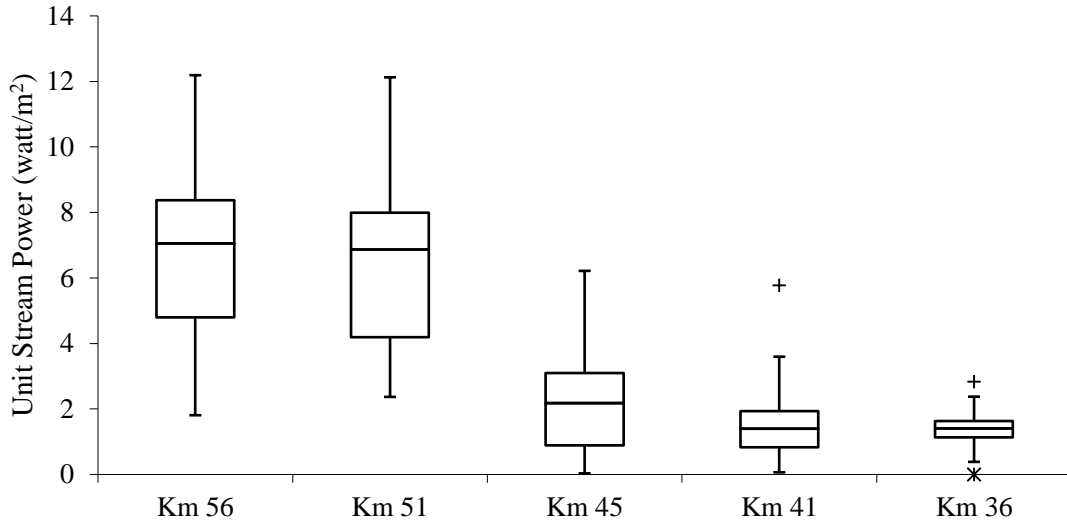
Figure 3.8: Cross-sectional stream power per unit channel width at five sites between km56 and km36.
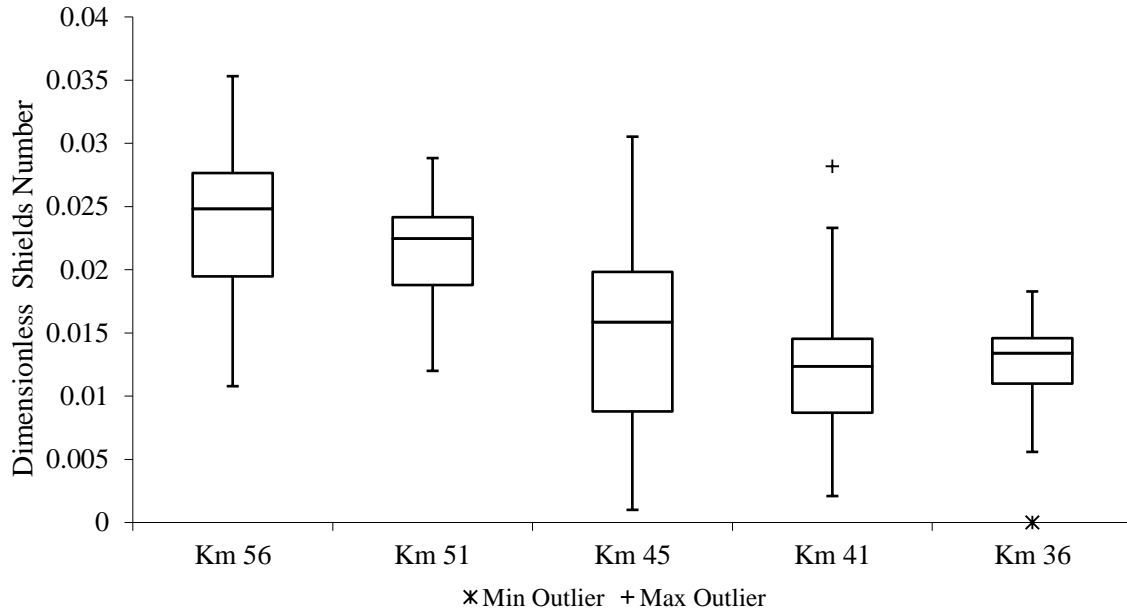
Figure 3.9: Shields number estimates at five sites between km56 and km36.

CHAPTER 4

SUMMARY AND CONCLUSIONS

Morphological and hydrological changes in rivers due to natural and anthropogenic induced changes were studied with the field and numerical investigations. Two studies were presented herein. The first study focused on the impacts of dam construction and channelization works on the Lower Missouri River, USA. The second study focuses on the changes in channel morphology and bed material characteristics in the fluvial-tidal transition zone of Altamaha River, USA.

The major findings of these two study cases are separately summarized below.

4.1 CHANGES IN RIVER MORPHOLOGY AND HYDROLOGY DUE TO IMPACT OF DAM CONSTRUCTION AND CHANNEL MODIFICATION: CASE STUDY OF THE LOWER MISSOURI RIVER, USA

The Lower Missouri River is the ~1300 km long reach of the Missouri River starting at Gavins Point Dam, SD, and ending at the Mississippi River – Missouri River confluence, MO. The Lower Missouri River basin is regulated by dams and river-engineering structures. In particular, the closure of dams causes a significant truncation for peak flows below the dam and hold fine sediment in dam reservoirs. While channel bank stabilization and narrowing prevent lateral bank erosion and create a *stable channel* for navigation purposes.

The morphological and hydrological response of the Lower Missouri River to river engineering works were approached through the field measurement analysis and numerical simulations. We first collected and analyzed the available mean daily flow and suspended sand load data for pre-and post-dam downstream the Gavins Point Dam, SD, to the Mississippi River – Missouri River confluence at St. Louis, MO. Suspended sand load data for major tributaries at the study reach also collected and analyzed to account for lateral sand load feeding from major tributaries.

We then implemented a one-dimensional mathematical formulation of river morphodynamic to study the impact of dam closure and channel narrowing on the Lower Missouri River (large sand bed rivers). Model governing equations are the shallow water equation of open channel flow simplified with the aid of the quasi-steady approximation and the Exner equation of conservation of bed material. Flow resistances and suspended sand load were computed with the Wright and Parker (2004) formulation for large, low slope sand bed rivers. The model was zeroed based on pre-dam field scale by comparing model predication with field measurement. The major findings of this study were:

- The post-dam peak discharge and suspended sand load have reduced remarkably downstream the dam to the upstream of the Missouri River – Platte River confluence and recovered gradually to pre-dam levels downstream of the Missouri River – Grand River confluence when major tributaries meet the mainstem.

- The post-dam low flow magnitude (probability of exceedance smaller than 0.6) is significantly higher than pre-dam low flow in the entire reach due to ensuring a safe navigation depth during low discharge periods.

105

- Field observations showed that as the drainage basin increased the reduction in suspended sand load associated with flow regulation became less important. A decline in suspended sand load of about ~30% from pre-dam values occurred upstream of the Missouri River – Kansas River confluence. A ~20% decrease in suspended sand load from pre-dam values were observed at the USGS station downstream of the Missouri River – Kansas River confluence and virtually no change in suspended sand load was predicted and observed in the downstream of the Missouri River – Grand River confluence, i.e. Hermann, MO.

- Long term model simulation suggested that there is no significant change in mean annual suspended sand load at Hermann (RK 158), MO, if there is no change in flow regime.

- The Missouri River – Grand River confluence (903 km downstream of Gavins Point Dam) can be seen as the location that disconnects between the regulated and unregulated reach in term of changes in flow and sand load due to engineering works.

- One-dimensional simulations of river morphodynamics and field observations showed that the channel response to narrowing and flow regulation was characterized by widespread channel bed erosion. Larger erosion rates were observed and predicted in the upstream part of the domain, i.e. upstream of the Missouri River – Grand River confluence.

- The model reasonably predicted the magnitude and temporal change of water surface elevation associated with the engineering works. Model results obtained

106

with 20 year-long post-dam flow duration curves showed an overall better agreement with field data than the results obtained using a single flow duration curve for the 1955-2015 period.

These results of this study suggest that the observed decline in suspended sediment concentration near the Mississippi River – Missouri River confluence has to be associated with a decline is wash load more than suspended bed material (sand) load. Further, the long term impact of the engineering works on the Missouri River will not be a major reduction in suspended sand load downstream of the Missouri River – Grand River confluence and thus the sand supply to the Mississippi River will likely remain close to historical values if major changes in the Missouri River flow regime and geometry will not occur.

4.2 CHANGES IN CHANNEL MORPHOLOGY AND SEDIMENT CHARACTERISTICS ACROSS A FLUVIAL TIDAL TRANSITION ZONE: CASE STUDY OF THE ALTAMAHA RIVER, USA

The Altamaha River is a tide-affected river in Georgia, USA and it runs for ~200 km from the confluence of the Ocmulgee and Oconee rivers to the Atlantic Ocean. Recently, morphological studies have shown changes in channel characteristics and sediment grain size distribution across the fluvial tidal transition zone. The sources of these changes, however, are still poorly understood. In this study we use field data collected in the fluvial and tidal dominated reaches of Altamaha River to investigate the causes of the observed changes in channel geometry and sediment grain size.

107

The study reach is a ~47 km long section between 29-76 km (0 km at the mouth). The total study reach was splitted into two reaches depending on maximum upstream tide penetration during monitoring period: The upstream fluvial reach, which has no tide effect and the downstream mixed tidal-fluvial which experiences periodic tide effect. The statistical significance of the observed changes in channel geometry, river bed profile and sinuosity, and bed grain size data for both fluvial and tidal reaches were tested with Spearman's rho non-parametric test to reveal the trends of these parameters along the study reach.

Spatial changes in observed stream power and shields number were employed to explain the observed trends of channel geometry and bed material distribution. In particular, the spatial variability of the dimensionless Shields number is used as a physical approach to understand the spatial change in grain size distribution and to explain channel capacity to either entrain or mobilize. While the spatial variability of stream power is used to interpret some changes in channel geometry properties.

The following major findings were made in this case study.

- The fluvial-tidal transient reach is approximately 1-4 km long extending from km 51 to km 47. Over this relatively short distance reach, abrupt discontinuities in trends of cross-section area, hydraulic radius and depth, width to depth ratio, median grain size, sinuosity and channel bed and water surface slopes are detected. This discontinuity in the trend of the mentioned parameters addresses the fluvial and tidal dominated reaches with distinctive characteristics.

- The fluvial reach is characterized by an increasing trend of cross-sectional area, hydraulic radius and depth and a decreasing in the trend of width to depth ratio.

108

- The tidal-dominated reach is characterized by an increasing trend of width to depth ratio and a decreasing trend of cross-sectional area, hydraulic radius and depth.

- Channel width increases slightly along the fluvial reach and increases measurably along the tidal dominated reach. Median grain size and sinuosity decrease seaward with a sharp decline near the boundary between fluvial and tidal dominated reaches.

- The abrupt changes in trends of channel geometry and median grain size that can be associated with a remarkable decline in estimates of unit stream power and dimensionless Shields number which declined by 82% and 42%, respectively. These analyses further illustrate that the fluvial reach has higher stream power and transport capacity than the downstream tide-dominated reach.

- The distribution of stream power and Shields number can be used to explain some of the fluvial-tidal transition channel adjustments in channel hydraulics, geometry and planform, and it provides some insight on the channel conditions that transition from seaward-deepening along fluvial reach to seaward shallowing along the tidal reach, leading to adjustments in, for example, cross-section area of flow. This may explain why the channel planform displays meandering and associated dissipation of the excess energy and the maintenance of straight channel for tidal dominated reach to ensure enough power for sediment transport over the relatively low slope.

These results are consistent with recent observations from modern tide environments that have referenced spatial changes in channel morphology across the of fluvial-tidal transition zone (Torres, 2017; Kastner et al., 2017; Gugliotta et al., 2017; Gurnell, 1997; Ensign et al.,2012; Ensign et al.,2017). Together, these studies may

109

introduce a framework schematic models for geomorphological common features and trends of the fluvial-tidal transition zone. With respect to interpretation and explanation of these changes, this study suggests that the changes in the trend of channel geometry and grain size distribution at the boundary between fluvial and tidal reaches can be explained with respect to spatial changes in stream power and sediment transport capacity that represented here with dimensionless Shields number for initiation of sediment motion.

REFERENCES

Agha, O. M. M., & Şarlak, N. (2016). Spatial and temporal patterns of climate variables in Iraq. *Arabian Journal of Geosciences*, *9*(4), 302.

Allison, M.A., Demas, C.R., Ebersole, B.A., Kleiss, B.A., Little, C.D., Meselhe, E.A., Powell, N.J., Pratt, T.C. and Vosburg, B.M. (2012). A water and sediment budget for the lower Mississippi–Atchafalaya River in flood years 2008–2010: implications for sediment discharge to the oceans and coastal restoration in Louisiana. *Journal of Hydrology*, *432*, 84-97.

Andrews, E. D. (1986). Downstream effects of flaming gorge reservoir on the Green River, Colorado, and Utah. *Geological Society of America Bulletin*, *97*(8), 1012-1023.

Ashida, K., and M. Michiue (1972). Study on hydraulic resistance and bed-load transport rate in alluvial streams, In *Proceedings of the Japan Society of Civil Engineers*, 206: 59–69.

Bagnold, R. A. (1966). An approach to the sediment transport problem from general physics. *U.S. Geological Survey Professional Paper* 422-1, 37.

Bagnold, R. A. (1980). An empirical correlation of bedload transport rates in flumes and natural rivers. *Proceedings of the Royal Society of London* A: Mathematical, Physical and Engineering Sciences, 36, 469–471.

Baker, V. R., & Costa, J. E. (1987). Flood power. *In Catastrophic flooding*. Allen & Unwin; Binghamton Symposia in Geomorphology, International Series. 1–24

Benn, P. C., & Erskine, W. D. (1994). Complex channel response to flow regulation: Cudgegong River below Windamere Dam, Australia. *Applied Geography*, *14(*2): 153-168.

Blevins, D. W., Wilkison, D. H., & Niesen, S. L. (2014). Pre-and post-impoundment nitrogen in the lower Missouri River. *Hydrological Processes*, *28*(4): 2535-2549.

Blom, A. (2012). Three effects of bedforms on the river bed profile. *River Flow*– Murillo (Ed.) © 2012 Taylor & Francis Group, London, ISBN 978-0-415-62129-8, 581–587.

Blom, A., Viparelli, E., & Chavarrías, V. (2016). The graded alluvial river: Profile concavity and downstream fining. *Geophysical Research Letters*, *43*(12): 6285-6293.

Blum, M. D., & Roberts, H. H. (2014). Is sand in the Mississippi River delta a sustainable resource? *Nature Geoscience*, *7*(12): 851.

Blum, M., Martin, J., Milliken, K., & Garvin, M. (2013). Paleovalley systems: insights from Quaternary analogs and experiments. *Earth-Science Reviews,* 116, 128-169.

Boix-Fayos, C., Barberá, G. G., López-Bermúdez, F., & Castillo, V. M. (2007). Effects of check dams, reforestation and land-use changes on river channel morphology: case study of the Rogativa catchment (Murcia, Spain). *Geomorphology*, *91*(1-2): 103-123.

Bolla Pittaluga, M., Tambroni, N., Canestrelli, A., Slingerland, R., Lanzoni, S., & Seminara, G. (2015). Where river and tide meet: The morphodynamic equilibrium of alluvial estuaries. *Journal of Geophysical Research: Earth Surface*, 120(1), 75-94.

Brandt, S. A. (2000). Classification of geomorphological effects downstream of dams. *Catena*, *40*(4): 375-401.

Branyan, R. L. (1974). Taming the Mighty Missouri: A History of the Kansas City District Corps of Engineers 1907-1971. US Army Corps of Engineers, Kansas City District Corps.

Bridge, J. S. (1981). Hydraulic interpretation of grain-size distributions using a physical model for bedload transport. *Journal of Sedimentary Research*, *51*(4), 1109-1124.

Brownlie, W. R. (1981). Prediction of flow depth and sediment discharge in open channels. Keck Laboratory of Hydraulics & Water Resources, Caltech.

Buffington JM. (2012). Changes in channel morphology over human time scale. *In Gravel-Bed Rivers: Processes, Tools, Environments*, Church M, Biron P, Roy A (eds), 1st edn. John Wiley & Sons. 433-463.

Bull, W. B. (1979). Threshold of critical power in streams. *Geological Society of America Bulletin*, *90*(5), 453-464.

Cai, H., Savenije, H. H., & Yang, Q. (2016). Backwater hydrodynamics in a tidal river. *18th Physics of Estuaries and Coastal Seas Conference.*

Carlston, C. W. (1969). Longitudinal slope characteristics of rivers of the midcontinent and the Atlantic East Gulf Slopes. International Association of Scientific Hydrology. Bulletin, *14*(4): 21-31.

Chatanantavet, P., Lamb, M. P., & Nittrouer, J. A. (2012). Backwater controls of avulsion location on deltas. *Geophysical Research Letters*, *39*(1).

Chaudhry, M. H. (2008). Open-channel flow, in: 2nd Edition. Springer US, New York, :493-497.

Chen, M. S., Wartel, S., Van Eck, B., & Van Maldegem, D. (2005). Suspended matter in the Scheldt estuary. *Hydrobiologia*, *540*(1-3), 79-104.

Church, M. (1995). Geomorphic response to river flow regulation: Case studies and time-scales. *River Research and Applications*, *11*(1), 3-22.

Colquhoun, D. J. (1969) Geomorphology of the lower coastal plain of South Carolina: *South Carolina Div. Geology*, Pub. MS-15, 36 p.

Colquhoun, D.J. (1968) Coastal plains, *in* Fairbridge, R.W., ed., The Encyclopedia of Geomorphology: *New York, Reinhold Book Corp*., 1296 p.,

Cook, T. L., Sommerfield, C. K., & Wong, K. C. (2007). Observations of tidal and springtime sediment transport in the upper Delaware Estuary. Estuarine, *Coastal and Shelf Science*, 72(1), 235-246.

Couperthwaite, J. S. (1997). Downstream change in channel hydraulics along the River Severn , UK by School of Geography, UK (Doctoral dissertation, University of Birmingham), 63-66.

Cui, Y., Braudrick, C., Dietrich, W. E., Cluer, B., & Parker, G. (2006). Dam removal express assessment models (dream) part 2: Sample runs/sensitivity tests. *Journal of Hydraulic Research*, *44*(3), 308-323.

Dalrymple, R. W., & Choi, K. (2007). Morphologic and facies trends through the fluvial–marine transition in tide-dominated depositional systems: a schematic framework for environmental and sequence-stratigraphic interpretation. *Earth-Science Reviews*, 81(3), 135-174.

Dalrymple, R. W., Kurcinka, C. E., Jablonski, B. V. J., Ichaso, A. A., & Mackay, D. A. (2015). Deciphering the relative importance of fluvial and tidal processes in the fluvial–marine transition. Fluvial-tidal sedimentology: Oxford, United Kingdom, Elsevier, *Developments in Sedimentology*, 68, 3-45.

Dalrymple, R. W., Mackay, D. A., Ichaso, A. A., & Choi, K. S. (2012). Processes, morphodynamics, and facies of tide-dominated estuaries. *In Principles of Tidal Sedimentology* (pp. 79-107). Springer Netherlands.

Dalrymple, R. W., Zaitlin, B. A., & Boyd, R. (1992). Estuarine facies models: conceptual basis and stratigraphic implications: perspective. *Journal of Sedimentary Research*, 62(6).

Dashtgard, S. E., & La Croix, A. D. (2015). Sedimentological trends across the tidal–fluvial transition, Fraser River, Canada: A review and some broader implications. Fluvial–Tidal Sedimentology, *Developments in Sedimentology*, Elsevier, Amsterdam, 111-126.

Dashtgard, S. E., Venditti, J. G., Hill, P. R., Sisulak, C. F., Johnson, S. M., & La Croix, A. D. (2012). Sedimentation across the tidal–fluvial transition in the Lower Fraser River, Canada. SEPM, *The Sedimentary Record*, 10(4), 4-9.

de Vries, M. (1965). Considerations about non-steady bed-load transport in open channels. In: Proceedings of the *11*th Congress International Association for Hydraulic Research, Leningrad.

Donner, S. D., Kucharik, C. J., & Foley, J. A. (2004). Impact of changing land use practices on nitrate export by the Mississippi River. Global Biogeochemical Cycles, *18*(1).

Ensign, S. H., Doyle, M. W., & Piehler, M. F. (2013). The effect of tide on the hydrology and morphology of a freshwater river. *Earth Surface Processes and Landforms*, 38(6), 655-660.

Ensign, S. H., Noe, G. B., & Hupp, C. R. (2014). Linking channel hydrology with riparian wetland accretion in tidal rivers. *Journal of Geophysical Research: Earth Surface*, *119*(1), 28-44.

Ensign, S. H., Noe, G. B., Hupp, C. R., & Skalak, K. J. (2015). Head-of-tide bottleneck of particulate material transport from watersheds to estuaries. *Geophysical Research Letters*, *42*(24), 10-671.

Ferrell, J. R. (1993). Big dam era: A legislative and institutional history of the Pick-Sloan Missouri basin program. U.S Army Corps of Engineers, Missouri River Division, Omaha, NE., 252 pp. http://www.dtic.mil/get-tr-doc/pdf?AD=ADA635437

Freitas, P. T., Silveira, O. F., & Asp, N. E. (2012). Tide distortion and attenuation in an Amazonian tidal river. *Brazilian Journal of Oceanography*, 60 (4), 429-446.

Friedrichs, C. T. (1995). Stability shear stress and equilibrium cross-sectional geometry of sheltered tidal channels. *Journal of Coastal Research*, 1062-1074.

Futawatari, T., Kusuda, T., Koga, K., Araki, H., Umita, T., & Furumoto, K. (1988). Development of a new simulation method for suspended sediment transport in a tidal river. *Water Science & Technology*, 20(6-7), 103-112.

Galat, D. L., & Lipkin, R. (2000). Restoring ecological integrity of great rivers: historical hydrographs aid in defining reference conditions for the Missouri River. In *Assessing the Ecological Integrity of Running Waters* (pp. 29-48). Springer, Dordrecht.

Galat, D. L., J. W. Robinson, and L. W. Hesse. (1996). Restoring aquatic resources to the lower Missouri River: Issues and initiatives. *In Overview of river-floodplain ecology in the Upper Mississippi River Basin*, edited by D. L. Galat and A. G.

116

Frazier. Vol. 3 of *Science for floodplain management into the 21st century*, edited by J. A. Kelmelis. Washington, DC: U.S. Government Printing Office, 3:49-71

Galay, V. J. (1983). Causes of river bed degradation. *Water resources research*, *19*(5), 1057-1090.

Ganju, N. K., Schoellhamer, D. H., Warner, J. C., Barad, M. F., & Schladow, S. G. (2004). Tidal oscillation of sediment between a river and a bay: a conceptual model. *Estuarine, Coastal and Shelf Science*, 60(1), 81-90.

Garcia, M. H. (2008) Sediment transport and morphodynamics, Chapter 2 in M. H. Garcia eds. Sedimentation Engineering Processes, Measurements, Modeling and Practice, *ASCE Manuals and Reports on Engineering Practice* No. 110, Reston, VA.

Giese, B. S., & Jay, D. A. (1989). Modelling tidal energetics of the Columbia River estuary. *Estuarine, Coastal and Shelf Science*, *29*(6), 549-571.

Gregory, K. J. (2006). The human role in changing river channels. *Geomorphology*, *79*(3), 172-191.

Grey, J. R. and Simoes, J. M. (2008), Estimating Sediment Discharge, Appendix D in M. H. Garcia ed. Sedimentation Engineering Processes, Measurements, Modeling and Practice, *ASCE Manuals and Reports on Engineering Practice* No. *110*: 1067-1088.

Gugliotta, M., Saito, Y., Nguyen, V.L., Ta, T.K.O., Nakashima, R., Tamura, T., Uehara, K., Katsuki, K., Yamamoto, S. (2017). Process regime, salinity, morphological, and sedimentary trends along the fluvial to marine transition zone of the mixed-energy Mekong River delta, Vietnam. *Continental Shelf Research*, *147*, 7-26.

Guo, L., Van der Wegen, M., Roelvink, J. A., & He, Q. (2014). The role of river flow and

tidal asymmetry on 1-D estuarine morphodynamics. *Journal of Geophysical Research: Earth Surface*, *119*(11), 2315-2334.

Gurnell, A. M. (1997). Adjustments in River Channel Geometry Associated With Hydraulic Discontinuities Across the Fluvial – Tidal Transition of a Regulated River, *Journal of Earth Surface Processes and Landforms*, VOL 22, 967–985.

Gurnell, A. M. (1997). Adjustments in river channel geometry associated with hydraulic discontinuities across the fluvial–tidal transition of a regulated river. *Earth Surface Processes and Landforms: The Journal of the British Geomorphological Group*, *22*(10): 967-985.

Halberg, G. (1981). Historic changes along the Missouri River. Iowa Geol, 6: 10-12.

Hassan, M. A., Roberge, L., Church, M., More, M., Donner, S. D., Leach, J., & Ali, K. F. (2017). What are the contemporary sources of sediment in the Mississippi River? Geophysical Research Letters, *44*(17):8919-8924.

Heimann, D. C., Sprague, L. A., & Blevins, D. W. (2011). Trends in suspended-sediment loads and concentrations in the Mississippi River Basin, 1950–2009 (No. 2011-5200). US Geological Survey.

Heine, R. A., & Lant, C. L. (2009). Spatial and temporal patterns of stream channel incision in the loess region of the Missouri River. Annals of the Association of American Geographers, *99*(2): 231-253.

Hidayat, H., Vermeulen, B., Sassi, M. G., Torfs, P. J. J. F., & Hoitink, A. J. F. (2011). Discharge estimation in a backwater affected meandering river. *Hydrology and earth system sciences*, *15*(8), 2717-2728.

Holly Jr, F. M., & Karim, M. F. (1986). Simulation of Missouri River bed degradation. Journal of Hydraulic Engineering, *112*(6): 497-516.

Horowitz, A. J., Elrick, K. A., & Smith, J. J. (2001). Annual suspended sediment and trace element fluxes in the Mississippi, Columbia, Colorado, and Rio Grande drainage basins. Hydrological Processes, *15*(7): 1169-1207.

Horrevoets, A. C., Savenije, H. H. G., Schuurman, J. N., & Graas, S. (2004). The influence of river discharge on tidal damping in alluvial estuaries. *Journal of Hydrology*, *294*(4), 213-228.

Horsak, M., Bojková, J., Zahrádková, S., Omesova, M., & Helešic, J. (2009). Impact of reservoirs and channelization on lowland river macroinvertebrates: A case study from Central Europe. *Limnologica-Ecology and Management of Inland Waters*, *39*(2), 140-151.

ICOLD (1988). World Register of Dams, *Update. International Commission on Large Dams*, Paris.

Jacobson, R. B., & Galat, D. L. (2008). Design of a naturalized flow regime—an example from the lower Missouri River, USA. Ecohydrology, *1*(2): 81-104.

Jacobson, R. B., Blevins, D. W., & Bitner, C. J. (2009). Sediment regime constraints on river restoration—An example from the Lower Missouri River. *Geological Society of America Special Paper*, 451: 1-22.

Jiang, L. Q., Cai, W. J., & Wang, Y. (2008). A comparative study of carbon dioxide degassing in river-and marine-dominated estuaries. *Limnology and Oceanography*, *53*(6), 2603-2615.

Jordan, P. R. (1965). Fluvial Sediment of The Mississippi River at St. Louis, Missouri. US Government Printing Office in Cooperation with The U.S. Army Corps of Engineers. Washington.

Joshi, S., & Xu, Y. J. (2015). Assessment of suspended sand availability under different flow conditions of the Lowermost Mississippi River at Tarbert Landing during 1973–2013. *Water*, *7*(12): 7022-7044.

Julien, P. Y., & Wargadalam, J. (1995). Alluvial channel geometry: theory and applications. *Journal of Hydraulic Engineering*, *121*(4): 312-325.

Kang, K., & Di Iorio, D. (2006). Depth-and current-induced effects on wave propagation into the Altamaha River Estuary, Georgia. *Estuarine, Coastal and Shelf Science*, *66*(3-4), 395-408.

Kästner, K., Hoitink, A. J. F., Vermeulen, B., Geertsema, T. J., & Ningsih, N. S. (2017). Distributary channels in the fluvial to tidal transition zone. *Journal of Geophysical Research: Earth Surface*, *122*(3), 696-710.

Kemp, G. P., Day, J. W., Rogers, J. D., Giosan, L., & Peyronnin, N. (2016). Enhancing mud supply from the Lower Missouri River to the Mississippi River Delta USA: Dam bypassing and coastal restoration. Estuarine, Coastal and Shelf Science, *183*: 304-313.

Keown, M. P., Dardeau, E. A., & Causey, E. M. (1986). Historic trends in the sediment flow regime of the Mississippi River. *Water Resources Research*, *22*(11): 1555-1564.

Kiraga, M., & Popek, Z. (2016). Using a Modified Lane's Relation in Local Bed Scouring Studies in the Laboratory Channel. *Water*, 8(1), 16.

Knight, D. W. (1981). Some field measurements concerned with the behavior of resistance coefficients in a tidal channel. *Estuarine, coastal and shelf science*, 12(3), 303-322.

Knighton, A. D. (1999). Downstream variation in stream power. *Geomorphology*, 29(3-4), 293-306.

Knox, J. C. (2007). The Mississippi river system. In *Large Rivers: Geomorphology and Management*, (Gupta A(ed) John Wiley & Sons: Chichester; 145-182.

Lamb, M. P., Nittrouer, J. A., Mohrig, D., & Shaw, J. (2012). Backwater and river plume controls on scour upstream of river mouths: Implications for fluvio-deltaic morphodynamics. *Journal of Geophysical Research: Earth Surface*, *117*(F1).

Lane, E. W. (1955). Importance of fluvial morphology in hydraulic engineering. *Proceedings of American Society of Civil Engineers, 81*(745): 17.

Lane, E.W. (1937). Stable channels in erodible material. *American Society of Civil Engineers Transactions 102*: 123–142.

Lane, S. N., Tayefi, V., Reid, S. C., Yu, D., & Hardy, R. J. (2007). Interactions between sediment delivery, channel change, climate change and flood risk in a temperate upland environment. *Earth Surface Processes and Landforms*, *32*(3): 429-446.

Lauer, J. W., and G. Parker. (2008a). Modeling framework for sediment deposition, storage, and evacuation in the floodplain of a meandering river: Theory, *Water Resources Research*, 44, W04425, doi:10.1029/2006WR005528.

Lauer, J. W., and G. Parker. (2008b). Modeling framework for sediment deposition, storage, and evacuation in the floodplain of a meandering river: Application to the Clark Fork River, Montana, *Water Resources Research*, 44, W08404, doi:10.1029/2006WR005529.

Lawrence Oghale O. O., Edeme Antia, Soronnadi-Ononiwo G. C., Powedei Debekeme. Grain Size Distribution of a Modern Tidal River: A Case Study of Calabar River, South-South Nigeria. *International Journal of Science and Research* (IJSR), 4 (1). 2015.

Leonardi, N., Kolker, A. S., & Fagherazzi, S. (2015). Interplay between river discharge and tides in a delta distributary. *Advances in Water Resources*, 80, 69-78.

Leopold, L. B., & Maddock Jr, T. (1953). The hydraulic geometry of stream channels and some physiographic implications. *Geological Survey Professional Paper 252*, Washington, DC: United States Government Printing Office.

Leopold, L.B., Wolman, M.G., and Miller, J.P. (1964). Fluvial processes in geomorphology: *San Francisco, W.H. Freeman, and Co.*, 241- 246.

Li, Y., Sun, Z., Liu, Y., & Deng, J. (2009). Channel degradation downstream from the Three Gorges Project and its impacts on flood level. *Journal of Hydraulic Engineering*, *135*(9): 718-728.

Livesey, R. H. (1965). Channel armoring below Fort Randall Dam. In *Proceedings of the Federal Inter-Agency Sedimentation Conference 1963*. US Department of Agriculture Miscellaneous Publication 970: 461–470.

Mackin, J.H. (1948). Concept of the graded river. *Geological Society of America Bulletin*, *59*(5): 463-512.

Magilligan, F. J., & Nislow, K. H. (2005). Changes in hydrologic regime by dams. *Geomorphology*, *71*(1-2): 61-78.

Martinius, A. W., & Gowland, S. (2011). Tide-influenced fluvial bedforms and tidal bore deposits (Late Jurassic Lourinhã Formation, Lusitanian Basin, Western

Portugal). *Sedimentology*, 58(1), 285-324.

Meade, R. H., & Moody, J. A. (2010). Causes for the decline of suspended-sediment discharge in the Mississippi River system, 1940–2007. *Hydrological Processes*, *24*(1): 35-49.

Meade, R. H., & Parker, R. S. (1985). Sediment in rivers of the United States. *US Geological Survey Water-Supply Paper, 2275*: 49-60.

Meade, R. H., Rayol, J. M., Da Conceicão, S. C., & Natividade, J. R. (1991). Backwater effects in the Amazon River basin of Brazil. *Environmental Geology and Water Sciences*, *18*(2), 105-114.

Meade, R. H., Yuzyk, T. R., & Day, T. J. (1990). Movement and storage of sediment in rivers of the United States and Canada. IN: *Surface Water Hydrology*, vol. O-1, Wolman MG, Riggs HC (eds.) Geological Society of America, The Geology of North America: Boulder, Colorado. p 255-280.

Nittrouer, J. A., & Viparelli, E. (2014). Sand as a stable and sustainable resource for nourishing the Mississippi River delta. *Nature Geoscience*, *7*(5): 350-354.

Ortega, J. A., Razola, L., & Garzón, G. (2014). Recent human impacts and change in dynamics and morphology of ephemeral rivers. *Natural Hazards and Earth System Sciences*, *14*(3): 713-730.

Parker, G. (2004). sediment transport morphodynamics with applications to rivers and turbidity currents, Chapters 2, 5 and 6. This is an e-book with PowerPoint presentations, Excel worksheets with embedded working programs in Visual Basic for Applications, Word files with extended explanation and video clips. http://hydrolab.illinois.edu/people/parkerg/morphodynamics_e-book.htm

Parker, G., (2008). Transport of gravel and sediment mixtures, Chapter 3 in M. H. Garcia eds. Sedimentation Engineering Processes, Measurements, Modeling and Practice, *ASCE Manuals and Reports on Engineering Practice* No. 110, Reston, VA. *110*: 165-251.

Pegg, M. A., & Pierce, C. L. (2002). Classification of reaches in the Missouri and lower Yellowstone Rivers based on flow characteristics. *River Research and Applications*, *18*(1): 31-42.

Pegg, M. A., Pierce, C. L., & Roy, A. (2003). Hydrological alteration along the Missouri River basin: a time series approach. Aquatic Sciences, *65*(1): 63-72.

Petersen-Overleir, A. (2006). Modelling stage—discharge relationships affected by hysteresis using the Jones formula and nonlinear regression. *Hydrological sciences journal*, *51*(3), 365-388.

Petts, G. E. (1979). Complex response of river channel morphology subsequent to reservoir construction. *Progress in Physical Geography*, *3*(3): 329-362.

Petts, G. E., & Gurnell, A. M. (2005). Dams and geomorphology: research progress and future directions. *Geomorphology*, *71*(1-2): 27-47.

Phillips, J. D. (1992). Delivery of upper-basin sediment to the lower Neuse River, North Carolina, USA. *Earth Surface Processes and Landforms*, *17*(7), 699-709.

Phillips, J. D., & Slattery, M. C. (2007). Downstream trends in discharge, slope, and stream power in a lower coastal plain river. *Journal of Hydrology*, *334*(1-2), 290-303.

Pickup, G. (1976). Alternative measures of river channel shape and their significance. *Journal of Hydrology (New Zealand)*, 15, 9-16.

Piest, R. F., & Spomer, R. G. (1968). Sheet and gully erosion in the Missouri Valley loessial region. *American Society of Agricultural Engineers Transactions*, *11*(6): 850-0853.

Pinter, N., & Heine, R. A. (2005). Hydrodynamic and morphodynamic response to river engineering documented by fixed-discharge analysis, Lower Missouri River, USA. *Journal of Hydrology*, *302*(1): 70-91.

Pišút, P. (2002). Channel evolution of the pre-channelized Danube River in Bratislava, Slovakia (1712–1886). *Earth Surface Processes and Landforms*, *27*(4), 369-390.

Pritchard, D. W. (1967). What is an estuary: physical viewpoint. *Estuaries*, 83, 3-5.

Renwick, W. H., & Ashley, G. M. (1984). Sources, storages, and sinks of fine-grained sediments in a fluvial-estuarine system. *Geological Society of America Bulletin*, 95(November), 1343–1348. http://doi.org/10.1130/0016-7606(1984)95<1343:SSASOF>2.0.CO;2.

Rijn, L. C. V. (1984). Sediment transport, part II: suspended load transport. *Journal of hydraulic engineering*, 110(11), 1613-1641.

Roebuck Jr, J. A., Medeiros, P. M., Letourneau, M. L., & Jaffé, R. (2018). Hydrological controls on the seasonal variability of dissolved and particulate black carbon in the Altamaha River, GA. *Journal of Geophysical Research: Biogeosciences*. 123. https://doi/epdf/10.1029/2018JG004406.

Sassi, M. G., Hoitink, A. J. F., Brye, B., & Deleersnijder, E. (2012). Downstream hydraulic geometry of a tidally influenced river delta. *Journal of Geophysical Research: Earth Surface*, 117(F4).

Savenije, H. H. (2015). Prediction in ungauged estuaries: An integrated theory. *Water Resources Research*, *51*(4), 2464-2476.

Schumm, S. A. (1960). The shape of alluvial channels in relation to sediment type. USGS Professional Paper 352-B, 17–30. Retrieved from https://pubs.er.usgs.gov/publication/pp352B.

Schumm, S. A. (1963). Sinuosity of alluvial rivers on the Great Plains. *Geological Society of America Bulletin*, *74*(9), 1089-1100.

Schumm, S. A., & Khan, H. R. (1972). Experimental study of channel patterns. *Geological Society of America Bulletin*, 83(6), 1755-1770.

Schumm, S.A. (1968). River Adjustment to Altered Hydrologic Regimen: *Murrumbidgee River and Paleochannels, Australia*. United States Geological Survey, Professional Paper 598.

Seminara, G., Lanzoni, S., Tambroni, N., & Toffolon, M. (2010). How long are tidal channels? *Journal of Fluid Mechanics*, 643(2005), 479. http://doi.org/10.1017/S0022112009992308

Sheldon, J. E., & Alber, M. (2002). A comparison of residence time calculations using simple compartment models of the Altamaha River Estuary, *Georgia. Estuaries*, 25(6), 1304-1317.

Simon, A. (1989). A model of channel response in disturbed alluvial channels. *Earth Surface Processes and Landforms*, *14*(1): 11-26.

Simon, A., & Rinaldi, M. (2000). Channel instability in the loess area of the Midwestern United States. *Jawra Journal of the American Water Resources Association*, *36*(1): 133-150.

Simon, A., & Rinaldi, M. (2006). Disturbance, stream incision, and channel evolution: The roles of excess transport capacity and boundary materials in controlling channel response. *Geomorphology*, *79*(3): 361-383.

Simon, A., Dickerson, W., & Heins, A. (2004). Suspended-sediment transport rates at the 1.5-year recurrence interval for ecoregions of the United States: transport conditions at the bankfull and effective discharge? *Geomorphology*, *58*(1): 243-262.

Skalak, K. J., Benthem, A. J., Schenk, E. R., Hupp, C. R., Galloway, J. M., Nustad, R. A., & Wiche, G. J. (2013). Large dams and alluvial rivers in the Anthropocene: The impacts of the Garrison and Oahe Dams on the Upper Missouri River. *Anthropocene*, *2*, 51-64.

Torres, R. (2017). Channel geomorphology along the fluvial-tidal transition, Santee River, USA. *GSA Bulletin*, *129*(11-12), 1681-1691.

U.S. Army Corps of Engineers. (1993). Aggradation, degradation, and water quality conditions: Missouri River mainstem Reservoir System. U.S. Army Corps of Engineers, Omaha District, Reservoir Control Center Technical Report ADA371403, 135p. http://oai.dtic.mil/oai/oai?verb=getRecord&metadataPrefix=html&identifier=ADA371403

U.S. Army Corps of Engineers. (2012). Missouri River stage trends: Omaha, Nebraska, U.S. Army Corps of Engineers, Northwestern Division, Reservoir Control Center Technical Report Ja-07, 36p. http://www.nwd-mr.usace.army.mil/rcc/reports/pdfs/MRStageTrends2012.pdf

U.S. Army Corps of Engineers. (2017). Missouri River Stage Trends. U.S. Army Corps of Engineers, Northwestern Division, Reservoir Control Center Technical Report A04: Omaha, NE; 43. http://www.nwd-mr.usace.army.mil/rcc/reports/pdfs/MRStageTrends2017.pdf

US Army Corps of Engineers. (2006). Upper Columbia Alternative Flood Control and Fish Operations, Columbia River Basin Final Environmental Impact Statement, U.S. Army Corps of Engineers, Seattle District, Appendix C. https://www.usbr.gov/pn/fcrps/documents/ucaaltflood.pdf

USDA, Natural Resources Conservation Service. (2007). Lower Missouri River Sub-basin. For more information: https://www.nrcs.usda.gov/Internet/FSE_DOCUMENTS/nrcs144p2_010958.pdf

Viparelli, E., Gaeuman, D., Wilcock, P., & Parker, G. (2011). A model to predict the evolution of a gravel bed river under an imposed cyclic hydrograph and its application to the Trinity River. *Water Resources Research*, *47*(2). W02533

Viparelli, E., Nittrouer, J. A., & Parker, G. (2015). Modeling flow and sediment transport dynamics in the lowermost Mississippi River, Louisiana, USA, with an upstream alluvial-bedrock transition and a downstream bedrock-alluvial transition: Implications for land building using engineered diversions. *Journal of Geophysical Research: Earth Surface, 120*(3): 534-563.

Wang, Z., Chen, Z., Li, M., Chen, J., & Zhao, Y. (2009). Variations in downstream grain-sizes to interpret sediment transport in the middle-lower Yangtze River, China: A pre-study of Three-Gorges Dam. *Geomorphology*, *113*(3-4), 217-229.

Williams, G. P., & Wolman, M. G. (1984). Downstream effects of dams on alluvial rivers. *Geological Survey Professional Paper 1286*: 8-12.

Wright, L. D., Coleman, J. M., & Thom, B. G. (1973). Processes of channel development in a high-tide-range environment: Cambridge Gulf-Ord River Delta, Western Australia. *The Journal of Geology*, *81*(1), 15-41.

Wright, L. D., Coleman, J. M., & Thom, B. G. (1973). Processes of channel development in a high-tide-range environment: Cambridge Gulf-Ord River Delta, Western Australia. *The Journal of Geology*, *81*(1): 15-41.

Wright, S., & Parker, G. (2004a). Density stratification effects in sand-bed rivers. *Journal of Hydraulic Engineering*, *130*(8): 783-795.

Wright, S., & Parker, G. (2004b). Flow resistance and suspended load in sand-bed rivers: simplified stratification model. *Journal of Hydraulic Engineering*, *130*(8): 796

Yankovsky, A. E., Torres, R., Torres-Garcia, L. M., & Jeon, K. (2012). Interaction of tidal and fluvial processes in the transition zone of the Santee River, SC, USA. *Estuaries and coasts*, *35*(6), 1500-1509. http://doi.org/10.1007/s12237-012-9535-6.

Yue, S., Pilon, P., & Cavadias, G. (2002). Power of the Mann–Kendall and Spearman's rho tests for detecting monotonic trends in hydrological series. *Journal of hydrology*, *259*(1-4), 254-271.

APPENDIX A

MEAN ANNUAL SUSPENDED SAND LOAD BASED ON SUSPENDED

SEDIMENT CONCENTRATION CURVE

Mean annual suspended sand loads are calculated from the available data collected at five USGS stations on the Missouri River mainstem. The station information (name and USGS ID) is reported in Tables A.1 with the estimated pre- and post-dam suspended sand loads, the period of record of suspended sediment concentration and the number of measurements used in the analysis. The procedures used to estimate the mean annual suspended sand loads is illustrated below.

Table A.1: Pre- and Post-dam Mean Annual Suspended Sand Load in the Lower Missouri River based on suspended sediment concentration rating curves. The asterisks identify measurements for which the volume fraction content of sand was not recorded.

U. S Geological Survey ID	Pre-dam load	Post-dam load	Period of available record	Number of measurements used in analysis
USGS ID: 06467500 Missouri River at Yankton, South Dakota	6.62	0.57	2000-2008	57
USGS ID: 06610000 Missouri River at Omaha, Nebraska	10.95	5.09	1953-1954*; 1971-1986, 1996-2015	2*; 432
USGS ID: 06818000 Missouri River at St. Joseph, Missouri	15.16	10.05	1948-1976*; 1977-1993, 2002-2015	600*; 400
USGS ID: 06893000 Missouri River at Kansas City, Missouri	23.18	14.4	1948-1968*;1989-1991, 2009-2015	255*; 231
USGS ID: 06934500 Missouri River at Hermann, Missouri	30.22	23.05	1948-1971*; 1972-2015	5049*; 811

In the pre-dam period, a limited number of suspended sediment concentration measurements are available at four stations on the Missouri River (Omaha, NE, St. Joseph, MO, Kansas City, MO, and Hermann, MO), but the volume fraction content of sand in suspension is not reported. To determine a pre-dam suspended sediment concentration rating curve, the suspended sediment concentrations were estimated from of the measured suspended sediment load, the flow discharge and the volume fraction content of sand in suspension (Grey and Simoes, 2008). Heimann et al. (2011) report the average fractions of sand in suspension were set equal to 0.43 at Omaha, NE, (39 samples); 0.26 at St. Joseph, MO, (13 samples); 0.15 at Kansas City, MO, (9 samples); and 0.2 at Hermann, MO, (12 samples), and these fractions have been used to estimate the pre-dam suspended sand rating curves. At Yankton, SD, where pre-dam suspended sediment concentration data are not available, the suspended sediment concentration rating curve based on data collected between 2000 and 2008 was assumed to be representative of pre- and post-dam suspended sediment concentration.

The post-dam suspended sand rating curves at the five stations on the Missouri River of Table A.1 were built with all the available data collected after the 1954 for which the volume fraction content of sand in suspension was reported. Due to the lack of measurements of instantaneous discharge for a significant number of post-dam data and for all the pre-dam data, the suspended sand load was estimated by using the rating curve between daily discharge and suspended sand concentration. Figure A.1 to A.4 shows pre- and post-dam suspended sediment concentration rating curves at four USGS stations on the Missouri River mainstem.
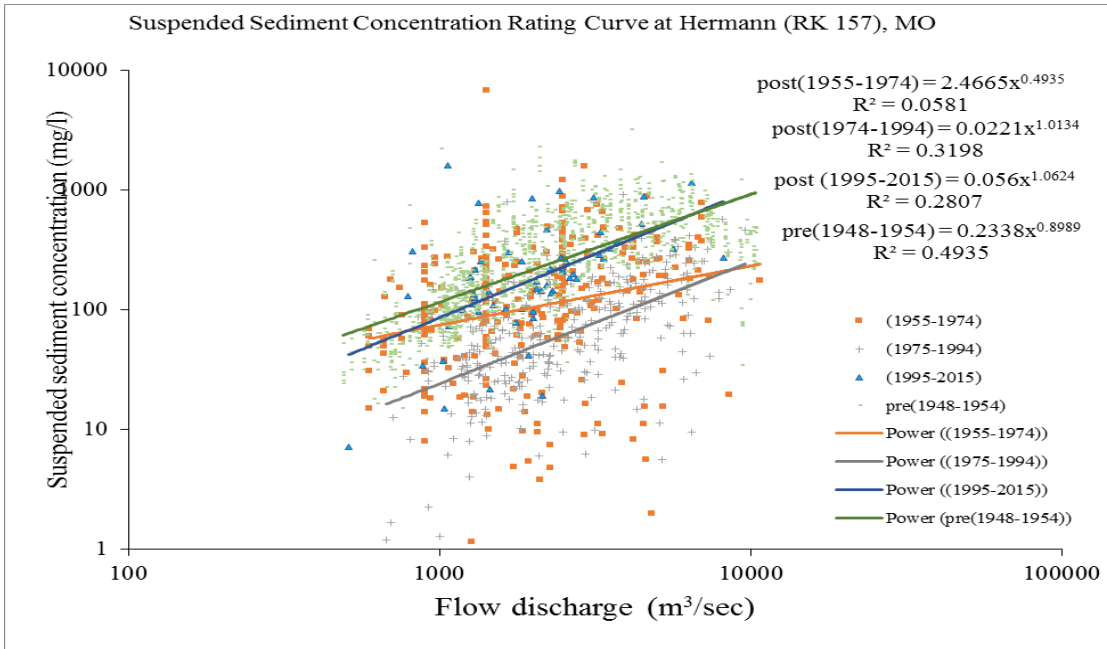
Figure A.1: Pre- and post-dam suspended sediment concentration rating curve of Missouri River at Hermann (RK 157), MO.
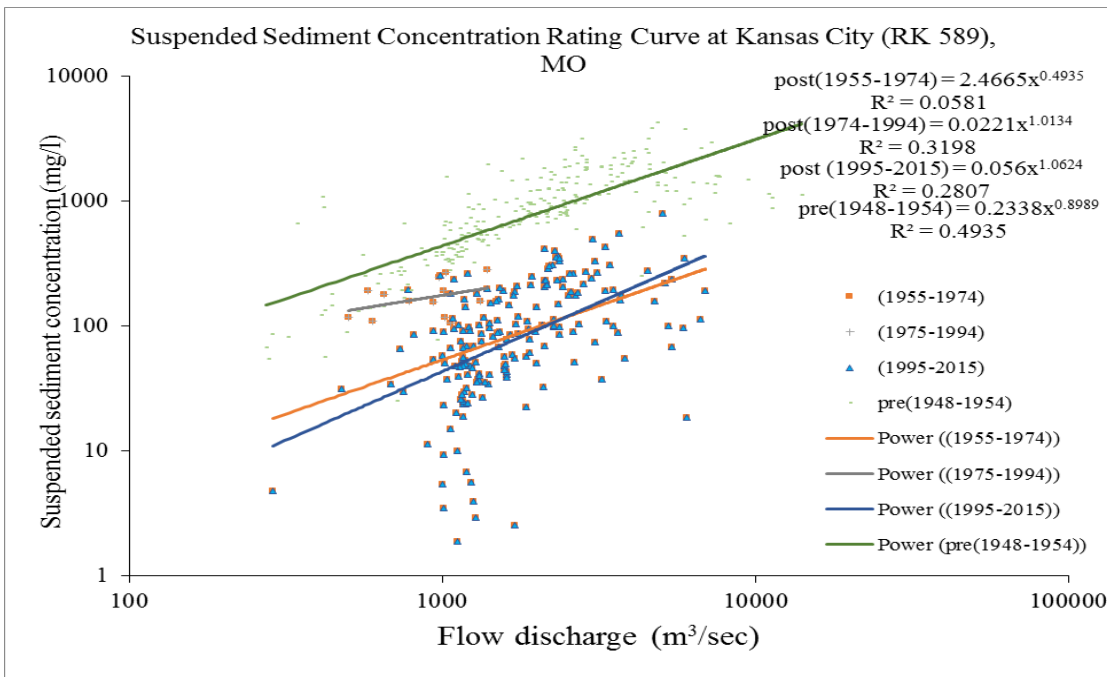

Figure A.2: Pre- and post-dam suspended sediment concentration rating curve of Missouri River at Kansas City (RK 589), MO.
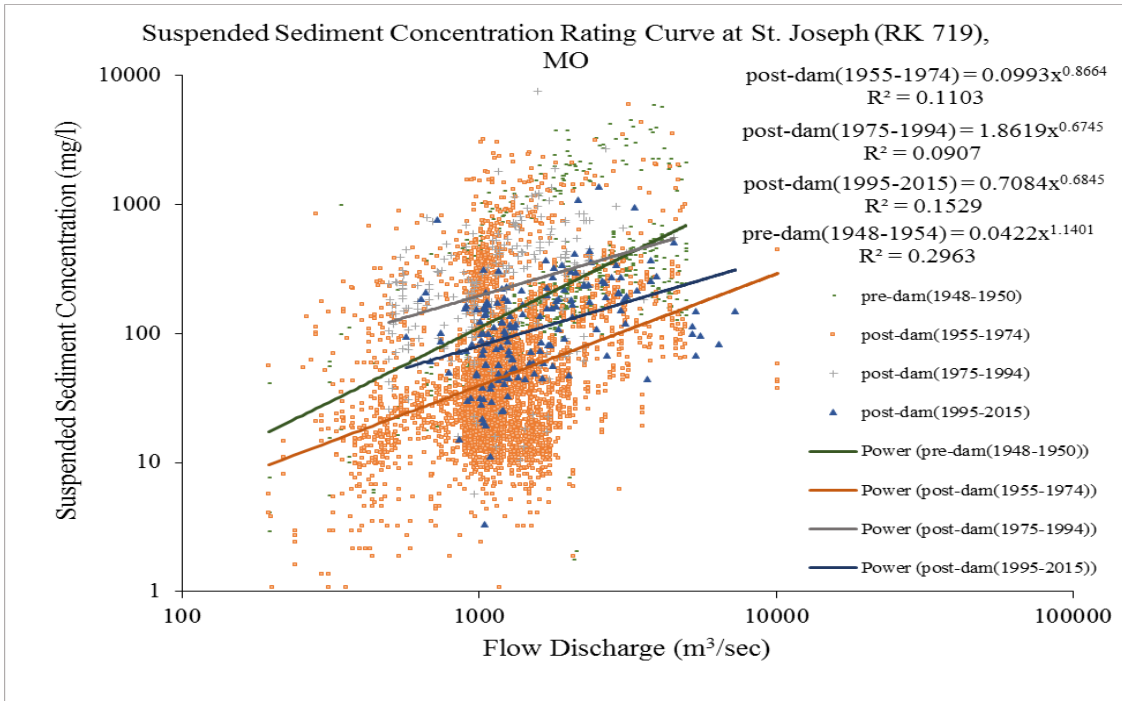
132

Figure A.3: Pre- and post-dam suspended sediment concentration rating curve of Missouri River at St. Joseph (RK 719), MO.
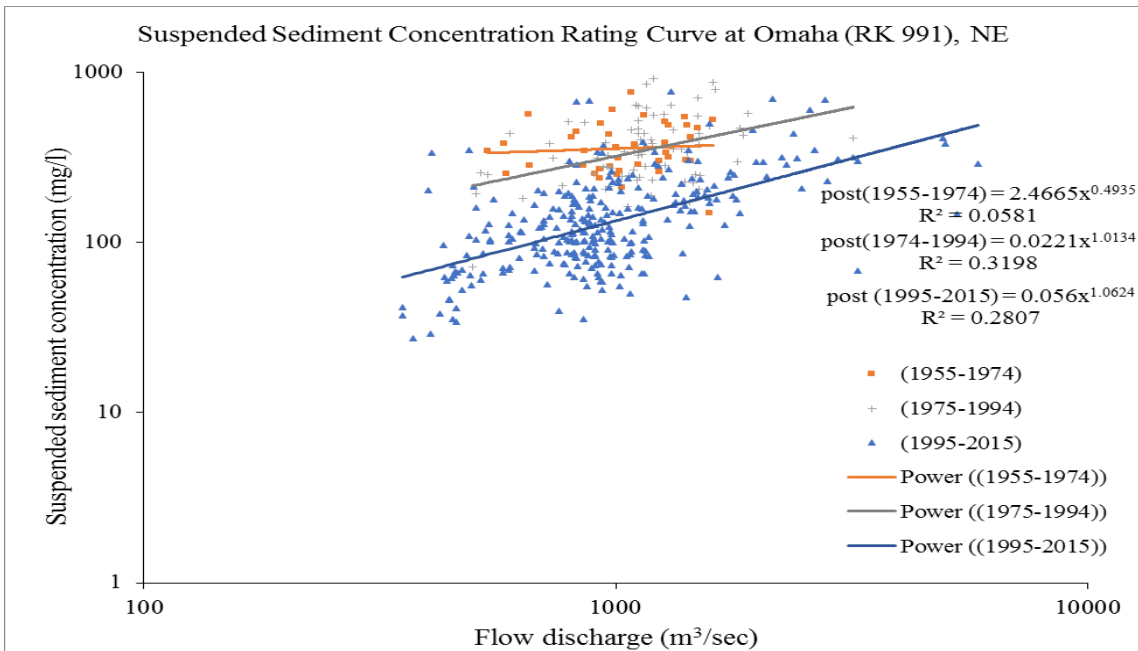

Figure A.4: Pre- and post-dam suspended sediment concentration rating curve of Missouri River at Omaha (RK 991), NE.

133

The pre- and post-dam mean annual suspended sand loads of Table A1 were computed as the average sand transport rate over the pre- and post-dam flow duration curves. In particular, the flow duration curves of Figure 2.2 were modeled in terms of 36 characteristics discharges, Q_i, with p_i being the average fraction of the year in which the flow was equal to Q_i. Estimated suspended sediment concentration for each characteristic discharge Ci is computed from suspended sediment concentration rating curve. The suspended sand transport capacity, Q_{si}, for each characteristic discharge was then computed as the product of the estimated suspended sediment concentration and the flow discharge (Horowitz, 2003; USACE, 2006).

$$Q_{si} = K * Ci * Qi$$

where K is constant and equal to 0.0864 when Ci in (mg/L), Q_i in (m^3/sec) and Q_{si} in (tan/day).

The mean annual suspended sand load, $Q_{bm,s}$ was finally estimated as:

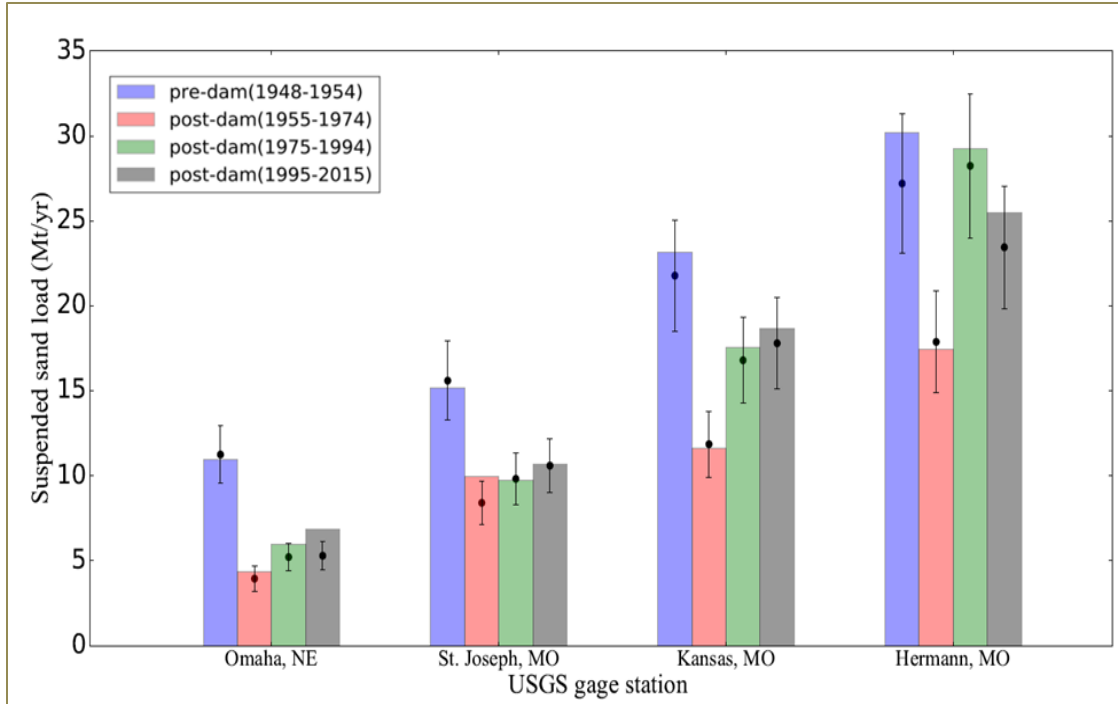$$Q_{bm,s} = \sum_{i=1}^{n} p_i Q_{si}$$

134

Figure A.5: Pre- and post-dam mean annual sand load. Field estimates and model results are respectively represented with colored bar and black dots. The error bars indicate ±15% of the numerical value. Due to limited suspended sediment concentration recorded values for post-dam(1955-1974) at St. Joseph and Kansas City, average fractions of sand in suspension were set equal to 0.33 at St. Joseph, MO, and 0.27 at Kansas City, MO, is used estimated the mean annual suspended sand load (Heimann et al., 2011). Pre-dam mean annual sand load based on suspended sediment concentration rating curve at Omaha, NE is determined based on only two available records.

135